FEDERAL UNIVERSITY OF SANTA CATARINA
CAMPUS FLORIANOPOLIS
POSTGRADUATE PROGRAM IN ELECTRICAL ENGINEERING

Sandra Cossul

A Data-Driven Strategy Combining Heart Rate Variability, Empirical Mode Decomposition and Machine Learning for Early Cardiac Autonomic Neuropathy Detection in Diabetes

Florianopolis
2024

Sandra Cossul

A Data-Driven Strategy Combining Heart Rate Variability, Empirical Mode Decomposition and Machine Learning for Early Cardiac Autonomic Neuropathy Detection in Diabetes

Thesis submitted to the Postgraduate Program in Electrical Engineering of the Federal University of Santa Catarina as a prerequisite to the Doctorate title in Electrical Engineering.

Supervisor: Professor Jefferson Luiz Brum Marques, PhD.

Florianopolis

2024

Cossul, Sandra
A Data-Driven Strategy Combining Heart Rate Variability, Empirical Mode Decomposition, and Machine Learning for Early Cardiac Autonomic Neuropathy Detection in Diabetes / Sandra Cossul ; orientador, Jefferson Luiz Brum Marques, 2024.
160 p.

Tese (doutorado) - Universidade Federal de Santa Catarina, Centro Tecnológico, Programa de Pós-Graduação em Engenharia Elétrica, Florianópolis, 2024.

Inclui referências.

1. Engenharia Elétrica. 2. Complicações Diabetes Mellitus. 3. Variabilidade Frequência Cardíaca. 4. Decomposição de Modo Empírico. 5. Aprendizado de máquina. I. Marques, Jefferson Luiz Brum. II. Universidade Federal de Santa Catarina. Programa de Pós-Graduação em Engenharia Elétrica. III. Título.

Sandra Cossul

A Data-Driven Strategy Combining Heart Rate Variability, Empirical Mode Decomposition, and Machine Learning for Early Cardiac Autonomic Neuropathy Detection in Diabetes

O presente trabalho em nível de Doutorado foi avaliado e aprovado, em 22 de fevereiro de 2024, pela banca examinadora composta pelos seguintes membros:

Prof.(a) Daiana Petry Rufato, Dra.
UDESC – Universidade do Estado de Santa Catarina

Prof. Cesar Augusto Prior, Dr.
UFSM – Universidade Federal de Santa Maria

Prof. Maurício Cagy, Dr.
UFRJ – Universidade Federal do Rio de Janeiro

Certificamos que esta é a versão original e final do trabalho de conclusão que foi julgado adequado para obtenção do título de Doutora em Engenharia Elétrica.

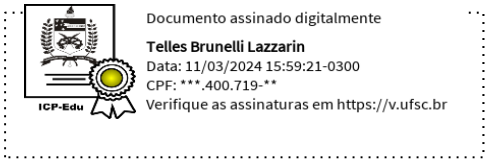

Prof. Telles Brunelli Lazzarin, Dr.
Coordenação do Programa de Pós-Graduação

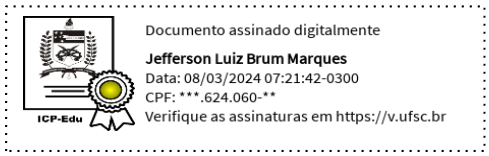

Prof. Jefferson Luiz Brum Marques, PhD.
Orientador

Florianópolis, 2024.

AGRADECIMENTOS

Ao meu orientador, Professor Jefferson Luiz Brum Marques, por não somente aceitar o compromisso da orientação, mas também por seu constante incentivo, sempre mostrando novas possibilidades e compartilhando seu conhecimento. Agradeço sinceramente por todo o tempo que dedicou ao longo destes anos na minha formação acadêmica. Por fim, agradeço pelo seu exemplo de dedicação e conduta, tanto pessoal quanto profissional.

À minha família, minha mãe, Márcia, e meu pai, Cláudio, que sempre me incentivaram a buscar meus objetivos, por meio do exemplo do trabalho, resiliência e integridade. Agradeço também aos meus irmãos, Scheila e Vitor, pelo incentivo e apoio incondicional.

Ao João Pedro, que esteve ao meu lado, dia após dia, sendo meu suporte emocional em tantos momentos. Agradeço profundamente pela paciência, pelo amor e companheirismo. Essa é uma conquista compartilhada, que não teria sido possível sem o teu apoio.

Aos meus amigos e colegas, especialmente ao Mateus A. Favretto e ao Felipe R. Andreis, que tornaram um pouco mais leve essa trajetória acadêmica. Obrigado por sempre estarem disponíveis para compartilharmos as dificuldades, pela troca de experiências e por todo o auxílio. O crescimento pessoal e profissional que alcançamos juntos é, sem dúvida, um dos retornos mais valiosos dessa jornada.

Aos professores do Instituto de Engenharia Biomédica da Universidade Federal de Santa Catarina e a todos os professores que contribuíram para meu conhecimento de alguma forma.

Ao CNPq pelo apoio financeiro.

Things are not always right because they are hard, but if they are right,
One must not mind if they are also hard. (CHURCHILL, W.)

ACADEMIC PRODUCTION

1. **COSSUL, S**. ANDRES, F.A., FAVRETTO, M.A.; MARQUES, J.L.B.M. The use of Empirical Mode Decomposition on Heart Rate Variability Signals to Assess Autonomic Neuropathy Progression in type 2 Diabetes. APPLIED SCIENCES, **2023,** 13, 7824. DOI: https://doi.org/10.3390/app13137824

2. FAVRETTO, M. A.; ANDREIS, F. A.; **COSSUL, S.**; NEGRO, F.; SOUZA, A. O.; MARQUES, J. L. B. Differences in motor unit behaviour during isometric contractions in patients with diabetic peripheral neuropathy at various disease severities. JOURNAL OF ELECTROMYOGRAPHY AND KINESIOLOGY, **2023,** 68, 102725. DOI: https://doi.org/10.1016/j.jelekin.2022.102725

3. FAVRETTO, M. A.; **COSSUL, S.**; ANDREIS, F. R.; NAKAMURA, L. R.; RONSONI, F.; TESFAYE, S.; SELVARAJAH D.; MARQUES, J. L. B. Alterations of tibialis anterior muscle activation pattern in subjects with type 2 diabetes with peripheral neuropathy. BIOMEDICAL PHYSICS & ENGINEERING EXPRESS, **2022**, 8, 025001. DOI: 10.1088/2057-1976/ac455b

4. OLIVEIRA, I.; FAVRETTO, M. A.**; COSSUL, S.;** MARQUES, J. L. B. Development of a MATLAB-based graphical user interface for analysis of high-density surface electromyography signals. XXVII Brazilian Congress on Biomedical Engineering – CBEB 2020. IFMBE PROCEEDINGS, **2022**, 83, 1829-1835. DOI: https://doi.org/10.1007/978-3-030-70601-2_267

5. WEBER, T. R.; DA SILVA, R. L.; COSSUL, S.; ALVES, M. S. L; LEE, S. V. S.; MARQUES, J. L. B. Avaliação Ecocardiográfica na diabetes mellitus tipo 1. REVISTA PORTUGUESA DE CARDIOLOGIA, **2021,** 1,1. DOI: https://doi.org/10.1016/j.repc.2020.11.012

6. **COSSUL, S.**; FAVRETTO, M. A.; ANDREIS, F. R.; DE CASTRO; A. A. JR.; MARQUES, J. L. B. A portable microcontroller-based electrostimulation system for nerve conduction studies. IET SCIENCE MEASUREMENT & TECHNOLOGY. **2020**,14,1. DOI: https://doi.org/10.1049/iet-smt.2019.0174

7. ANDREIS, F. R.; FAVRETTO, M. A.; **COSSUL, S.**; NAKAMURA, L. R.; BARBETTA, P. A.; MARQUES, J.L.B. Linear mixed-effects models for the analysis of high-density electromyography with application to diabetic peripheral neuropathy. MEDICAL & BIOLOGICAL ENGINEERING & COMPUTING, **2020,** 58,1625-1636. DOI: https://doi.org/10.1007/s11517-020-02181-1

8. UCKER, M.; **COSSUL, S.**; FAVRETTO, M. A.; LOPES, L. B.; TERRA, T. G.; FRANCO, M. V. B.; MARQUES, J. L. B. Desenvolvimento de um sistema de aquisição de imagens de pupilometria dinâmica utilizando módulos OpenMV. ANAIS DO XII SIMPÓSIO DE ENGENHARIA BIOMÉDICA - IX SIMPÓSIO DE INSTRUMENTAÇÃO E IMAGENS MÉDICAS, Uberlândia, **2019**. DOI: 10.5281/zenodo.3461153

9. **COSSUL, S**.; FAVRETTO, M. A.; ANDREIS, F. R.; MARQUES, J. L. B. Ulnar Motor Nerve Conduction Studies: Reference Values and Effect of Age, Gender and Anthropometric Factors. IFMBE PROCEEDINGS, **2019**, 70(2), 881-886. DOI: https://doi.org/10.1007/978-981-13-2517-5_137

10. FAVRETTO, M. A.; **COSSUL, S**.; ANDREIS, F. R.; MARQUES, J. L. B. Evaluation of Rate of Muscular Force Development in Type 2 Diabetic Individuals with and without Diabetic Peripheral Neuropathy. IFMBE PROCEEDINGS, **2019**, 70(1), 31-36. DOI: https://doi.org/10.1007/978-981-13-2119-1_5

11. ANDREIS, F. R.; FAVRETTO, M. A.; **COSSUL, S**.; BARBETTA, P. A.; MARQUES, J. L. B. Reliability of Maximal Voluntary Isometric Contraction of Ankle Dorsiflexion in Male Subjects. IFMBE PROCEEDINGS, **2019,** 70(1), 353-357. DOI: https://doi.org/10.1007/978-981-13-2119-1_55

12. FAVRETTO, M. A.; **COSSUL, S**.; ANDREIS, F. R; BALOTIN, A. F.; MARQUES, J. L. B. High Density Surface EMG System based on ADS1298-front end. IEEE LATIN AMERICA TRANSACTIONS, **2018**, 16, 1616-1622. DOI: 10.1109/TLA.2018.8444157

RESUMO

A neuropatia autônomica cardiovascular (NAC), complicação do diabetes mellitus (DM), é uma condição que afeta a regulação neural do sistema cardiovascular. O objetivo desta tese é analisar sinais de variabilidade da frequência cardíaca (VFC) usando a decomposição de modo empírico (DME) e técnicas estabelecidas de análise da VFC para identificar alterações precoces ou subclínicas na função autonômica de indivíduos com DM que possuem NAC. A tese está estruturada em três seções: (a) o desenvolvimento e validação de uma *ferramenta de processamento de sinais de VFC* integrada a um banco de dados para o pré-processamento de sinais de eletrocardiograma (ECG) e fotopletismografia (PPG), permitindo a análise da VFC e sensibilidade barorreflexa, bem como a implementação do método DME e extração de parâmetros, que foi a base para ambos os estudos desta tese; (b) o *Primeiro Estudo* investigou a relevância das características baseadas na DME extraídas dos sinais de VFC para diferenciar entre os níveis de progressão da NAC em pacientes com DM tipo 2. Este estudo envolveu 60 participantes igualmente divididos em três grupos: semNAC - ausência de NAC, subNAC - NAC subclínica e estNAC - NAC estabelecida. Seis características da DME (ASR_{area} - área do sinal analítico; $SODP_{area}$ - área do gráfico de diferenças de segunda ordem; $SODP_{CTM}$ – medida da tendência central do gráfico de diferença de segunda ordem; PSD_{pkamp} – amplitude de pico da estimativa da densidade espectral de potência; e PSD_{mfreq} - frequência média da estimativa da densidade espectral de potência) foram extraídas dos sinais de intervalo RR e comparadas entre os grupos. Os resultados revelaram diferenças significativas entre os indivíduos semNAC e estNAC para todos os parâmetros da DME e seus componentes, exceto para PSD_{mfreq}. Além disso, apenas alguns componentes da DME de cada parâmetro mostraram diferenças significativas entre indivíduos semNAC ou estNAC e aqueles com subNAC. Também houve uma redução gradual na variabilidade e distribuição de potência dos componentes da DME correlacionada com os estágios de gravidade da NAC e; (c) o *Segundo Estudo*, que avaliou o desempenho de vários modelos de aprendizado de máquina supervisionados e diferentes técnicas de seleção de características para a classificação multiclasse dos níveis de gravidade da NAC. O estudo utilizou um conjunto de dados composto por dados de ECG e PPG de 250 indivíduos com DM tipo 1 ou tipo 2, categorizados em três classes de progressão da NAC. Três conjuntos de características foram considerados: um contendo parâmetros convencionais da VFC (incluindo domínios de tempo, frequência e parâmetros não lineares), outro composto exclusivamente por características baseadas na DME derivadas da VFC, e o último incorporando uma combinação de todas essas características derivadas da VFC. Os principais resultados indicaram que os modelos de aprendizado de máquina que utilizaram o conjunto composto resultaram na maior acurácia de classificação (88,4%), com características de todos os métodos de análise da VFC contribuindo para esse resultado. Ambos os estudos demonstraram que as medidas extraídas da DME podem contribuir para caracterizar alterações subclínicas associadas à manifestação da NAC em conjunto com parâmetros tradicionais da VFC. Esses resultados demonstram o potencial de medidas baseadas na DME como uma ferramenta de triagem viável para o diagnóstico precoce da NAC.

Palavras-chave: Complicações Diabetes Mellitus; Neuropatias Diabéticas; Variabilidade Frequência Cardíaca; Eletrocardiograma; Decomposição Modo Empírico; Aprendizado de Máquina.

ABSTRACT

Cardiovascular autonomic neuropathy (CAN), a diabetes mellitus (DM) complication, is a condition that disrupts the neural regulation of the cardiovascular system. This thesis aims to analyse heart rate variability (HRV) signals using the empirical mode decomposition (EMD) and established HRV analysis techniques, to identify early or subclinical autonomic function alterations in DM individuals with CAN. The thesis is structured into three sections: (a) the development and validation of an *HRV signal processing tool* integrated with a database for preprocessing electrocardiogram (ECG) and photoplethysmogram (PPG) signals, allowing for HRV and baroreflex sensitivity analysis, along with the implementation of the EMD method and feature extraction, which was the basis for both the studies of this thesis; (b) the *First Study,* that investigated the relevance of EMD-based features extracted from HRV signals to differentiate between progression levels of CAN among type 2 DM patients. This study involved 60 participants equally divided into three groups: noCAN - no presence of CAN, subCAN - subclinical CAN, and estCAN - established CAN. Six EMD features (ASR_{area} – the area of the analytical signal; $SODP_{area}$ - area of the second-order difference plot; $SODP_{CTM}$ - the central tendency measure of the second-order difference plot; PSD_{pkamp} - peak amplitude of the power spectral density estimation; PSD_{bpow} - band power of the power spectral density estimation; and PSD_{mfreq} - mean frequency of the power spectral density estimation) were extracted from the RR interval signals and compared between groups. The results revealed significant differences between the noCAN and estCAN individuals for all EMD features and their components, except for the PSD_{mfreq}. Moreover, only some EMD components of each feature showed significant differences between individuals with noCAN or estCAN and those with subCAN. Also, there was a gradual reduction in variability and power distribution of the EMD components correlated to the stages of CAN severity; and (c) the *Second Study* assessed the performance of several supervised machine learning models and different feature selection techniques for the multiclass classification of CAN severity levels. The study employed a dataset comprising ECG and PPG data from 250 individuals with either type 1 or type 2 DM, categorized into three classes of CAN progression. Three feature sets (FS) were considered: one containing conventional HRV features (including time, frequency domains, and nonlinear parameters), another consisting solely of EMD-based features derived from HRV, and the last one incorporating a combination of all these HRV-derived features. The main findings revealed that the ML models using the composite FS resulted in the highest classification accuracy (88.4%), with features from all HRV analysis methods contributing to this outcome. Both studies demonstrated that EMD outcome measures can contribute to characterizing subclinical changes associated with CAN manifestation in conjunction with traditional HRV features. These findings demonstrate the potential of EMD-based measures as a viable screening tool for early CAN diagnosis.

Keywords: Diabetes Mellitus Complication; Diabetic Neuropathies; Heart Rate Variability; Electrocardiogram; Empirical Mode Decomposition; Machine Learning

RESUMO EXPANDIDO

Introdução

A diabetes mellitus (DM) é uma doença crônica que ocorre quando o corpo não consegue produzir insulina suficiente ou não consegue usar efetivamente a insulina que produz, resultando em níveis elevados de glicose no sangue. Os distúrbios metabólicos da DM levam a danos difusos e generalizados nos nervos periféricos, autonômicos e nos pequenos vasos sanguíneos. Dentre esses danos, destaca-se a neuropatia autonômica cardiovascular (NAC), caracterizada por lesões nas fibras nervosas autônomas que inervam o coração, levando a alterações na frequência cardíaca e na dinâmica cardiovascular. Embora seja uma condição grave, a NAC é frequentemente subdiagnosticada, uma vez que os sintomas clínicos (por exemplo, taquicardia em repouso, hipotensão ortostática e regulação anormal da pressão arterial) só aparecem em estágios avançados da doença. Assim, a detecção precoce da NAC, especialmente em sua fase subclínica (ou seja, quando os sintomas característicos da doença ainda não são aparentes ou totalmente desenvolvidos, mas podem haver alterações subjacentes), é essencial para iniciar intervenções que visem atrasar a progressão da doença ou, até mesmo, reverter seu curso. No diagnóstico da NAC, os testes de reflexo cardiovascular são considerados o padrão-ouro, sendo utilizados para avaliar a resposta do sistema cardiovascular a estímulos específicos. No entanto, a NAC apresenta uma manifestação silenciosa e pode não exibir sintomas nos estágios iniciais, o que dificulta o diagnóstico precoce apenas por meio dos testes de reflexo cardiovascular. Nos estágios iniciais ou subclínicos da NAC, observam-se principalmente anormalidades nos reflexos barorreceptores e alterações na variabilidade da frequência cardíaca (VFC). Os reflexos barorreceptores são respostas automáticas do sistema nervoso autônomo (SNA) a mudanças na pressão arterial, enquanto a VFC refere-se à variação no intervalo de tempo entre os batimentos cardíacos. A VFC é utilizada para avaliar a regulação cardiovascular, em que níveis adequados de variabilidade indicam uma resposta equilibrada entre os componentes simpático e parassimpático do SNA. Os índices de VFC são derivados de análises no domínio do tempo e da frequência, além de incorporar medidas não lineares. Dentre as abordagens não lineares, um método que tem sido aplicado na análise de sinais de VFC e sinais biomédicos em geral é a decomposição de modo empírico (DME). A DME decompõe um sinal complexo em componentes intrínsecas e adaptativas, conhecidas como modos empíricos, as quais representam diferentes escalas de variabilidade presentes no sinal original.

Objetivos

O objetivo principal desta tese é analisar sinais de VFC usando a DME e técnicas estabelecidas de análise da VFC para identificar alterações precoces ou subclínicas na função autonômica de indivíduos com DM que possuem NAC. Os objetivos específicos são: (a) *sistema de processamento de sinais de VFC:* desenvolver um sistema de processamento de sinais de VFC integrado a um banco de dados para o pré-processamento de sinais de eletrocardiograma (ECG) e fotopletismografia (PPG), permitindo a análise da VFC e sensibilidade barorreflexa, bem como a implementação do método DME e extração de parâmetros; (b) *primeiro estudo:* investigar a relevância das métricas baseadas na DME extraídas dos sinais de VFC para diferenciar entre os níveis de progressão da NAC em pacientes com DM tipo 2 (DM2) e; (c) *segundo estudo:* avaliar o desempenho de modelos de aprendizado de máquina na

classificação multiclasse dos níveis de progressão da NAC usando uma combinação de métricas de VFC e métricas derivadas da DME aplicada ao sinal de VFC.

Sistema de processamento de sinais de VFC

Metodologia

O sistema de processamento de sinais de VFC foi desenvolvido no MATLAB e integrado a um banco de dados criado no Access. Esse sistema recebe sinais de ECG e PPG como entrada, realiza o pré-processamento desses sinais e extrai o sinal de VFC. A análise do sinal de VFC inclui o cálculo de parâmetros nos domínios do tempo e da frequência, análises não lineares e a aplicação do método de DME. O sistema também inclui um módulo para análise da sensibilidade barorreflexa, utilizando os sinais de VFC e PPG. Todos esses parâmetros calculados são enviados e armazenados no banco de dados para análise posterior. Para validação do sistema, foram coletados dados de ECG de 25 indivíduos saudáveis. Em seguida, foram calculadas 19 medidas de VFC nos domínios do tempo, frequência e não lineares. Essas medidas foram comparadas com as mesmas medidas calculadas no Kubios HRV Standard, um software validado cientificamente para análise de VFC. A validação utilizou análises estatísticas com cálculo do coeficiente de correlação intraclasse (ICC) e gráficos de Bland-Altman.

Resultados e Discussão

O sistema de processamento e análise da VFC foi desenvolvido como uma ferramenta personalizada para análise dos sinais de ECG e PPG, sendo utilizado como base para o desenvolvimento de ambos os estudos apresentados nesta tese. Na validação, os gráficos de Bland-Altman, nos quais a maioria dos pontos estava dentro dos limites de concordância, em conjunto com as medidas de ICC, predominantemente acima de 0,9, demonstraram a consistência entre as medidas dos dois sistemas, indicando a confiabilidade do software desenvolvido.

Primeiro estudo

Metodologia

Este estudo envolveu 60 participantes com DM2 igualmente divididos em três grupos: semNAC - ausência de NAC, subNAC - NAC subclínica e estNAC - NAC estabelecida. Seis características foram extraídas dos modos empíricos após a DME dos sinais de VFC: ASR_{area} - área do sinal analítico, $SODP_{area}$ - área do gráfico de diferenças de segunda ordem, $SODP_{CTM}$ – medida da tendência central do gráfico de diferença de segunda ordem, PSD_{pkamp} – amplitude de pico da estimativa da densidade espectral de potência e PSD_{mfreq} - frequência média da estimativa da densidade espectral de potência. Para comparar as diferenças médias dos parâmetros entre os grupos foi conduzida uma análise de variância (ANOVA) no R.

Resultados e Discussão

Os resultados da ANOVA revelaram diferenças significativas entre os indivíduos semNAC e estNAC para todos os parâmetros da DME e seus componentes, exceto para PSD_{mfreq}. Além disso, apenas alguns componentes da DME de cada parâmetro mostraram diferenças significativas entre indivíduos semNAC ou estNAC e aqueles com subNAC. Também houve uma redução gradual na variabilidade e distribuição de potência dos componentes da DME correlacionada com os estágios de gravidade da NAC. Os resultados deste estudo sugerem que as medidas de resultados baseadas

em DME são promissoras na caracterização de mudanças associadas à progressão de NAC em indivíduos com DM2.

Segundo estudo

Metodologia

Neste estudo, utilizou-se um conjunto de dados composto por dados de ECG e PPG de 250 indivíduos com DM tipo 1 ou DM2. Esses participantes foram categorizados em três classes de progressão da NAC (semNAC - ausência de NAC, subNAC - NAC subclínica e estNAC - NAC estabelecida). Considerou-se três conjuntos de características: o primeiro com parâmetros convencionais da VFC (incluindo domínios de tempo, frequência e parâmetros não lineares); o segundo com características derivadas da VFC utilizando a DME; e o terceiro, um conjunto composto, que incorpora uma combinação de todas essas características incluindo métricas da DME e métricas convencionais da VFC. Para a seleção de características foram aplicadas técnicas como selectKbest, eliminação de características recursivas e análise de componentes principais. Os modelos de aprendizado de máquina multiclasse supervisionados utilizados incluíram máquina de vetor de suporte, K vizinhos mais próximos, análise de discriminante linear e quadrática, regressão logística, classificador adaboost e árvore de decisão. O estudo foi desenvolvido utilizando a linguagem Python e o ambiente Jupyter Notebook.

Resultados e Discussão

Os principais resultados indicaram que os modelos de aprendizado de máquina que utilizaram o conjunto composto resultaram na maior acurácia de classificação, obtendo uma acurácia de 88,4% com o classificador K vizinhos mais próximos e a técnica de seleção de eliminação de características recursivas. Além disso, as características derivadas de todos os métodos de análise da VFC contribuíram para esse resultado. Por fim, os modelos de classificação utilizando os conjuntos de métricas individuais (somente VFC ou somente DME) não obtiveram uma acurácia na classificação superior a 76,5%.

Considerações Finais

Ambos os estudos demonstraram que as medidas extraídas da DME em conjunto com parâmetros tradicionais da VFC podem contribuir para caracterizar alterações subclínicas associadas à manifestação da NAC. Esses resultados evidenciam o potencial das medidas baseadas na DME como uma ferramenta adicional de triagem para complicações cardiovasculares decorrentes da DM, auxiliando no diagnóstico precoce da NAC.

Palavras-chave: Complicações Diabetes Mellitus; Neuropatias Diabéticas; Variabilidade Frequência Cardíaca; Eletrocardiograma; Decomposição Modo Empírico; Aprendizado de Máquina.

LIST OF FIGURES

LIST OF TABLES

LIST OF ABBREVIATIONS AND ACRONYMS

ANS	Autonomic nervous system
ANN	Artificial neural network
AI	Artificial intelligence
ASR	Analytical signal representation
AUC	Area under the ROC curve
BP	Blood pressure
BRS	Baroreflex sensitivity
CAN	Cardiovascular autonomic neuropathy
CART	Cardiac autonomic reflex test
CV	Cross-validation
CVD	Cardiovascular disease
CTM	Central tendency measure
DAN	Diabetic autonomic neuropathies
DBMS	Database management system
DBP	Diastolic blood pressure
DM	Diabetes mellitus
DN	Diabetic neuropathies
DT	Decision tree
DPN	Diabetic peripheral neuropathy
ECG	Electrocardiogram
EMD	Empirical mode decomposition
EstCAN	Established CAN
FFT	Fast Fourier transform
HbA1c	Glycated Haemoglobin
HF	High-frequency
HR	Heart rate
HRV	Heart rate variability
ICC	Intraclass correlation coefficient
IDF	International Diabetes Federation
IMF	Intrinsic mode function
KNN	K-nearest neighbours
LR	Logistic regression

LF	Low-frequency
ML	Machine learning
NoCAN	No presence of CAN
PAT	Pulse arrival time
PCA	Principal component analysis
PNS	Parasympathetic nervous system
PPG	Photoplethysmogram
PSD	Power spectral density
PTT	Pulse transit time
PWW	Pulse wave velocity
ROC	Receiver operating characteristic curve
SBP	Systolic blood pressure
SCD	Sudden cardiac death
SNP	Sympathetic nervous system
SQL	Structured query language
SODP	Second-order difference plot
SubCAN	Subclinical CAN
SVM	Support vector machine
T1DM	Type 1 diabetes mellitus
T2DM	Type 2 diabetes mellitus
VLF	Very-low-frequency

SUMMARY

1 INTRODUCTION

This section presents a contextualization and motivation of the studies developed in this thesis and presents the thesis' objectives.

1.1 CONTEXTUALIZATION

According to the International Diabetes Federation (IDF, 2021), it is estimated that 537 million people are living with diabetes mellitus (DM), which represents 10.5% of the world's population. DM is a chronic disorder that occurs when the body cannot produce enough insulin or cannot effectively use the insulin it produces, resulting in raised blood glucose levels (American Diabetes Association, 2021). The metabolic disorders of DM lead to diffuse and widespread damage to the peripheral and autonomic nerves and small vessels. Among these, damage to the autonomic nerve fibres that innervate the heart and blood vessels is known as cardiovascular autonomic neuropathy (CAN), resulting in abnormalities in heart rate and vascular dynamics (Vinik *et al.*, 2018). Data indicate a varied prevalence of CAN in type 1 and 2 DM, varying from 17% to 73%, depending on clinical and demographic factors (Williams *et al.*, 2022).

Cardiovascular autonomic neuropathy (CAN) is an autonomic dysfunction that affects the neural regulation of the cardiovascular system, occurring as a result of diabetes mellitus (DM) (Spallone, 2019). The strongest risk factors for the development of CAN in type 1 DM are the duration of diabetes and hyperglycaemia. In contrast, in type 2 DM, multifactorial risk factors, such as obesity, hypertension, and hyperlipidaemia, play a significant role (Andersen *et al.*, 2018; Williams *et al.*, 2022). CAN is associated with morbidity, high cardiovascular mortality, and sudden cardiac death (Spallone, 2019). Although it is a serious condition, CAN is frequently under-recognized since the clinical symptoms (*e.g.*, weakness, resting tachycardia, orthostatic hypotension, abnormal blood pressure regulation) only appear in advanced stages of disease (Ang *et al.*, 2020). Thus, the early detection of CAN, especially in its subclinical stage (*i.e.*, when the characteristic disease symptoms are not yet apparent or fully developed, but there might be underlying changes or abnormalities), is essential to initiate timely interventions.

The gold standard for CAN diagnosis is the series of cardiac autonomic reflex tests (CARTs), which measure the heart rate and blood pressure responses to simple interventions such as deep breathing, the Valsalva manoeuvre, and lying-to-standing (Williams *et al.*, 2022). These responses are compared to normal and age-adjusted cut-off values (O'Brien; O'Hare; Corrall, 1986). Nevertheless, CAN has a silent presentation and may exhibit no symptoms or have subtle symptoms, making it challenging to identify and diagnose in the initial stages with only the CARTs (Vinik *et al.*, 2018). In addition, CARTs must follow consistent and standardized protocols, which require active patient collaboration (Ang *et al.*, 2020). Early or subclinical CAN is limited to baroreceptor abnormalities and changes in heart rate variability (HRV) (Fisher; Tahrani, 2017). Hence, HRV indices are a different approach to CARTs for assessing autonomic function, as they are easier and quicker than CARTs, patient-independent, and sensitive to early dysfunction (Spallone, 2019).

HRV refers to the time elapsed between two successive R-waves of the QRS complex on the electrocardiogram (ECG) (*i.e.*, the RR interval) (Acharya; Kannathal; Krishnan, 2004). HRV indices are amongst the simplest and most reliable ways to assess CAN. They are obtained by time- and frequency-domain methods, which measure, respectively, the overall magnitude of the fluctuations of the RR interval between each heartbeat around the average values and the magnitude of fluctuations in a predetermined range of frequency (Rolim; de Souza; Dib, 2013). Despite having a wide basis of evidence for the supportive value of HRV analysis in CAN diagnosis and risk stratification in diabetic individuals (Cardoso *et al.*, 2023; Castiglioni *et al.*, 2022; Pop-Busui *et al.*, 2022), HRV methods and indices for decision-making and, most importantly, CAN severity quantification remain an active and expanding research topic (Benichou *et al.*, 2018).

HRV reflects the dynamic changes in the autonomic nervous system's regulation and is determined by the combined inputs of the sympathetic and parasympathetic systems (Williams *et al.*, 2022). HRV signals involve nonlinear contributions and are essentially non-stationary (Acharya; Kannathal; Krishnan, 2004). Thus, measures from information and invariant domains that can accurately describe the nonlinear properties of HRV signals are strongly recommended to be used in conjunction with traditional techniques because they may provide supplementary information about the underlying mechanisms involved in cardiovascular regulation (Bravi; Longtin; Seely, 2011; Sassi *et al.*, 2015). Several studies have demonstrated

the usefulness of the nonlinear analysis of HRV for assessing cardiac abnormalities and have explored techniques such as the correlation dimension, Poincare plots, entropy parameters, recurrence plots, and detrended fluctuation analysis (Faust *et al.*, 2012; Jelinek *et al.*, 2013; Khandoker; Jelinek; Palaniswami, 2009; Rajendra Acharya *et al.*, 2013; Roy; Ghatak, 2013).

Among these techniques, a nonlinear method that has been explored for HRV analysis is empirical mode decomposition (EMD). EMD is a data analysis method proposed by Huang *et al*. (1998) that decomposes a time series into a set of simpler and more interpretable oscillatory modes called intrinsic mode functions (IMFs). The Hilbert transform can be applied to IMFs to obtain their analytical signal, from which additional information can be calculated, such as the instantaneous frequency and the amplitude and phase modulation of the IMF (Maheshwari; Kumar, 2014). EMD is an adaptive and data-driven technique, which makes it well-suited to analysing signals that have complex, nonlinear, and non-stationary characteristics. Compared to other methods of time-frequency analysis of signals, EMD addresses some of these limitations. For example, the Fourier transform is a linear technique that assumes the signal is stationary over time (Maheshwari; Kumar, 2014), which is not the case for HRV signals that exhibit nonlinear interactions between different frequency components (Benichou *et al.*, 2018). On the other hand, the Wavelet transform is a frequency-based method that selects an appropriate wavelet basis function and scale, while EMD is a time-based method that does not require a priori knowledge of the signal frequency content (Maheshwari; Kumar, 2014).

As a result of its different approach and the advantages over the analysis of complex and nonlinear time-series signals, the use of the EMD technique has gained increasing attention and has been adopted for a variety of biomedical signals, such as the electroencephalogram for epileptic seizure classification (Bajaj; Pachori, 2012; Pachori; Patidar, 2014), emotion recognition (Abdulrahman; Baykara; Alakus, 2022; Salankar; Mishra; Garg, 2021), and the identification of autism severity level (Hadoush; Alafeef; Abdulhay, 2019), electromyography for the analysis of amyotrophic lateral sclerosis (Mishra *et al.*, 2016, 2017) or for the classification of neuromuscular disorders (Dubey *et al.*, 2022; Naik; Selvan; Nguyen, 2016) and ECG signals for the classification of cardiovascular diseases (Hasan; Bhattacharjee, 2019), ECG denoising (Kumar; Panigrahy; Sahu, 2018; Rakshit; Das, 2018), the classification of ventricular arrhythmias (Mohanty *et al.*, 2021), the prediction of sudden cardiac death (-Bautista

et al., 2023), and the detection of hypertension (Soh *et al.*, 2020) or the extraction of foetal ECG (Barnova *et al.*, 2021).

The study by Echeverria *et al*. (2001) was one of the first to propose the application of EMD to HRV analysis, concluding that EMD and the associated Hilbert spectral representation are powerful techniques for HRV time-frequency analysis due to their capabilities of independently isolating the main frequency components and dealing with non-stationary and nonlinear features of the ECG signal. Subsequently, a study by Souza Neto *et al*. (2004) also showed that EMD is a flexible processing method that enhances the assessment of cardiovascular autonomic control, overcoming the limitations posed by the linearity and stationarity assumptions inherent in traditional spectral techniques. Pachori *et al*. (2015) proposed a set of EMD-based features applied to the RR interval signals that allowed differentiation between subjects with and without diabetes. In the same context, Pachori et al. (2016) presented a methodology for screening patients with DM by applying the EMD method to decompose HRV signals, achieving a classification accuracy of 95.63%. Acharya *et al*. (2017) subjected HRV signals to the EMD technique to identify and classify normal and congestive heart failure, obtaining an accuracy of 97.01%. Sood *et al*. (2016) proposed a methodology for discriminating between normal and coronary artery disease subjects using heart rate signals, showing statistically significant EMD-based features. Similarly, Shi *et al*. (2020) investigated EMD-based features applied to HRV signals on sudden cardiac death (SCD), predicting subjects at risk earlier with an accuracy of 96.1% and outperforming the classical linear estimators of SCD. These studies highlighted that analysing HRV signals using the EMD technique provides relevant information about overall cardiac abnormalities.

This understanding is especially significant in the context of the cardiovascular system, which continually adapts to changes in internal and external conditions to maintain blood pressure homeostasis through complex and dynamic feedback mechanisms that simultaneously affect several processes such as heart rate, cardiac output, blood pressure, respiration, and peripheral resistance. In this way, there is a need for nonlinear, non-stationary, and multivariate approaches to assess cardiovascular interactions and their causal structure in health and disease (Orini *et al.*, 2017). Furthermore, it is necessary to develop biomarkers for early and precise prediction of diabetes complications, which are specific, stage-related, and non-invasive (Ahluwalia *et al.*, 2019). However, single biomarkers will likely have inherent

limitations; therefore, combining several biomarkers may be more precise in identifying those at high risk for developing diabetes or identifying complications when DM is already established (Dorcely *et al.*, 2017). The identification of biomarkers, metrics, or patterns of risk based on data generated by a monitoring device (*e.g.*, ECG and PPG data) combined with clinical data is facilitating the development of risk-prediction models for diabetes and diabetes-related complications that will, in turn, change the DM control to a personalized approach with personalized treatment and management strategies leading to precision medicine in DM (Fagherazzi; Ravaud, 2019).

In connection with this, applying artificial intelligence (AI) will facilitate the analysis of extensive datasets to create predictive models, which offer valuable insights for patients and healthcare providers to enhance the control and treatment of DM and its complications (Fagherazzi; Ravaud, 2019). Predictive models can be used to estimate the probability or risk of a specific outcome or to classify that a particular outcome is present/absent (diagnostic prediction model) or will happen within a specific timeframe (prognostic prediction model) in an individual (Cichosz; Johansen; Hejlesen, 2016). The development of predictive models for the onset of chronic microvascular complications in patients suffering from DM could contribute to evaluating the relationship between exposure to an individual factor and the risk of the onset of a specific complication, to stratifying the patient's population in a medical centre concerning this risk, and to developing tools for the support of informed clinical decision in patient's treatment (Dagliati *et al.*, 2018).

Recently, several studies have proposed the use of AI through the use of machine learning algorithms for CAN classification based on HRV features (Abdalrada *et al.*, 2017; Alkhodari *et al.*, 2021; Carricarte Naranjo *et al.*, 2017b; Cornforth; Tarvainen; Jelinek, 2013, 2014; Hassan *et al.*, 2022; Khandoker; Jelinek; Palaniswami, 2009b; Nedergaard *et al.*, 2023; Wehler *et al.*, 2021). Most existing approaches have successfully identified CAN through binary classification, primarily focusing on distinguishing between patients with CAN and without CAN. Some studies evaluated CAN in a multiclass approach (Abdalrada *et al.*, 2017; Hassan *et al.*, 2022; Nedergaard *et al.*, 2023), achieving good results, but they did not evaluate the use of features calculated from the HRV signal components derived from the EMD method.

In this context, this thesis' significance is based on four complementary aspects: (a) identifying parameters that characterize the subtle changes occurring in the early stages of CAN (*i.e.*, the subclinical phase, where the disease is present but symptoms

are not yet evident or are very mild), enabling the initiation of preventive treatment to control symptoms and potentially slow or reverse the disease progression (Fisher; Tahrani, 2017; Williams *et al.*, 2022); (b) introducing a novel application of the EMD method, since the EMD method has not been applied to analyse HRV signals of DM patients with CAN at different levels of severity. Previous studies of the EMD method have been limited to binary CAN or DM classification; (c) proposing the utilization of HRV indices as a complementary method for CARTs in CAN diagnosis and monitoring, offering the advantages of time-effectiveness, patient-independence, and providing quantitative measurements; and d) contributing to ongoing research on the relevance of nonlinear HRV analysis approaches in investigating the neural control of the cardiovascular system in the presence of CAN.

The work is organized in three parts outlined as follows: (1) the development and validation of an HRV processing tool to serve as the basis for conducting analyses of ECG and PPG data, along with the calculation of EMD extracted features; (2) the first study, which evaluates the relevance of EMD derived features for CAN severity levels differentiation and; (3) the second study, which focuses on the evaluation of machine learning models for multiclass classification of CAN severity levels, using both traditional HRV features and EMD-derived features.

1.2 OBJECTIVES

1.2.1 Main Objective

The main objective of this study is to investigate the complexity of heart rate variability signals by combining nonlinear methodologies with conventional techniques. This approach aims to assess early changes in the autonomic function of diabetic individuals with cardiovascular autonomic neuropathy.

1.2.2 Specific Objectives

1.2.2.1 HRV Processing Tool

To develop an HRV signal processing tool integrated with a database connection, facilitating the analysis of ECG and PPG data, enabling the computation of HRV-derived features, and conducting EMD analysis.

1.2.2.2 First Study

To investigate the relevance of the EMD-based features extracted from HRV signals to differentiate between progression levels of cardiovascular autonomic neuropathy among type 2 DM patients (*i.e.*, no CAN, subclinical CAN, and established CAN).

1.2.2.3 Second Study

To assess the performance of machine learning models in the multiclass classification of CAN severity levels (*i.e.*, no CAN, subclinical CAN, and established CAN) using a combination of HRV features and EMD-derived features.

2 LITERATURE REVIEW

The literature review is subdivided into four sections: 2.1) Cardiovascular System, with an overall description focusing on the electrocardiogram derivation and definition of HRV; 2.2) Autonomic Nervous System with an initial description of its structure and functionality, primarily related to the cardiovascular control; 2.3) Diabetes Mellitus, with a general explanation about the disease and its complications, and; 2.4) Cardiac Autonomic Neuropathy, detailing this complication, how it is diagnosed and its association with HRV analysis and BRS.

2.1 CARDIOVASCULAR SYSTEM

The cardiovascular system comprises the heart and a network of blood vessels circulating blood to tissues and organs. The heart works as a pump by forcing blood into the arterial circulation to deliver oxygen and nutrients to tissues and remove carbon dioxide and waste products from these tissues into the venous circulation that carries blood back to the heart (Biaggioni *et al.*, 2022; Goldberger; Goldberger; Shvilkin, 2013).

The ability to contract without any outside signal gives the heart its unique property, which comes from the specialized myocardial cells known as autorhythmic cells (or pacemaker cells) in the cardiac muscle. The autorhythmic cells' action potential depolarization phase is caused by Ca^{2+} influx, followed by the repolarization phase due to K^{+} efflux. So, an action potential originates spontaneously in the heart's pacemaker cells and spreads into the contractile cells of the cardiac muscle through gap junctions. The action potentials of myocardial contractile cells have a depolarization phase created by Na^{+} influx and a repolarization phase due to K^{+} efflux with a plateau phase created by Ca^{2+} influx (Silverthorn, 2019).

2.1.1 Electrocardiogram

The electrocardiogram (ECG) records the heart's electrical activity produced by the spread of the stimuli through the atria and ventricles, followed by the return of the stimulated atrial and ventricular muscle to the resting state. The ECG is an extracellular

recording representing the sum of multiple action potentials in many heart muscle cells (Goldberger; Goldberger; Shvilkin, 2013; Silverthorn, 2019).

Each phase of cardiac electrical activity produces a specific wave or complex, and each one reflects depolarization or repolarization of the atria and ventricles (see Figures 1 and 2). The heart's depolarization begins in the sinoatrial or sinus node (SA), autorhythmic cells in the right atrium (RA) that serve as the heart's primary pacemaker. The P wave represents the atria depolarization. The depolarization wave spreads rapidly to the atrioventricular node (AV) via intermodal pathways. Conduction slows through the AV node, allowing sufficient time for complete atrial depolarization and contraction. From the AV node, the depolarization rushes through the ventricular conducting system to the apex of the heart, resulting in ventricular depolarization. The QRS complex represents the progressive wave of ventricular depolarization, followed by ventricular repolarization during the T wave (Silverthorn, 2019).

Figure 1 - Representation of the electrical activity on the heart and respective electrocardiogram reading. Purple and peach regions, respectively, represent depolarization and repolarization. Typically, the cardiac stimulus is generated in the sinoatrial or sinus node (SA), represented by the P wave. The stimulus then spreads through the right atrium (RA) and left atrium (LA). Next, it spreads through the atrioventricular node (AV), passing into the left ventricle (LV) and right ventricle (RV), represented by the QRS complex. The T wave represents ventricular repolarization, which reinitiates the cardiac cycle.

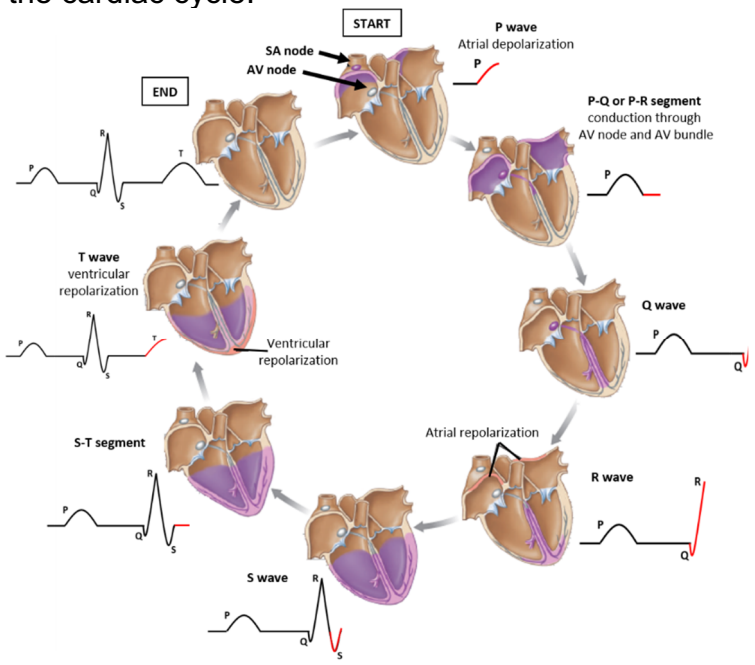

Source: Adapted from (Silverthorn, 2019).

2.1.2 Heart Rate Variability

Heart rate variability (HRV) is a reliable reflection of many physiological factors modulating the normal heart's rhythm, allowing us to assess the overall cardiac health and the state of the heart's autonomic neural regulation. HRV analysis is based on the RR interval time series, the sequence of intervals between successive points of R peaks of QRS complexes in the ECG (see Figure 2) (Kamath; Watanabe; Upton, 2016). HRV analysis is considered a non-invasive methodology of substantial utility to evaluate autonomic control mechanisms and identify patients with increased cardiac mortality (Orini *et al.*, 2017).

HRV indicates the heart's ability to respond to multiple physiological and environmental events (*e.g.*, breathing, physical exercise, mental stress, hemodynamic and metabolic changes, sleep, and orthostatism) and compensate for disease-induced disorders (Kim *et al.*, 2018). Thus, an optimal level of HRV is associated with healthy self-regulatory capacity, and adaptability or resilience (Shaffer; Ginsberg, 2017), modulated by separate rhythmic contributions from the sympathetic and parasympathetic autonomic activity at distinct frequencies.

Figure 2 - Components of the electrocardiogram with waves, segments, and intervals. A typical electrocardiogram has five waves or deflections called P, Q, R, S, and T waves; PR and ST segments between the waves and PR, QT, and RR intervals, which consist of a combination of waves and segments. RR interval is the time between successive QRS complexes.

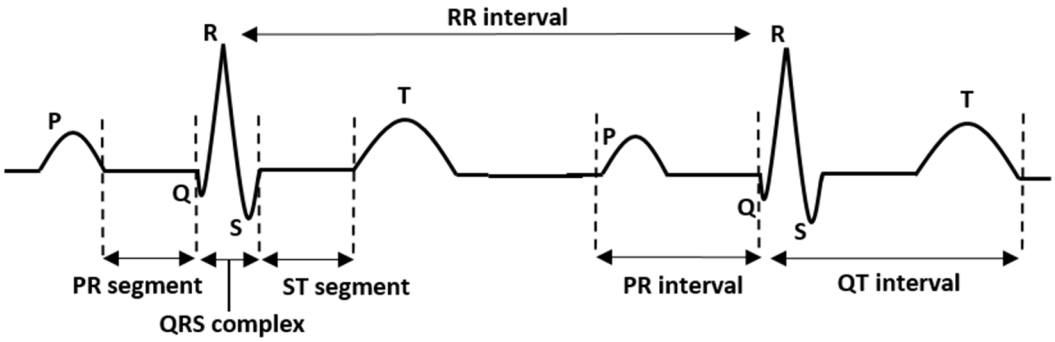

Source: Elaborated by the author.

2.2 AUTONOMIC NERVOUS SYSTEM

The autonomic nervous system (ANS) is structurally and functionally positioned to coordinate bodily functions ensuring homeostasis (*e.g.*, cardiovascular and

respiratory control, thermal regulation, gastrointestinal motility, urinary and bowel excretory functions, reproduction and metabolic and endocrine physiology) and adaptive responses to stress (*i.e.*, flight or fight response) (Biaggioni *et al.*, 2022). Traditionally, the organization of physiological control of the ANS is divided into two main branches: the sympathetic nervous system (SNP) and the parasympathetic nervous system (PNS). Stimulation of the SNP mediates physiological responses of fight and flight, manifested as increased heart rate (HR) and blood pressure (BP), mobilization of needed energy stores, and heightened arousal. In contrast, stimulation of PNS tends to produce effects that are opposite to those of the SNS, such as slowing of HR and cardiac contractility and enhanced digestive functions. Although these systems appear to have opposing effects, for any given situation, the system must be considered in its entity because it is necessary to coordinate the firing and response of both arms of the ANS (Vinik; Erbas; Casellini, 2013). The effects on different end organs due to stimulation of either the PNS or SNP are shown in Table 1.

The autonomic nervous system (ANS) is a key regulator of metabolic processes, controlling glucose metabolism and regulating the physiological function of essential organs involved in this metabolism (Hoshi *et al.*, 2019). This process occurs directly through neuronal input and indirectly via circulation, influencing insulin and glucagon release and hepatic glucose production. Sympathetic nerve activation increases glucagon secretion from the pancreatic alpha cells, while vagal stimuli increase insulin secretion. In the liver, sympathetic activation increases blood glucose levels, while parasympathetic stimulation decreases blood glucose. The ANS may also impact insulin regulation indirectly by modulating the immune and inflammatory reaction driven toward beta cells (Hoshi *et al.*, 2019; Vinik; Erbas; Casellini, 2013). Also, the ANS plays a primary role in maintaining homeostasis by regulating arterial pressure and all significant cardiovascular variables.

Table 1 - Autonomic Nervous System Functions.

Organ	Sympathetic Nervous System	Parasympathetic Nervous System
Eye		
Pupils	Dilatation	Constriction
Ciliary muscle	Relax (far vision)	Constrict (near vision)
Lacrimal gland	Slight secretion	Secretion
Parotid gland	Slight secretion	Secretion
Submandibular gland	Slight secretion	Secretion
Heart	Increased rate Positive inotropism	Slowed rate Negative inotropism
Lungs	Bronchodilation	Bronchoconstriction
Gastrointestinal tract	Decreased motility	Increased motility
Kidney	Decreased output	None
Bladder	Relax detrusor muscle Contract sphincter	Contract detrusor muscle Relax sphincter
Sweat glands	Secretion	Palmar sweating
Piloerection muscles	Contraction	None

Source: Adapted from (Biaggioni *et al.*, 2022).

2.2.1 Neural Control of the Cardiovascular System

The ANS continuously regulates the cardiovascular system through the sympathetic and parasympathetic divisions. This is carried out by a network of neurons located in the medulla oblongata that receive inputs from other central structures (*e.g.*, the hypothalamus, cerebral cortex, and medullary chemoreceptors) and peripheral reflexes arising from baroreceptor, chemoreceptor, mechanoreceptor, thermoreceptor, and nociceptor afferents (located in the blood vessels, heart, lungs, skeletal muscles, skin and viscera) (Biaggioni *et al.*, 2022; Orini *et al.*, 2017).

In a healthy human heart, there is a dynamic relationship between the PNS and SNS. The PNS tone predominates over the sympathetic tone at rest. PNS stimulation causes a decrease in heart rate and strength of contraction, almost no effect on blood vessels, and provokes a decrease in arterial pressure but does not affect peripheral vascular resistance. On the other hand, the SNP has a predominant role in cardiovascular regulation due to its effect in increasing cardiac rate and contractility,

causing constriction of arteries and veins and, consequently, increasing blood pressure (Biaggioni *et al.*, 2022; Cardinali, 2017; Orini *et al.*, 2017). A summary of the effects of PNS and SNP on the cardiovascular system is presented in Table 2.

Heart rate is initiated by autorhythmic cells in the SA node, but it is modulated by neural and hormonal input. The ANS connection with the pacemaker cells influences the permeability of the channel to K^+, $Na^{+,}$ and Ca^{2+}, causing depolarisation velocity effects. The parasympathetic neurotransmitter acetylcholine (ACh) delays the onset of the action potential in the pacemaker through an increase of K^+ permeability and a decrease of Ca^{2+} permeability, which slows the heart rate. On the other hand, sympathetic activation increases the permeability of the channel to Na^+ and Ca^{2+} influx, which speeds up the pacemaker depolarization rate and consequently increases heart rate (Silverthorn, 2019).

Table 2 - Effect of the autonomic nervous system on the cardiovascular system.

Organ	**Sympathetic stimulation**	**Parasympathetic stimulation**
Heart	Increased rate	Slowed rate
Heart	Increased force of contraction	Decreased force of contraction
Coronaries	Constricted (α), Dilated (β_2)	Dilated
Vessel	Constricted	No effect
Arterioles (resistance vessels)	Constricted	No effect
Adrenal medullae	Release of epinephrine	No effect
Arterial pressure	Short-term increase	Short-term decrease

Source: Adapted from Orini *et al.* (2017).

2.2.2 Baroreflex

The central nervous system's primary function is to ensure adequate blood flow to the brain and heart by maintaining sufficient mean arterial pressure. The baroreceptor reflex is the primary pathway for homeostatic mean arterial blood pressure control. The baroreflex is a negative feedback system that buffers short-term fluctuations in arterial pressure by modifying the heart rate and peripheral resistance according to the input from pressure-sensing baroreceptors. The changes in blood pressure occur by the indirect stretch sense of blood vessels via baroreceptors, which

are sensory afferent nerve endings located in walls of the carotid arteries and the aorta, where they continuously monitor the pressure of blood flowing to the brain (carotid baroreceptors) and the body (aortic baroreceptors) (Kamath; Watanabe; Upton, 2016; Orini *et al.*, 2017; Silverthorn, 2019).

The blood pressure regulatory system can be considered to be a feedback system consisting of sensors (the baroreceptor that measures blood pressure at select locations in the body), a processing unit (residing in the central nervous system), and an output unit (the autonomic nervous system, which adjusts blood pressure by changing HR, cardiac contractility and resistance of peripheral blood vessels) (Kamath; Watanabe; Upton, 2016).

The last section (Section 2.2.1) describes that the ANS regulates the cardiovascular system through the sympathetic and parasympathetic divisions (see Table 2). So, an increase in arterial blood pressure increases the baroreceptor activity, which leads to a decrease in sympathetic neural outflow, decreasing vasoconstrictor tone, myocardial contractility (to decrease stroke volume), and slowing down the heart rate. These sympathetic influences work with parasympathetic influences on the sinoatrial node to decrease heart rate. Conversely, the opposite occurs during a decrease in blood pressure (Biaggioni *et al.*, 2022; Silverthorn, 2019). An illustration of this mechanism is presented in Figure 3.

Figure 3 – The baroreceptor reflex mechanism.

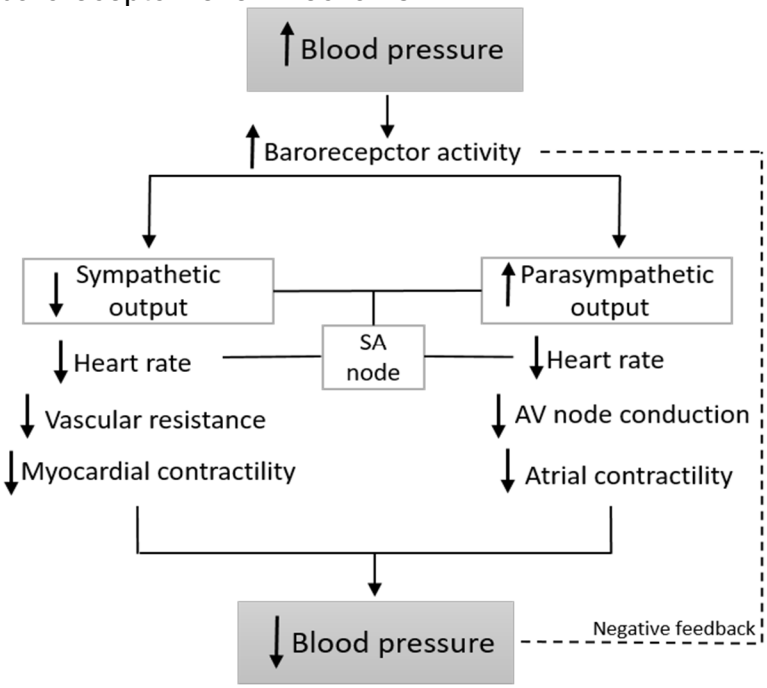

Source: Adapted from Biaggioni *et al*. (2022) and Silverthorn (2019).

2.3 DIABETES MELLITUS

Diabetes mellitus (DM) represents a series of metabolic conditions associated with hyperglycaemia caused by partial or total insulin insufficiency from a medical perspective. From the patient's perspective, diabetes is a life-long condition requiring daily attention to diet, lifestyle, and self-monitoring of blood glucose, with frequent medication administration. Besides that, it is frequently associated with varying degrees of anxiety, depression, and multiple visits to healthcare providers (Egan; Dinneen, 2019).

DM can be classified into the following major categories: (a) Type 1 (T1DM): pancreatic beta-cells are destroyed, usually by autoimmune inflammatory mechanism, which typically leads to absolute insulin deficiency, with a variable rate of progression; (b) Type 2 (T2DM): complex metabolic disorder associated with beta-cell dysfunction and varying degrees of insulin resistance; (c) Gestational: carbohydrate intolerance with onset or first recognition during pregnancy, is associated with an increase in adverse outcomes and increased risk of type 2 diabetes in later life and; (d) Less common types: inherited diabetes associated with a mutation in certain beta-cell or hepatic genes, diabetes associated with a pancreatic disease or endocrinopathies, drug or chemical-induced diabetes and others (Egan; Dinneen, 2019).

People with diabetes have an augmented risk of developing several life-threatening health problems, increasing medical care costs, falls, causing pain, and consequently lowering the quality of life. Diabetic neuropathies (DN) are the most prevalent chronic complications of DM, being characterized by a set of clinical syndromes that affect distinct regions of the nervous and peripheral systems, individually or combined (Pop-Busui *et al.*, 2017; Vinik; Casellini; Névoret, 2016). The prevalence of neuropathy in T2DM ranges from 8 to 51% and 11 to 50% in T1DM individuals, increasing with disease duration (Feldman *et al.*, 2019).

The duration of diabetes and HbA1c (a measurement of glycated haemoglobin as a surrogate for average daily glucose levels) are significant predictors of DN. They are commonly associated with other metabolic factors such as obesity (the most influential), insulin resistance, and hypertension (particularly in T2DM) (Callaghan *et al.*, 2020). Other independent risk factors for DN development include smoking, alcohol abuse, increased height, and older age (Feldman *et al.*, 2019). Among the various forms of DN, diabetic peripheral neuropathy (DPN) and diabetic autonomic

neuropathies, particularly cardiovascular autonomic neuropathy (CAN), are by far the most prevalent (Feldman *et al.*, 2019; Pop-Busui *et al.*, 2017).

Diabetic Peripheral Neuropathy is one of the major complications in patients with Type 1 and Type 2 DM (Tesfaye; Selvarajah, 2012). A simple definition of DPN for clinical practice is “the presence of symptoms and/or signs of peripheral nerve dysfunction in people with diabetes after excluding other causes” (Boulton; Gries; Jervell, 1998). Also, it is defined as a “symmetrical, length-dependent sensorimotor polyneuropathy attributable to metabolic and micro-vessel alterations as a result of chronic hyperglycaemia exposure and cardiovascular risk covariates” (Tesfaye *et al.*, 2010). The prevalence of diabetes-related peripheral neuropathy ranges from 16% to as much as 87 %, with painful diabetes-related neuropathy reported in about 26% of adults with diabetes (International Diabetes Federation, 2021).

Peripheral nerve fibres are classified into large myelinated fibres, small thinly myelinated fibres, and unmyelinated fibres. DPN involves both small and large nerve fibres in a length-dependent pattern. Small nerve fibre injuries occur earlier than large ones (Won; Park, 2016). Thus, sensory symptoms are more prominent than motor symptoms and usually involve the lower limbs with a stocking-like distribution. The main symptoms are pain, paraesthesia, hyperesthesia, deep aching, burning, and sharp stabbing sensations. All sensory modalities can be affected, particularly vibration, touch, and position perception that are indicative of considerable Aα/β fibre damage and pain, with abnormal heat and cold temperature perception that is a characteristic of small thinly myelinated Aδ and unmyelinated C-fibre damage (Feldman *et al.*, 2019; Vinik; Casellini; Névoret, 2016), as represented in Figure 4.

As stated, the sensory nerve fibres are the most affected in the early course of DPN; however, as the disease progresses, muscle weakness becomes present, affecting distal leg muscles. These muscle alterations affect the foot (or gait) dynamics and plantar pressure distribution, leading to foot deformities and, ultimately, foot ulceration (Amin; Doupis, 2016; Suda *et al.*, 2018). Furthermore, DPN is the leading cause of disability due to foot ulceration, amputation, gait disturbance, and fall-related injury (Juster-Switlyk; Smith, 2016). In summary, foot ulceration is considered the primary precursor of lower extremity amputation among patients with diabetes (Amin; Doupis, 2016).

Figure 4 – Peripheral nervous system and type of nerve fibres. Clinical presentation of small and large fibre neuropathies.

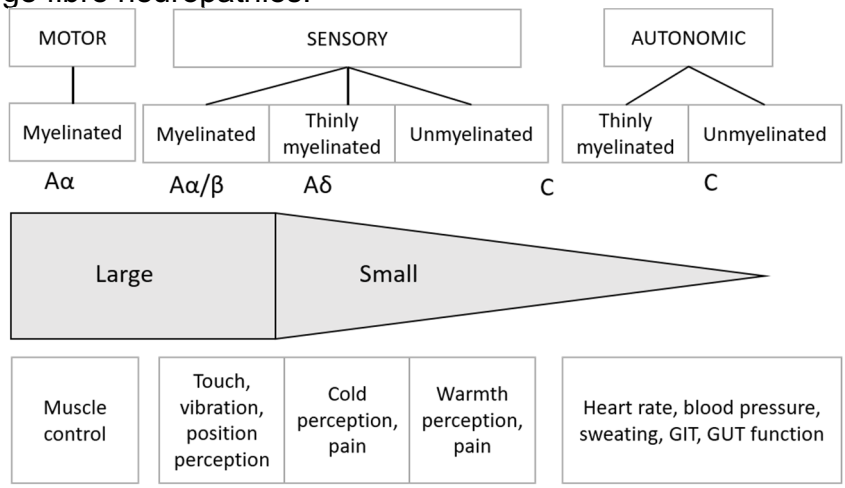

Abbreviations: GIT, gastrointestinal; GUT, genitourinary.

Source: Adapted from Vinik; Casellini and Névoret (2016).

Diabetic autonomic neuropathies (DAN) are disorders caused by impairment of the sympathetic and parasympathetic nervous system, associated with various specific symptoms (Feldman *et al.*, 2019). DAN may be either clinically evident or subclinical. DAN typically occurs as a system-wide disorder affecting all parts of the ANS; the vagus nerve, which is the longest of the ANS nerves, accounts for ~75 % of all parasympathetic activity, and DAN manifests first in longer nerves, so even early effects of DAN are widespread (Vinik; Erbas; Casellini, 2013). Major clinical manifestations of DAN include hypoglycaemia unawareness, resting tachycardia, exercise intolerance, orthostatic hypotension, constipation, gastroparesis, erectile dysfunction, sudomotor dysfunction, impaired neurovascular function, and brittle diabetes (*i.e.*, hard-to-control-diabetes) (Pop-Busui *et al.*, 2017).

Among the autonomic neuropathies, Cardiac Autonomic Neuropathy (CAN) is the most serious and clinically relevant of the complications, as CAN is an independent risk factor for cardiovascular mortality, arrhythmia, silent ischemia, myocardial dysfunction, or any major cardiovascular event (Pop-Busui *et al.*, 2017). CAN is the focus of this work; thus, it is further addressed in the next section.

2.4 CARDIAC AUTONOMIC NEUROPATHY

The metabolic disorders of diabetes lead to diffuse and widespread damage of peripheral and autonomic nerves and small vessels. When diabetic neuropathy affects the autonomic nervous system (ANS), it can damage the cardiovascular, gastrointestinal, genitourinary, and neurovascular systems. Of these, damage to the autonomic nerve fibres that innervate the heart and blood vessels is known as cardiac autonomic neuropathy (CAN), resulting in abnormalities in heart rate control and vascular dynamics (Vinik; Erbas; Casellini, 2013).

CAN in DM is among the strongest risk markers for future global and cardiovascular mortality, and the increase of other micro- and macrovascular complications increases the probability of having CAN in both types of DM, being more pronounced in T2DM (Motataianu *et al.*, 2018). The prevalence of CAN in unselected people with type 1 and type 2 diabetes is approximately 20%, but it can be as high as 65% with increasing age and diabetes duration (Vinik; Erbas; Casellini, 2013). Clinical correlates or risk markers for CAN are age, diabetes duration, glycaemic control, microvascular complications (peripheral polyneuropathy, retinopathy, and nephropathy), hypertension, obesity, smoking, and dyslipidaemia (Cha *et al.*, 2018). The study by Andersen *et al*. (2018) reported that higher HbA1c, weight, body mass index (BMI), and triglycerides were associated with prevalent CAN.

In parallel to the development of peripheral neuropathy, DM affects cardiac autonomic neurons in an ascending fashion, with pathological changes affecting first the longest nerve fibres, which in the ANS is the vagus nerve that modulates approximately 75% of all parasympathetic activity (Kuehl; Stevens, 2012). Thus, in an early phase of CAN, there is a loss of parasympathetic function due to denervation, with a resulting compensatory increase of sympathetic tone. Later, sympathetic denervation follows, causing an increase in cardiac sympathetic tone, which seems to correlate with the progression of peripheral neuropathy (Kuehl; Stevens, 2012; Vinik; Erbas; Casellini, 2013). The imbalance of sympathetic/parasympathetic observed in CAN patients is a significant cause of morbidity and mortality associated with a high risk of cardiac arrhythmias and sudden death, possibly related to silent myocardial ischemia; cardiovascular disease (CVD) remains the main cause of excess mortality among patients with type 1 and type 2 DM (Vinik, 2012).

2.4.1 CAN Diagnosis

The Toronto Consensus established four reasons why the diagnosis of CAN is relevant to clinical practice: (a) for diagnosing and staging CAN (initial, definite, and advanced or severe), (b) for the differential diagnosis of clinical manifestations (*e.g.*, resting tachycardia, orthostatic hypotension) and their respective treatment, (c) for stratifying the degree of cardiovascular risks and the risk of other diabetic complications, and (d) to adjust the goal of glycated haemoglobin (HbA1c) in each patient (Bernardi *et al.*, 2011).

Screening for autonomic dysfunction should be performed at the diagnosis of type 2 diabetes and five years after the diagnosis of type 1 diabetes, particularly in patients at higher risk due to a history of poor glycaemic control, cardiovascular risk factors, diabetic peripheral neuropathy, and macro or microangiopathic diabetic complications (Vinik, 2012). The body's functional response to the immediate metabolic needs is regulated by the beat-to-beat variation, where a high variability reflects the cardiac ability to adapt and implies good health. At the same time, disturbances to this control system result in lower HRV values (Balcıoğlu, 2015).

Early or subclinical autonomic dysfunction may exhibit no symptoms, and it can only be detected by lower indices of HRV and abnormal BRS (which can be present at the time of DM diagnosis). Initial parasympathetic denervation enables augmentation of sympathetic tone in the early stages of CAN. Over time, sympathetic denervation follows and correlates clinically with advanced CAN patients who present resting tachycardia (>100 bpm) and/or a fixed HR, as well as orthostatic hypotension (OH), intolerance to exercise and syncope (Kuehl; Stevens, 2012; Vinik *et al.*, 2018). The most common symptoms of CAN occur upon standing and include light-headedness, weakness, palpitations, faintness, and syncope; however, these symptoms may occur relatively late in the disease course (Pop-Busui *et al.*, 2017). The CAN staging is summed up in Figure 5.

High resting HR is the least specific sign of CAN and can also reflect vagal impairment and/or sympathetic overactivity in cardiac diseases, poor fitness, obesity, or anaemia; it has a prognostic value in the general and diabetic population (Spallone, 2019). In the ADVANCE study of 11140 T2DM patients, a higher HR was associated with an increased risk of all-cause mortality and cardiovascular death; however, it is unclear whether a high HR is directly conditioned to a higher risk or is a marker for

other factors (Hillis *et al.*, 2012). The study of Zafrir *et al*. (2016) also demonstrated that resting tachycardia and reduced heart rate recovery are independently and additively associated with long-term mortality, myocardial infarction, or stroke in T2DM without known coronary heart disease.

Figure 5 – The stages of cardiovascular autonomic neuropathy.

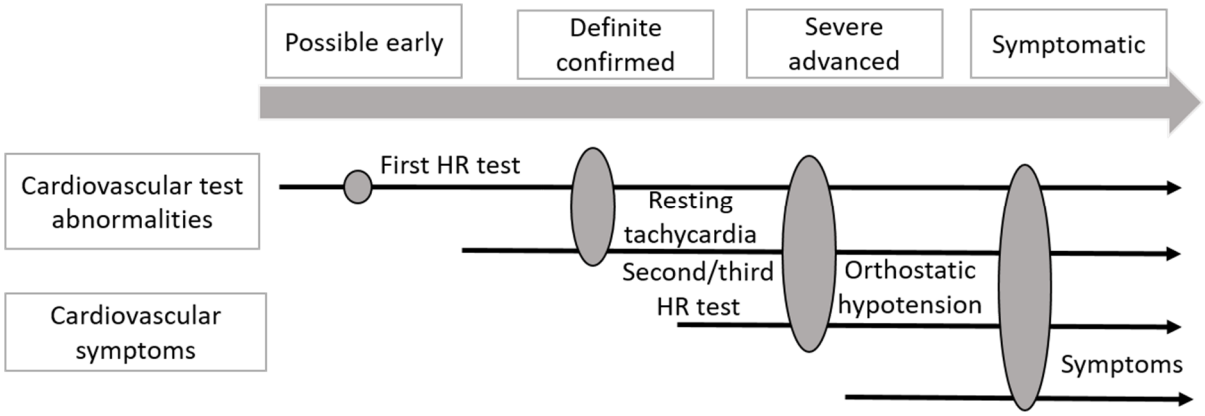

Source: Adapted from Vinik; Erbas and Casellini (2013).

The Toronto Consensus Panel (Bernardi *et al.*, 2011), the European Society of Cardiology, the North American Society of Pacing and Electrophysiology (Dillingham *et al.*, 2016), and the American Diabetes Association Position Statement on Diabetic Neuropathy (Pop-Busui *et al.*, 2017) recommend the following regarding CAN assessments for clinical trials measuring a targeted intervention or for prognostication (Vinik *et al.*, 2018):

a) standardized cardiovascular reflex tests (CARTs);
b) heart rate variability analysis (see section 3.1);
c) resting tachycardia (> 100 bpm) and/or a fixed heart rate;
d) measurement of QT corrected interval on ECG recording;
e) baroreflex sensitivity (see Section 3.3).

Functional diagnostics of the cardiovascular autonomic system are intended to help assess individual autonomic reflex arcs' functional integrity. The more common way to assess cardiovascular autonomic function is through an indirect evaluation by measuring the end-organ response (*e.g.*, heart rate, blood pressure, respiration, or blood flow) after provocative physiological tests, which is the cardiovascular reflex tests (CARTs) proposal (Ziemssen; Siepmann, 2019).

CARTs were first proposed in the study of Ewing *et al*. (1985), as detailed in Table 3. CARTs evaluate short-term RR alterations, and the five tests are the gold standard for decades in clinical practice to identify CAN in patients with diabetes. Most recent evidence has reduced the diagnostic utility of the handgrip test (Körei *et al.*, 2017). These tests have good sensitivity, specificity, and reproducibility and are non-invasive, safe, well-standardized, and easily performed (Vinik, 2012).

Table 3 - Summary of the Ewing tests.

Test	Interpretation	Normal Response
HR response during paced deep breathing	E:I ratio (longest RR during expiration divided by shortest RR during inspiration)	HR > 15 beats/min difference is normal, and HR < 10 beats/min is abnormal. E:I ratio > 1.17*
HR response to standing	30:15 ratio (RR around the 30th heartbeat divided by RR around the 15th heartbeat)	Typically, tachycardia is followed by reflex bradycardia. 30:15 ratio > 1.03
Valsalva manoeuvre: the subject exhales into the mouthpiece of a manometer to 40 mmHg for 15 s	Evaluates the ratio of the longest RR divided by the shortest RR during and after a provoked increase in intrathoracic pressure.	The ratio of longest to shortest RR interval > 1.2
BP response to standing	Evaluate the difference in both SBP and DBP, measured in a supine position, and after 2 min, the patient is standing.	The usual response is a drop of <10 mmHg in SBP Abnormal is a drop of <20 mmHg in SBP or a drop of <10 mmHg in DBP
BP response to isometric exercise	A squeeze of the handgrip dynamometer for 5 min at 30 % maximum	The usual response is a rise of >16 mmHg in the diastolic BP in the other arm

Abbreviations: RR, RR interval; HR, heart rate; E:I, expiration: inspiration; BP, blood pressure; SBP, systolic blood pressure; DBP, diastolic blood pressure; bpm, beats per minute. *Ratio values are adjusted by age. Source: Adapted from Vinik *et al.* (2018).

CARTs also allow for CAN staging, according to the number of test abnormalities: the presence of one abnormal or two borderline CART results identifies possible or early CAN to be confirmed over time; at least two abnormal cardiovagal

results are required for a definite or a confirmed diagnosis of CAN; and the presence of orthostatic hypotension identifies severe or advanced CAN (Ewing *et al.*, 1985; Spallone, 2019; Vinik *et al.*, 2018).

HRV indices are the easiest and most reliable way to assess cardiac autonomic neuropathy, obtained by time- and frequency-domain methods, which measure, respectively, the overall magnitude of the fluctuations of the RR interval between each heartbeat around the average values (statistical analysis) and the magnitude of fluctuations in a predetermined range of frequency (spectral analysis) (Rolim; de Souza; Dib, 2013). HRV time- and frequency-domain indices should be considered as additional and not an alternative to CARTs in clinical practice, thus allowing for supplemental early and prognostic information to current CARTs (Spallone, 2019).

Due to the long experience and validation of traditional time and frequency-domain HRV analysis, these remain the methods for assessing ANS physiology and pathophysiological modelling, making them the most reliable tools. However, measures from information and invariant domains that may describe the nonlinear properties of HRV signal accurately are strongly recommended to be used in conjunction with the traditional ones since they may provide supplementary or different information about underlying mechanisms involved in cardiovascular regulation (Sassi *et al.*, 2015).

The evaluation of HRV in DM patients has been assessed in several studies using time- and frequency-domain methods, as well as nonlinear approaches. For further details on the HRV analysis technique, see section 3.1.

As previously discussed, low HRV is a marker for autonomic dysfunction, a known feature of both types of DM. In the study of Coopmans *et al*. (2020), both prediabetes and T2DM patients were independently associated with lower HRV (both in the time and frequency domain), strongly suggesting that cardiac autonomic dysfunction is already present in prediabetes and HRV indices could be useful to identify subclinical CAN. In the same context, the study of Jaiswal *et al*. (2013) compared HRV parameters in T1DM and healthy individuals, exploring potential contributors of altered HRV and concluding that T1DM presented a reduced overall HRV and parasympathetic loss with sympathetic override, being connected to hyperglycaemia. The study of Silva *et al*. (2017) reinforced that T1DM individuals showed decreased sympathetic and parasympathetic activities through HRV indices discriminating from healthy individuals.

According to a recent systematic review that included T2DM patients and healthy controls during 24-hour electrocardiogram, T2DM patients presented an overall decrease in HRV; both sympathetic and parasympathetic activity was decreased, which can be explained by the effects of altered blood glucose levels on HRV. In this review, T2DM patients presented significantly lower values for the following parameters: RR-intervals, RMSSD, pNN50, total power, low-frequency (LF), and high-frequency (HF) (Benichou *et al.*, 2018).

The study of Tarvainen *et al*. (2014) considered the risk factors associated with CAN and reported that high glycaemic values have an unfavourable effect on cardiac autonomic function, and this effect is pronounced in long-term T2DM patients. In this same study, HR was increased, and HRV decreased in hyperglycaemia; besides, mean RR, SDNN, RMSSD, pNN50, HRVI, TINN, LF, HF, and total power decreased in T2DM patients. In the same context, a Brazilian longitudinal study concluded that decreased HRV is an independent risk predictor for the incidence of diabetes within four years; from the six HRV indices analysed, five (SDNN, pNN50, RMSSD, LF, and HF) showed an increased relative risk of developing diabetes with low HRV (Hoshi *et al.*, 2019).

Besides time- and frequency-domain indices, non-linear measurements can detect changes related to a disease occurrence in the time series. Physiological complexity is associated with the ability of living systems to adjust to an ever-changing environment, which requires integrative multiscale functionality. In contrast, under free-running conditions, a sustained decrease in complexity reflects a reduced ability of the system to function in specific dynamical regimes, possibly due to decoupling or degradation of control mechanisms (Costa; Goldberger; Peng, 2005). Some studies have demonstrated the association between diabetes and abnormal non-linear HRV parameters (Roy; Ghatak, 2013; Silva-E-Oliveira *et al.*, 2017).

The study of Hsu *et al*. (2012) stated that the features of heart rate dynamics could be better identified by dynamic analysis of Poincaré plot than by traditional HRV analysis techniques, providing a qualitatively and quantitatively visual measure of the ANS activity, which then, provides prognostic information on patients with heart failure and patients vulnerable to life-threatening arrhythmias.

In the same context, the study of Khandoker; Jelinek; Palaniswami (2009) presented the usefulness of HRV and complexity analysis from short-term ECG recordings as a screening tool for CAN. The results demonstrated that CAN subjects

had reduced Poincare plot patterns and significantly lower sample entropy (SampEn) values, demonstrating the potential utility of these HRV markers in CAN diagnosis and prognosis.

A systematic review that analysed studies of HRV as a tool for diagnostic evaluation in individuals with DM also demonstrated the reduction of HRV and loss of complexity in individuals with DM, suggesting that some parameters such as Sample Entropy, SD1/SD2 (ratio of the Poincaré plot standard deviation perpendicular to the line of identity by the Poincaré plot standard deviation along the line of identity), SDANN (standard deviation of the mean of normal RR-intervals), high frequency, Recurrence Plot, Approximate Entropy (ApEn), Detrended fluctuation analysis (DFA), Correlation Dimension (CD), Lyapunov exponent and heart rate turbulence of tilt have better discriminatory power to detect autonomic dysfunction (Da Silva *et al.*, 2016). Similarly, Rajendra Acharya *et al*. (2013) study determined whether or not DM is present by determining cardiac health using non-linear HRV analysis (*e.g.*, ApEn and DFA), achieving high accuracy.

Related to the usage of entropies for HRV analysis, sample entropy has been associated with changes to blood glucose level and glycated haemoglobin (HbA1c), indicating that hyperglycaemia induces changes in RR time series complexity, which is not detectable by standard linear methods (Tarvainen *et al.*, 2014). In another study, HRV complexity increased with hyperglycaemia, as indicated by increases in Shannon and multiscale entropy (Tarvainen *et al.*, 2013). Also, a study to diagnose the ECG signals and detect arrhythmia demonstrated that spectral entropy could provide good separation among different ECG beats (Asgharzadeh-Bonab; Amirani; Mehri, 2020).

Applying the MSE method to the analysis of RR intervals of healthy subjects, subjects with heart failure (HF), and subjects with atrial fibrillation (AF) shows that the healthy dynamics are the most complex. Under pathological conditions, the time series structure may change in two ways: loss of variability and the emergence of more regular patterns in patients with HF and random types of output in patients with AF. MSE reveals decreased system complexity (Costa; Goldberger; Peng, 2005).

Likewise, the study of (Xiao *et al.*, 2018) assessed MSE in a group of upper-middle-aged non-diabetic subjects and diabetic subjects; the results demonstrated consistent and significant reductions of large-scale MSE, highlighting its ability to identify diabetes-associated vascular changes, which is consistent with the fact that diabetes impairs vascular structural integrity. In the same study, the large-scale MSE

also had a significant negative association with fasting blood sugar and HbA1c levels, further highlighting the adverse impact of diabetes on vascular endothelial function in both acute and chronic hyperglycaemia, respectively.

Still exploring the entropies as HRV analysis methods, the study of (Liu *et al.*, 2013) proposed the use of ApEn, SampEn, fuzzy entropy (FuzzyEn), and a new entropy measure based on FuzzyEn, named fuzzy measure entropy, for HRV analysis on healthy subjects and subjects with heart failure. The results demonstrated that the fuzzy-based entropies better classified the two groups. Similarly, the study of (Carricarte Naranjo *et al.*, 2017) proposed to explore the potential of permutation entropy (PermEn) in the analysis of HRV complexity for the assessment of CAN in type 1 diabetic subjects. They found that for some specific temporal scales, PermEn indicators were significantly lower in CAN patients than those calculated for controls, concluding that PermEn analysis of HRV is a promising method for CAN assessment since PermEn seems to provide additional information to that obtained with traditional HRV methods.

2.4.2 Baroreflex Sensitivity

The baroreflex sensitivity (BRS) is a technique to assess cardiac vagal and sympathetic baroreflex function, in which a depressed BRS is a further marker for subclinical CAN (Kuehl; Stevens, 2012). BRS is a sensitive indicator of CAN in DM patients (Frattola *et al.*, 1997) and is associated with cardiovascular events (Spallone, 2019).

Some studies have shown that BRS abnormalities occur before abnormalities of conventional autonomic function tests, allowing early detection of CAN (Frattola *et al.*, 1997). Similarly, the study of Kück *et al*. (2020) investigated BRS early in the course of both type 1 and type 2 diabetes and its temporal sequence over five years; the results demonstrated that T2DM patients showed early baroreflex dysfunction, likely due to insulin resistance and hyperglycaemia, albeit without progression over five years. The study of Svačinová *et al.* (2013) found that type 1 diabetics, compared with controls, had a decreased mean BRS. Similarly, the study of Petry *et al*. (2020) demonstrated that BRS indices distinguished T1DM individuals with subclinical and established CAN, which could be an early sign of autonomic dysfunction and contribute to CAN detection in its asymptomatic stage.

Recently, short-term glycaemic variability (GV) and long-term GV, represented by HbA1c variability, an independent risk factor for cardiovascular events, were reported as risk factors for CAN (Spallone, 2019). In addition, the study of Matsutani *et al*. (2018) investigated the relationship between long-term GV and BRS in T2DM patients, concluding that visit-to-visit HbA1c variability was inversely related to BRS independently of the mean HbA1c in patients with T2DM, which might be a marker of reduced BRS.

Besides the clinical relevance of BRS to detecting early impairment of autonomic function, BRS also provides information of prognostic value. For example, BRS is an independent predictor of mortality in patients with DM (Gerritsen *et al.*, 2001) and a predictor of mortality following a recent myocardial infarction (La Rovere *et al.*, 1998). The BRS impairment in T2DM patients may be reversible or improved after weight loss, combined exercise training (aerobic and resistance), and during slow breathing manoeuvres (Spallone, 2019).

3 METHODS

This section describes the main methods that were used for the development of this work. The section is divided into the following sub-sections: (3.1) HRV Analysis and Indices; (3.2) Empirical Mode Decomposition Method and Extracted Parameters; (3.3) Baroreflex Sensitivity Analysis Calculation and; (3.4) Machine Learning Methods.

3.1 HEART RATE VARIABILITY ANALYSIS

This section describes the analysis methods for HRV that can be divided into *time-domain*, *frequency-domain,* and *non-linear* methods. The derivation of the HRV signal is explained in section 2.1.2.

3.1.1 Time-Domain Parameters

The time-domain indices of HRV quantify the variability in measurements of the normal-to-normal (NN) intervals (*i.e.,* the time between successive heartbeats resulting from sinus node depolarization). Time-domain indices can be divided into two subgroups: statistical indices and geometric indices obtained from the probability density function of NN intervals. A summary of the indices with a short description is presented in Table 4.

Time-domain measures do not provide a means to adequately quantify autonomic dynamics or determine the rhythmic or oscillatory activity generated by the different physiological control systems; however, since they are always calculated the same way, data of different studies are comparable considering the same recording length (Shaffer; McCraty; Zerr, 2014)

Table 4 - Summary of heart rate variability in time-domain measures.

Parameter	Unit	Description
SDNN	ms	The standard deviation of NN intervals
NN mean	ms	Mean of NN intervals
RMSSD	ms	Root mean square of successive NN interval differences
SDSD	ms	The standard deviation of differences between adjacent NN intervals
NN50	count	Number of successive NN intervals that differ by more than 50 ms
pNN50	%	NN50 count divided by the total number of NN intervals
NN20	count	Number of successive NN intervals that differ by more than 20 ms
pNN20	%	NN20 count divided by the total number of NN intervals
HR change	bpm	Difference between the maximum and minimum heartbeat
HTI	-	HRV triangular index: integral of the density of the RR interval histogram divided by its height
TINN	ms	Triangular interpolation; baseline width of the NN interval histogram
SI	-	Baevsky's stress index

Source: Elaborated by the author.

3.1.2 Frequency-Domain Parameters

The main idea behind the frequency domain analysis of HRV is the observation that HRV is composed of certain well-defined rhythms, which are related to different regulatory mechanisms of cardiovascular control, so to obtain more detailed information on the dynamics and frequency components of HRV, the power spectral density can be applied. PSD analysis provides the basic information of how power (*i.e.*, signal energy) distributes as a function of frequency, which allows the autonomic balance to be quantified at any given time and also to distinguish between the activity of the sympathetic and parasympathetic nervous system (Kamath; Watanabe; Upton, 2016).

For short-term recordings, three main spectral components are distinguished: very-low-frequency (VLF), low-frequency (LF), and high-frequency (HF) rhythms that operate within different frequency ranges. Frequency-domain measurements can be expressed in *absolute power*, calculated as milliseconds squared divided by cycles per

second (ms²/Hz), or as *relative power,* estimated in a percentage of total HRV power or in normalised units (n.u.), which divides the absolute power for a specific frequency band by the summed absolute power of the LF and HF bands (Shaffer; Ginsberg, 2017). The frequency-domain parameters are summarized in Table 5.

The *VLF band* (0.003 – 0.04 Hz) comprises rhythms between 25 and 300 s, related to the fluctuation in vasomotor tonus associated with thermoregulation and sweating (sympathetic control). There is uncertainty regarding the physiological mechanisms responsible for activity within this band; however, experimental evidence suggests that the heart's intrinsic nervous system contributes to the VLF rhythm and the SNS influences the amplitude and frequency of its oscillations. Although all low values on HRV measurements predict a higher risk of adverse outcomes, VLF power is more strongly associated with all-cause mortality than HF or LF power. Low VLF power is associated with arrhythmic death and posttraumatic stress disorder, high inflammation, and has been correlated with low testosterone levels (McCraty; Shaffer, 2015; Shaffer; Ginsberg, 2017).

The *LF band* (0.04 – 0.15 Hz) reflects mainly baroreceptor activity during resting conditions. Studies suggest that both the PNS and SNP may produce LF power, with recent evidence demonstrating how the LF band can be affected by parasympathetic dynamics. The centre frequency of the LF band is 0.1 Hz, produced by the SNS, while the PNS can be observed to affect heart rhythms down to 0.05 Hz (Shaffer; Ginsberg, 2017; Valenza *et al.*, 2018).

Lastly, the *HF band* (0.15 – 0.40 Hz) reflects parasympathetic control or vagal activity, called the *respiratory band,* because it corresponds to HR variations related to the respiratory cycle, known as respiratory sinus arrhythmia (RSA). The modulation of vagal tone helps maintain the dynamic autonomic regulation important for cardiovascular health and reduced parasympathetic (high frequency) activity has been found in many cardiac pathologies. Regarding psychological regulation, lower HF power is associated with stress, panic, anxiety, or worry. The LF/HF ratio reflects the interaction of both types of autonomic modulation (Kamath; Watanabe; Upton, 2016; Shaffer; Ginsberg, 2017; Shaffer; McCraty; Zerr, 2014; Vinik, 2012).

Table 5 - Summary of heart rate variability in frequency-domain measures.

Parameter	Band	Unit	Description
VLF power	0.003 – 0.04 Hz	ms²	The absolute power of the very-low-frequency band
LF power	0.04 – 0.15 Hz	ms²	The absolute power of the low-frequency band
LF peak		Hz	The peak frequency of the low-frequency band
LF norm		n.u.	The relative power of the low-frequency band in normalised units. LF/(Total power-VLF) x 100
HF power	0.15 – 0.40 Hz	ms²	The absolute power of the high-frequency band
HF peak		Hz	The peak frequency of the high-frequency band
HF norm		n.u.	The relative power of the high-frequency band in normalised units. HF/(Total power-VLF) x 100
Total power		ms²/Hz	The sum of energy in the VLF, LF, and HF bands
LF/HF		%	The ratio of LF to HF power

Source: Elaborated by the author.

3.1.3 Non-linear Parameters

The non-linear analysis methods do not assess the magnitude of the variability but rather the signal quality, scaling, and correlation property, allowing a more subtle characterization of autonomic balance (Vinik *et al.*, 2018). Non-linear measurements quantify the unpredictability of a time series, which results from the complexity of the mechanisms that regulate HRV (Shaffer; Ginsberg, 2017).

Due to the difficulty of frequency band separations over sympathetic and parasympathetic activities, the non-linear measures are becoming increasingly important for investigating and interpreting the pathophysiological behaviour of HRV under various conditions and enhancing its prognostic values (Vinik *et al.*, 2018). Besides that, nonlinear indices correlate with specific frequency and time-domain measurements when generated by the same process (Shaffer; Ginsberg, 2017).

One alternative for characterizing the heart rate variability is to measure the regularity or complexity of the fluctuations without specifying the form of repeating patterns. In this context, *entropy* is a general approach for quantifying the data's regularity or information content; therefore, different entropy measures are included in the non-linear analysis (Kamath; Watanabe; Upton, 2016). As already discussed, the ANS adapts HR to the current needs, which might change continuously. Thus, the RR

series is irregular with high entropy; however, when the system becomes less responsive to environmental stimuli, the entropy decreases, and the RR signal becomes more "ordered". In this way, highly-ordered (low values of entropy) signals are more predictable than low-ordered (high values of entropy) signals (Sassi *et al.*, 2015).

The nonlinear measures explored in this work are detailed below and summarized in Table 6.

Table 6 – Summary of non-linear heart rate variability measures.

Parameter	**Unit**	**Description**
SD1	ms	Poincaré plot standard deviation perpendicular to the line of identity
SD2	ms	Poincaré plot standard deviation along the line of identity
S		The area of the ellipse adjusted to the Poincare plot
SD1/SD2	%	Ratio of SD1/SD2
CSI		Cardiac Sympathetic Index
CVI		Cardiac Vagal Index
ApEn		Approximate entropy
SampEn		Sample entropy
MSE (Area S, Area L, Slope S)		Multiscale entropy, area calculations of short and long-time scales
FuzzyEn		Fuzzy entropy
ShEn		Shannon entropy
SpEn		Spectral entropy
PermEn		Permutation entropy
DFA α_1		Detrended fluctuation analysis, which describes short-term fluctuations
DFA α_2		Detrended fluctuation analysis, which describes long-term fluctuations
CD, D2		Correlation dimension

Source: Elaborated by the author.

3.1.3.1 The Poincaré Plot

The Poincaré plot is obtained by plotting every RR interval against the prior interval, creating a scatter plot. A quantitative plot analysis can be made by adjusting it to an ellipse, as represented in Figure 6. The following non-linear measurements can be derived: ***SD1***, the standard deviation of the instantaneous (short-term) beat-to-beat RR interval variability (minor axis of the ellipse or ellipse's width)*;* ***SD2****,* the standard deviation of the long-term RR interval variability (major axis of the ellipse or ellipse's length)*;* ***S****,* which corresponds to the area covered by the ellipse calculated by doing the product of π, SD1 and SD2 and; the ratio of ***SD1/SD2*** (Hsu *et al.*, 2012; Piskorski; Guzik, 2007; Shaffer; Ginsberg, 2017; Tayel; AlSaba, 2015).

SD1 correlates with baroreflex sensitivity and HF power, reflecting parasympathetic activity, while SD2 reflects sympathetic modulation and correlates with BRS and LF power. The SD1/SD2 ratio correlates with the LF/HF ratio and measures autonomic balance. An elongated, torpedo-like shape with decreased SD1/SD2 ratio is associated with an elevated sympathetic tone, and a more oval, fan-shaped configuration resulting from increased SD1/SD2 indicates less sympathetic tone; the points get more scattered when vagal activity increases or sympathetic activity decreases (Hsu *et al.*, 2012; Piskorski; Guzik, 2007; Shaffer; Ginsberg, 2017; Tayel; AlSaba, 2015).

In addition to the cited parameters, TOICHI et al. (1997) proposed two new measures employing the Poincaré plot to assess cardiac autonomic function: a) **CSI**, the cardiac sympathetic index, and b) **CVI**, the cardiac vagal index. The CSI and CVI metrics are calculated from Equations (1) and (2), respectively.

$$\text{CSI} = \frac{SD1}{SD2} \tag{1}$$

$$\text{CVI} = \log (\text{SD1} \,.\, \text{SD2}) \tag{2}$$

Figure 6 – Illustration of a standard Poincaré plot of RR intervals.

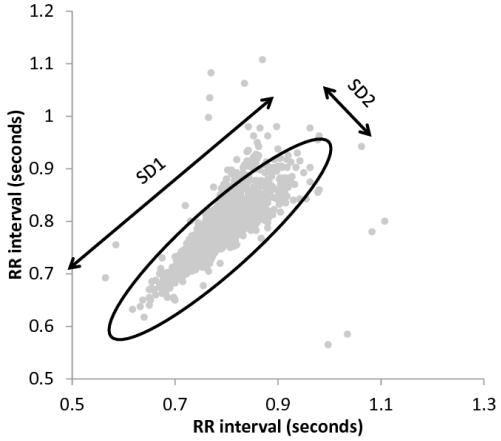

Source: Adapted from Jelinek *et al*. (2014).

3.1.3.2 Approximate Entropy (ApEn)

ApEn measures the regularity and complexity of a time series. This method examines time series for similar epochs: more frequent and more similar epochs lead to lower values of ApEn, which reflects a high degree of regularity and predictability. ApEn (m, r, N) depends on three parameters: the length m of the vector being compared, the tolerance parameter r, and the number of N data points. In practice, ApEn is biased since it is heavily dependent on the record length and is uniformly lower than expected for short records, which implies greater regularity of the signal that may be present (Kamath; Watanabe; Upton, 2016; Richman; Moorman, 2000; Shaffer; Ginsberg, 2017).

3.1.3.3 Sample Entropy (SampEn)

The sample Entropy provides a less biased and more reliable measure of signal regularity and complexity when compared to ApEn measures. The interpretation and use of SampEn remain the same as for ApEn, in which a lower value of SampEn also indicates more self-similarity in the time series. Also, SampEn may be calculated from a much shorter time series (*e.g.*, fewer than 200 values) (Richman; Moorman, 2000).

3.1.3.4 Multiscale Entropy (MSE)

The multiscale entropy development has been motivated by three hypotheses: a) the complexity of a biological system reflects its ability to adapt and function in an ever-changing environment; b) biological systems need to operate across multiple spatial and temporal scales, and hence their complexity is also multi-scaled; and c) a broad class of disease states, as well as ageing, which reduce the adaptive capacity of the individual, appear to degrade the information carried by output variables. So, complexity measurement, defined as MSE, quantifies the information expressed by the physiologic dynamics over multiple time scales (Costa; Goldberger; Peng, 2005).

The MSE calculation is comprised of two steps: (a) coarse-graining the signals into different time scales and (b) quantifying the degree of irregularity in each coarse-grained time series using sample entropy (SampEn). In this way, the entropy is calculated as a scale function, providing a measure of information richness embedded in different time scales (Costa; Goldberger; Peng, 2005).

Regarding cardiac inter-beat interval time series, we can refer to “large” and “small” time scales when the scales are larger or smaller than one typical respiratory cycle length, approximately five cardiac beats. Small-scale represents autonomic nervous activity, whereas large-scale reflects vascular regulatory function. Thus, three different parameters can be derived: a) summation of quantitative values of scale 1-5 (Area S); b) summation of quantitative values of scale 6-20 (Area L); and c) linear-fitted slope of the first five scales (Slope S), as represented in Figure 7 (Costa; Goldberger; Peng, 2005).

Figure 7 - Illustrative graph of multiscale entropy-derived parameters.

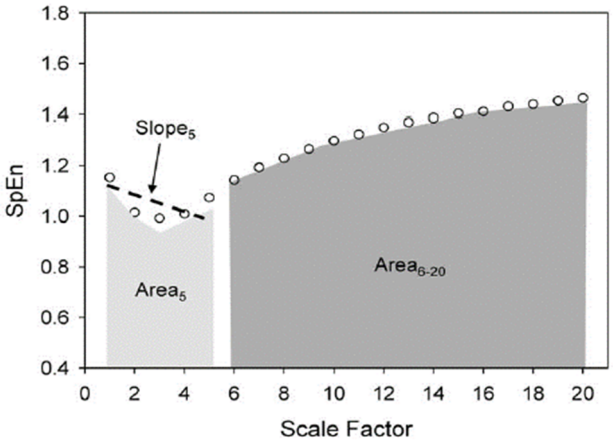

Source: Ho *et al*. (2011).

3.1.3.5 Fuzzy Entropy (FuzzyEn)

The ApEn and SampEn entropy measures have poor statistical stability since the vector's similarity is defined based on the Heaviside function of the classical sets, which is a two-state classifier that judges two vectors as either "similar" or "dissimilar", with no intermediate states. Thus, a fuzzy entropy measure was proposed, importing the concept of fuzzy sets, where the vector's similarity is defined by fuzzy similarity degree (graduated similarity classifier), achieving better statistical stability. The advantages of FuzzyEn are: a) insensitive to noise, b) highly sensitive to changes in the information content, and c) less dependent on data length than ApEn and SampEn (Acharya *et al.*, 2015; Chen *et al.*, 2009).

3.1.3.6 Shannon Entropy (ShEn)

Shannon's entropy measures a set of relational parameters that vary linearly with the logarithm of the number of possibilities. ShEn of a random variable X that takes the values x_1, x_2… x_N is defined as Equation (3), where p (x_i) are probabilities of acceptance by the random variable X values x_i.

$$\text{lEn} = -\sum_{i=1}^{n} p(x_i)\, log_a\, p(x_i)\,,\ a > 1 \qquad (3)$$

ShEn is also a measure of data spread and is most commonly used to assess the dynamical order of a system. It is characterized by a degree of uncertainty associated with the occurrence of the result; a higher value gives a more uncertain outcome and is more difficult to predict. When applied to an RR time series, x_i can be considered an RR interval, and p (x_i) is estimated by counting the number of RR intervals in a given recording (Borowska, 2015; Orini *et al.*, 2017).

3.1.3.7 Spectral Entropy (SpEn)

Spectral entropy measures how the information in the signal is distributed across different frequencies (Acharya *et al.*, 2015). SpEn is a normalized form of Shannon's entropy, which uses the power spectrum amplitude components of the time series for entropy evaluation, quantifying the spectral complexity of the signal. SpEn is

obtained by multiplying the power in each frequency p_f by the logarithm of the same power, as represented in Equation (4) (Acharya *et al.*, 2015; Borowska, 2015).

$$\text{SpEn} = -\sum_f p_f \log(p_f) \quad (4)$$

3.1.3.8 Permutation Entropy (PermEn)

Permutation entropy is a complexity estimation of time series by identifying the couplings between the time-series signal. The signal dynamics can be derived by assessing the presence and absence of permutation patterns of different elements in the given time-series signal. At high frequencies, PermEn elevates with an asymmetry of the time series, while at low frequencies, the permutations corresponding to peaks and troughs observed are seldom. The largest value of PermEn is one, which means the time series is completely random; the smallest value is zero, which means the time series is very regular (Acharya *et al.*, 2012; Brandt; Pompe, 2002).

In short, the PermEn refers to the local order structure of the time series and is a measure of chaotic and non-stationary time series in the presence of dynamical noise. The advantages of this entropy are: (a) it is simple, robust, and less prone to computational complexity; (b) it applies to real and noisy data; (c) it does not require any model assumption and is suitable for the analysis of nonlinear processes, and (d) it is useful to analyse huge data sets and requires less pre-processing time and fine-tuning of parameters (Acharya *et al.*, 2012; Brandt; Pompe, 2002).

3.1.3.9 Correlation Dimension (CD or D2)

The correlation dimension estimates the minimum number of variables required to construct a model of system dynamics—the more variables required to predict the time series, the higher its complexity. An attractor is a set of values (or a path) towards the system convergence, and the correlation dimension is one of the simplest methods for estimating a system's attractor dimension. This quantity cannot accurately define the real dimension of the system (the calculation of correct CD for biomedical signals is computationally not easily achieved), but it gives a measure of the complexity of the system, that is, when CD increases, the system becomes more complex (Kamath; Watanabe; Upton, 2016; Shaffer; Ginsberg, 2017).

3.1.3.10 Detrended Fluctuations Analysis (DFA, α1, α2)

DFA extracts the correlations (expressed by scaling properties) between successive RR intervals over different time scales. This analysis results in slope α_1, which describes brief fluctuations, and slope α_2, which describes long-term fluctuations. The long-range scaling exponent α_2 for a healthy person is ~1, while the short-range scaling exponent α_1 is usually between 0.5 and 1.5. Many factors affect it, such as the functioning of the baroreflex mechanism and breathing modulation (Shaffer; Ginsberg, 2017).

3.2 EMPIRICAL MODE DECOMPOSITION

The EMD method is an adaptive data analysis method applicable to nonlinear and non-stationary signals (Huang *et al.*, 1998). The EMD model decomposes data into finite intrinsic mode functions (IMFs) based on directly extracting the energy associated with various intrinsic time scales. With the Hilbert transform, the IMFs yield instantaneous frequencies as functions of time that give sharp identifications of embedded structures. The final presentation of the results is an energy-frequency-time distribution, designated as the Hilbert spectrum, which accurately represents non-stationary and nonlinear signals (Huang *et al.*, 1998).

Unlike Fourier analysis or wavelet transforms, EMD breaks down a time signal into a set of base signals derived from the data itself; this unique approach allows EMD to preserve the full non-stationarity of the signal (Maheshwari; Kumar, 2014). In addition to contrasting the Fourier analysis that produces a series of sine and cosine functions of fixed amplitudes to represent each frequency constituent in the signal, the IMFs are oscillatory modes whose amplitude and frequency vary over time (Huang *et al.*, 1998).

The EMD of a time-series signal x(t) can be represented as a sum of IMFs, $\mathrm{IMF_i(t)}$, and a residue component, $\mathrm{r_N(t)}$, as represented in Equation (5):

$$x(t) = \sum_{i=1}^{N} \mathrm{IMF_i(t)} + \mathrm{r_N(t)} \quad (5)$$

The algorithm to extract the IMFs of a time-series signal using EMD follows an iterative process known as the sifting process, summarized as follows (Huang *et al.*, 1998):

a) Identify the signal maxima and minima;

b) Compute the interpolated upper and lower envelopes and the instantaneous local mean of the envelopes;

c) Subtract the obtained local mean from the original signal x(t) to obtain the first component $\mathrm{IMF_i(t)}$;

d) Check whether the component $\mathrm{IMF_i(t)}$ satisfies the two basic conditions of the IMF:

- The number of extrema—maxima and minima—and the number of zero-crossings in a signal should be either equal or differ by a maximum of one;
- At any point, the mean value of two envelopes, one formed by connecting local maxima and the other by local minima, should be zero.

e) Repeat steps (a) to (c) until it satisfies the conditions of the IMF (or by applying a stopping criterion such as the number of repetitions);

f) Repeat steps (a) to (c) for calculating the next IMFs until no more components can be extracted (or by removing criteria such as the number of required IMFs).

After the signal decomposition, the Hilbert transformation applied to the obtained IMFs provides an analytical signal representation (ASR) of IMFs (*i.e.*, a complex-valued function with no negative frequency components). Any complex signal, z(t), can be considered the sum of its real part, $\mathrm{IMF_i(t)}$, and its imaginary part, Im(t), and rewritten in a polar coordinate system, as demonstrated in Equation (6). Equations (7) and (8) denote the instantaneous amplitude A(t) and phase Θ(t) of the complex analytic signal, respectively:

$$z(t) = \mathrm{IMF_i(t)} + j\mathrm{Im(t)} = A(t)\, e^{j\Theta(t)} \tag{6}$$

$$A(t) = \sqrt{\mathrm{IMF_i(t)^2} + \mathrm{Im(t)^2}} \tag{7}$$

$$\Theta(t) = \tan^{-1}\left(\frac{\mathrm{Im(t)}}{\mathrm{IMF_i(t)}}\right) \tag{8}$$

When applied to HRV analysis, the RR interval is decomposed into amplitude and frequency-modulated (AM–FM) signal components, the IMFs. The study of (Echeverria *et al.*, 2001) demonstrated that the isolation of the first four components of the EMD is necessary to recognize the spectral bands of the autonomic modulation. Thus, the studies limited the decomposition to four IMFs, considering they held the most significant signal variation.

3.2.1 The Features of EMD-derived IMFs

The features extracted from the EMD-derived IMFs were as follows: the area of analytical signal representation (ASR_{area}), the second-order difference plot area ($SODP_{area}$), and the central tendency measure of the second-order difference plot ($SODP_{CTM}$). Furthermore, the features extracted after power spectral density estimation of the IMFs were peak amplitude (PSD_{pkamp}), band power (PSD_{bpow}), and mean frequency (PSD_{mfreq}). The specifics of how these features were obtained are explained below.

3.2.1.1 The Area of Analytical Signal Representation (ASR_{area})

The IMF analytic signal s(n) can be plotted as the imaginary part, Im{s(n)}, against the real part, R{s(n)}. This IFM analytical signal representation (ASR) plot shows a circular pattern with a unique centre of rotation (Lai; Ye, 2003). Thus, a feature of the area can be estimated. One of the standard methods to summarize graph information is the central tendency measure (CTM). The CTM is computed by selecting a circular region of radius *r* around the origin, counting the number of points within the radius, and dividing by the total number of points N, as in the study of Cohen, Hudson, and Deedwania (1996). This procedure is demonstrated in Equations (9) and (10):

$$\text{CTM} = \frac{\sum_{n=1}^{N} D(n)}{N} \tag{9}$$

$$D(n) = \begin{matrix} 1 \text{ if } ([R\{s(n)\}]^2 + [Im\{s(n)\}]^2)^{0.5} < r \\ 0 \text{ otherwise} \end{matrix} \tag{10}$$

The radius of the plot is computed using the CTM. In this work, a radius of 95% CTM was chosen to calculate the ASR area. Finally, the ASR_{area} is computed as in Equation (11).

$$ASR_{area} = \pi \cdot r^2 \quad (11)$$

3.2.1.2 The Second-Order Difference Plots ($SODP_{area}$ and $SODP_{CTM}$)

The second-order difference plots (SODPs) are centred around the origin representing the variability rate; they help model biological systems, such as heart rate variations, to characterize the degree of theoretical chaos (Cohen; Hudson; Deedwania, 1996). The SODPs extract the rate of the data variability (*e.g.*, they assess the variability present in the IMFs of the RR interval signals) and provide a graphical representation of successive differences in the same series when plotted against each other (Hadoush; Alafeef; Abdulhay, 2019; Pachori *et al.*, 2015).

The SODP graph of a given signal x(n) can be obtained by plotting X(n) versus Y(n), as defined in Equations (12) and (13), respectively:

$$X(n) = \mathrm{IMF_i}(n+1) - \mathrm{IMF_i}(n) \quad (12)$$

$$Y(n) = \mathrm{IMF_i}(n+2) - \mathrm{IMF_i}(n+1) \quad (13)$$

Once the SODP is obtained, we used the 95% confidence ellipse area of the SODP graph to obtain the $SODP_{area}$. The procedure to calculate the ellipse area is given as the following process (Cavalheiro *et al.*, 2009; Pachori; Patidar, 2014).

Compute S_x, S_y, and S_{xy}, according to Equation (14) to Equation (16):

$$S_x = \sqrt{\frac{1}{N}\sum_{n=0}^{N-1} X(n)^2} \quad (14)$$

$$S_y = \sqrt{\frac{1}{N}\sum_{n=0}^{N-1} Y(n)^2} \quad (15)$$

$$S_{xy} = \frac{1}{N} \sum \mathrm{X(n)\ Y(n)} \quad (16)$$

Compute D, a, and b parameters according to Equations (17), (18), and (19):

$$\mathrm{D} = \sqrt{\left(S_x^2 + S_y^2\right) - 4(S_x^2 S_y^2 - S_{xy}^2)} \quad (17)$$

$$\mathrm{a} = 1.7321\sqrt{S_x^2 + S_y^2 + D)} \quad (18)$$

$$\mathrm{b} = 1.7321\sqrt{S_x^2 + S_y^2 - D)} \quad (19)$$

From parameters a and b, the $SODP_{area}$ is calculated as in Equation (20):

$$SODP_{area} = \pi \cdot \mathrm{a} \cdot \mathrm{b} \quad (20)$$

In addition, the CTM method was applied to the SODP graphs. The CTM was calculated for each IMF's fixed circular region around the SODP origin point. Therefore, a low-variable plot will have points clustered around the origin. Additionally, the diseased state of the heart exhibits a greater degree of chaos (Cohen; Hudson; Deedwania, 1996). The $SODP_{CTM}$ is defined as the ratio between the number of points within the fixed radius and the total number of points. The radius was defined by visual inspection as 0.02, 0.01, 0.002, and 0.001 for the 1st to 4th IMF, respectively.

3.2.1.3 The Power Spectral Density Estimation (PSD_{pkamp}, PSD_{bpow} and PSD_{mfreq})

The power spectral density (PSD) estimation describes the power distribution over frequency contained in a signal. The x-axis represents frequency, while the y-axis represents the magnitude or power of the signal at that frequency in units expressed in decibels (dB) or squared units of the original signal. Welch's method was used to estimate the PSD. In brief, it is an averaging method that divides the signal into overlapping segments, computes the periodogram of each segment, and averages these periodograms to obtain an estimate of the PSD over a certain frequency range (Subasi, 2019). In this study, the adopted frequency range was 0–0.5 Hz. Welch's PSD

was estimated for each of the four extracted IMFs. The PSD peak amplitude (PSD_{pkamp}) was defined as the absolute maximum height of the PSD waveform. The PSD band power (PSD_{bpow}) was calculated as the average power computed by integrating the PSD estimate curve, and, finally, the PSD mean frequency (PSD_{mfreq}), as the average frequency of the spectrum, was calculated as the weighted average of the frequencies, with the weights being the PSD values at each frequency.

3.3 BAROREFLEX SENSITIVITY ANALYSIS

This section presents the two steps for baroreflex analysis. First, the blood pressure estimation from ECG and PPG variables, and second, the methodology for BRS index estimation. Details about the baroreflex mechanism are described in section 2.2.2.

3.3.1 Blood Pressure Estimation

Blood pressure (BP) is an indicator of the state of the circulatory system, being one of the most dynamic physiologic variables routinely measured in clinical practice. BP consists of a series of pulse waves continuously changing in terms of both frequency and amplitude and represents the response of cardiovascular control mechanisms to environmental stimulations and to daily life challenges aimed at maintaining cardiovascular “homeostasis” (Bote; Recas; Hermida, 2020; Solà; Delgado-Gonzalo, 2019).

BP measurement methods can be categorized as invasive (*e.g.*, catheterization) and non-invasive (*e.g.*, auscultation or sphygmomanometer, oscillometry, and volume clamping, which employs an inflatable cuff). Catheterization is the gold standard method since the measurement is done by placing a strain gauge in fluid contact with blood at any arterial site. Auscultation is the standard clinical method; BP is measured by occluding an artery with a cuff and detecting the Korotkoff sounds using a stethoscope and manometer during cuff deflation. Oscillometry is an automatic method that measures BP using a cuff with a pressure sensor inside it (Mukkamala *et al.*, 2015; Solà; Delgado-Gonzalo, 2019).

With improvements in sensor technology, many approaches have been employed to study the BP relationship with ECG and photoplethysmography (PPG) parameters such as pulse arrival time (PAT), pulse transit time (PTT), and pulse wave velocity (PWW). PTT is the time delay for the pressure wave to travel between two arterial sites. At the same time, PAT is the time delay between the ECG waveform and a distal arterial waveform and is equal to the sum of the PTT and pre-ejection period, of which PEP is the time interval between the start of ventricular depolarization and the moment of aortic valve opening. Finally, PWW is the reciprocal of PTT (1/PTT). (Mukkamala *et al.*, 2015; Rajala; Lindholm; Taipalus, 2018). PAT is often calculated as the time delay between the R peak in the ECG signal and a certain feature in the PPG waveform (*i.e.*, peak, foot, or the maximum value of the first derivative) (Rajala; Lindholm; Taipalus, 2018), as demonstrated in Figure 8.

Figure 8 – Pulse arrival time (PAT) measurement. PAT calculated from the R peak of the electrocardiogram to (a) the maximum value of the first derivative, (b) the peak value, and (c) the foot value of the photoplethysmogram.

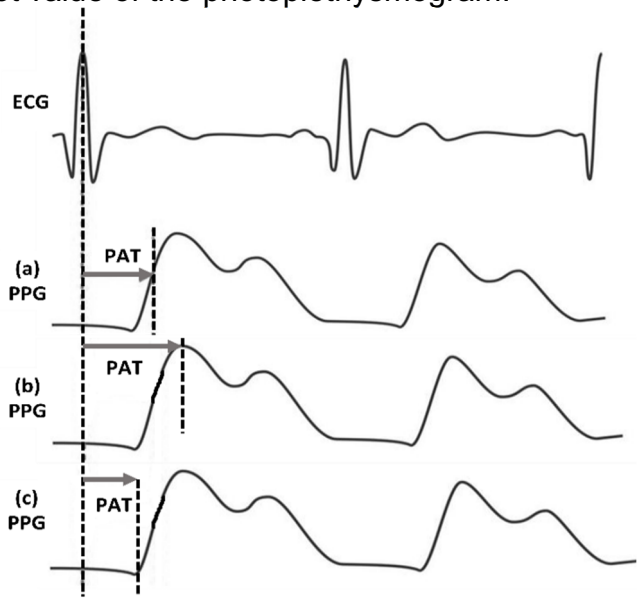

Source: Adapted from Ding *et al*. (2016).

Although these techniques based on PAT, PTT, or PWW cannot measure BP as accurately as the gold standard method, they can monitor BP continuously in a non-invasive, automatic, and cuff-less way. Among the different BP estimation models based on PAT and PTT, linear models are the most widely proposed due to their robustness against artefacts present in the waveforms. Also, multivariate models can be found in the literature that includes other variables (*e.g.*, heart rate, PPG parameters

such as systolic and diastolic time, PPG pulse width, PPG amplitude) that could improve the model's accuracy (Bote; Recas; Hermida, 2020; Mukkamala *et al.*, 2015; Rajala; Lindholm; Taipalus, 2018; Solà; Delgado-Gonzalo, 2019).

In this context, the study by Wong, Poon, and Zhang (2009) investigated the relationship between blood pressure and PTT proposing linear models of PTT-based estimation using the least squares method in first and repeatability tests; the results confirmed the linearity between systolic blood pressure and PTT achieving reasonable BP estimations. Another study proposed by Rajala, Lindholm, and Taipalus (2018) compared PPG signals measured from the wrist and finger to evaluate if wrist PPG could be used to calculate PAT and also investigated the correlation between PWW and systolic BP. From the results, wrist PPG can be used for PAT calculation, with the PPG foot or first derivative peak being the most suitable method for wrist PAT calculation. Also, the correlation between PWW and systolic BP was below 0.5, indicating that BP estimation still has challenges.

3.3.2 Baroreflex Sensitivity

Baroreflex sensitivity (BRS) is commonly measured as a ratio of the change in heart rate (quantified by its reciprocal, the RR interval) in response to a fixed change in the blood pressure, with the idea of characterising the "quality" of operation of the entire blood pressure regulatory system with a single numerical value. Its unit is "ms/mmHg" and is usually positive, in which a higher BRS value indicates that the system strongly reacts to pressure changes, *i.e.*, the system is more sensitive (Kuusela, 2013).

Traditional approaches to testing the sensitivity of baroreceptors of the carotid sinus and aortic arch include pharmacological stimulation and neck suction. More recent approaches enable the BRS to be estimated non-invasively from the RR interval changes associated with spontaneous fluctuations in blood pressure and are closely correlated with the results of the pharmacological method. These approaches include the slope method, the advanced slope method, the sequence method, and the spectral method. The slope and advanced slope methods perturb the blood pressure control system through the application of some medication and the measurement of the response to such a perturbation while simultaneously recording electrocardiogram and blood pressure waveforms (Kuusela, 2013; Zygmunt; Stanczyk, 2010).

The sequence method analyses the relations between fluctuations in blood pressure extracted in particular sequences and RR intervals. However, instead of concentrating on a singular pressure rise or fall (slope method), the calculation is performed multiple times during a recording, and, in this case, the pressure rise and fall are not externally induced since naturally occurring fluctuations of these signals are utilized (Kuusela, 2013; Zygmunt; Stanczyk, 2010).

In the sequence technique, represented in Figure 9, beat-by-beat blood pressure and RR interval recordings are scanned for sequences in which systolic blood pressure (SBP) and RR interval concurrently increase or decrease for at least three consecutive beats. Second, accepted sequences need a minimum change of 0.5mmHg in SBP and a change of 1 ms in the RR interval, which is advanced by one beat to compensate for an assumed adjustment delay between the BP and RR interval. Finally, identified sequences need to present a correlation coefficient greater than 0.85. Baroreflex sensitivity is then assessed from the relationship between systolic blood pressure and RR interval across these fragments, fitting a regression line to the sequence and the slope of the regression gives the BRS value (Kuusela, 2013; Zygmunt; Stanczyk, 2010).

The baroreflex mechanism may also be studied based on spectral analysis of heart rate and blood pressure variability signals. With this method, baroreflex sensitivity is assessed by analysing the RR interval changes associated with rhythmic blood pressure oscillations over a range of frequencies reported to reflect baroreflex function (Kamath; Watanabe; Upton, 2016; Zygmunt; Stanczyk, 2010).

Figure 9 - Illustration of the sequence method. Accepted sequences have a minimum of three consecutive rising (or falling) values in systolic blood pressure (SBP) and RR intervals, which must have a minimum increase/decrease of 0.5 mmHg in SBP (ΔSBP) and a minimum increase/decrease of 1 ms in RR intervals (ΔRR) advanced by one.

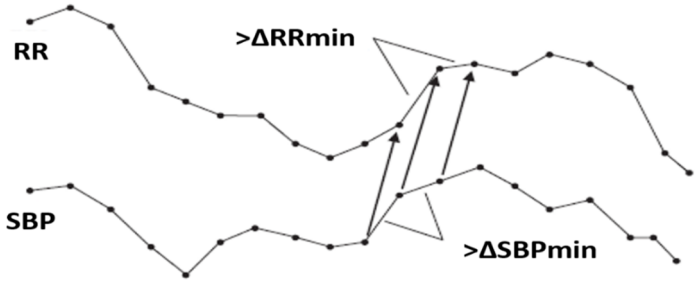

Source: Adapted from Kuusela (2013).

3.4 MACHINE LEARNING METHODS

This section describes fundamental concepts and methods to develop and evaluate a machine learning model. Also, it presents brief explanations about standard machine learning algorithms that were tested in this work.

3.4.1 Feature Selection

Feature selection is a solution to reduce the generalization error by choosing a simpler model with fewer parameters or reducing the final dataset's dimensionality. For biomedical signal processing, the analysis methods include the representation of biosignals as a feature vector that can be further analysed to identify the most representative features and reduce the final dataset's dimensionality (Remeseiro; Bolon-Canedo, 2019).

There are two different main approaches in the feature selection process. The first one is to make an independent assessment, based on general characteristics of data and is called the *filter method* since the feature set is filtered out before model construction. The second approach is the *wrapper method,* which uses a machine-learning algorithm to evaluate a different subset of features. Finally, it selects the one with the best performance on classification accuracy (Kavakiotis *et al.*, 2017), as represented in Figure 10. Some common approaches for feature selection are commented on in the next sub-sections.

Figure 10 - Feature selection methods based on how they combine the selection algorithm and the model building. (a) Filter Method. (b) Wrapper Method.

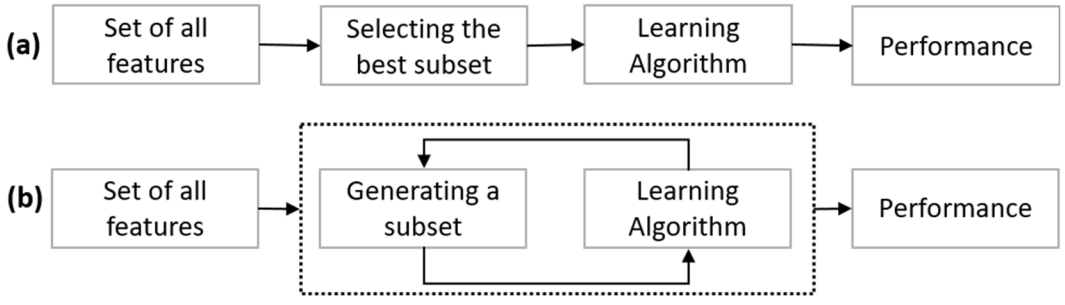

Source: Elaborated by the author.

3.4.1.1 Univariate Filter Methods

Univariate filter methods evaluate each feature individually and do not consider feature interactions; these methods provide a score for each feature, often based on statistical tests. The scores usually either measure the linear correlation (*e.g.*, Pearson correlation coefficient and Spearman's rank correlation coefficient) or evaluate each feature individually and rank the features based on specific criteria (*e.g.*, Chi-squared score, Mutual information, ANOVA, ROC-AUC). However, since each feature is considered separately, univariate methods only focus on feature relevance and cannot detect feature interaction or redundancy (Pudjihartono *et al.*, 2022).

Scores based on statistical tests provide a p-value that may be used to rule out some features, for example, if the p-value is above a certain threshold (typically 0.01 or 0.05). The p-value is proportional to the similarity of the two classes. In a classification scenario, we want the two classes to differ; hence, a low p-value is preferred. Therefore, a low p-value indicates a high probability that the individual classes are separable. In a diagnostic setting, a p-value below 0.05 indicates clinical significance (Rajendra Acharya *et al.*, 2013).

One example of a filter-based feature selection method is the SelectKBest. SelectKBest uses statistical tests like chi-squared test, ANOVA F-test, or mutual information score to score and rank the features based on their relationship with the output variable. Then, it selects the k features with the highest scores to be included in the final feature subset (Pedregosa *et al.*, 2011).

3.4.1.2 Multivariate Filter Methods

The multivariate filter methods consider a subset of features simultaneously and can model feature dependencies. Despite its advantages, the multivariate methods are more computationally heavy and independent from the classifier algorithm than univariate methods (Pudjihartono *et al.*, 2022).

One popular category of multivariate filter methods is the ReliefF-based algorithm (Remeseiro; Bolon-Canedo, 2019). ReliefF is a ranker approach that considers correlations between predictors because it is based on the nearest-neighbour procedure. The worth of each variable is estimated by considering how well its values distinguish between neighbours' subjects. So, a useful feature should have

values similar to examples from the same class and different from examples from the other classes (Remeseiro; Bolon-Canedo, 2019). In summary, it scores the importance of a feature according to how well the feature's value distinguishes samples that are similar to each other but belong to different classes (Pudjihartono *et al.*, 2022).

3.4.1.3 Wrapper Methods

In contrast to filter methods, wrapper methods use the performance of the chosen classifier algorithm as a metric to support the selection of the best feature subset. These methods tend to perform better than filter methods, with the cost of being dependent on the classifier used and computationally heavy due to the high number of computations required to generate and evaluate the feature subsets (Pudjihartono *et al.*, 2022).

One example of the wrapper-based method is the Recursive Feature Elimination (RFE). This approach starts with all features, builds a model, and discards the least important feature according to the model. A new model is built using all but the discarded features, and so on, until only prespecified numbers of features are left. So, when using RFE, two options need to be selected: a) the number of features to select and b) choice of the algorithm used to help choose features (*e.g.*, decision tree, logistic regression, random forest, etc.) (Müller; Guido, 2016).

3.4.2 Feature Extraction

Besides feature selection, feature extraction methods are another data dimensionality reduction technique. When compared to feature selection, the main difference is that feature extraction combines the original features and creates a set of new features, while feature selection selects a subset of the original features (Remeseiro; Bolon-Canedo, 2019).

The principal component analysis (PCA) is an example of a feature extraction technique used for deriving a low-dimensional set of features from a large set of variables. Given a large set of correlated variables, principal components allow summarizing this set with a smaller number of representative variables that collectively explain most of the variability in the original set (James *et al.*, 2014). PCA is a technique

for feature extraction related to dimensionality reduction, starting from an initial set of measured data and building derived values intended to be informative and non-redundant, facilitating the subsequent learning and generalization steps of ML algorithms (Müller; Guido, 2016).

Considering a dataset with *n* observations and *p* features, the idea is that each of the *n* observations lives in a *p*-dimensional space, but not all of these dimensions are equally interesting. PCA is a tool to find a low-dimensional representation of a data set that contains as much as possible of the variation. Each of the dimensions, namely principal components, found by PCA, is a linear combination of the *p* features. The finding of the principal components comes from the eigenvalue/eigenvectors problem, solving the characteristic equation of the correlation matrix of the observed variables.

For example, when reducing a set of features represented by two principal components, the first principal component vector (PC_1) defines the most correlated line with the data. At the same time, the second principal component (PC_2) is a linear combination of the variables that are uncorrelated with PC_1. The condition of zero correlation between PC_1 and PC_2 is equivalent to the requirement that their directions be perpendicular or orthogonal (James *et al.*, 2014), as represented in Figure 11.

Figure 11 – Representation of a principal component analysis into two principal components, the PC_1 and PC_2.

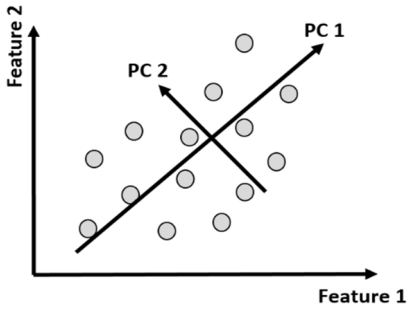

Source: Elaborated by the author.

3.4.3 Feature Scaling

Feature scaling is a method to normalize the range of independent variables or data features to prevent classification biases. Since the range of values of raw data may vary widely, ML functions may not work properly; for example, many classifiers calculate the distance between two points by the Euclidean distance, which will be a

problem with different magnitudes of features (Isler *et al.*, 2019; Müller; Guido, 2016). Some methods for feature scaling are presented in the next sub-sections.

3.4.3.1 Standardization

This method, also known as Z-score normalization, ensures that for each feature, the mean is 0 and unit variance, bringing all features to the same magnitude. This method is used in ML algorithms such as SVM, LR, PCA, and ANNs (Müller; Guido, 2016). The method is detailed in Equation (21), where x' is the standardized value, x is the original feature vector, $\bar{x}$ is the mean of the feature vector and σ is the standard deviation of the feature vector.

$$x' = \frac{x - \bar{x}}{\sigma} \quad (21)$$

If data contains many outliers, especially in small datasets, scaling using the mean and variance of the data is not recommended. One option is to scale the features according to the 1st and 3rd quartiles of the dataset, such that more extreme values and outliers become less pronounced (Müller; Guido, 2016; Raschka; Mirjalili, 2019).

3.4.3.2 Min-Max Normalization

Normalize the attributes to re-scale them to make all values fall into the same interval, between 0 and 1, as detailed in Equation (21), where x' is the normalized value, and x is the original value.

$$x' = \frac{x - min\,(x)}{\max(x) - \min(x)} \quad (21)$$

3.4.3.3 Mean Normalization

Like min-max normalization, it scales values between -1 and 1, as detailed in Equation (23), where x' is the normalized value and x is the original value.

$$x' = \frac{x - mean\,(x)}{\max(x) - \min(x)} \quad (23)$$

3.4.4 Machine Learning Algorithms

This section provides an overview of this study's supervised machine-learning algorithms. In the context of supervised learning, the construction of a model takes place using training data, which is subsequently evaluated on new, unseen data with the same characteristics as the training set. Successful predictions on this unseen data demonstrate the model's ability to generalize from the training set to the test set (Müller; Guido, 2016). A supervised learning model is represented in Figure 12.

Figure 12 - A supervised machine learning algorithm model.

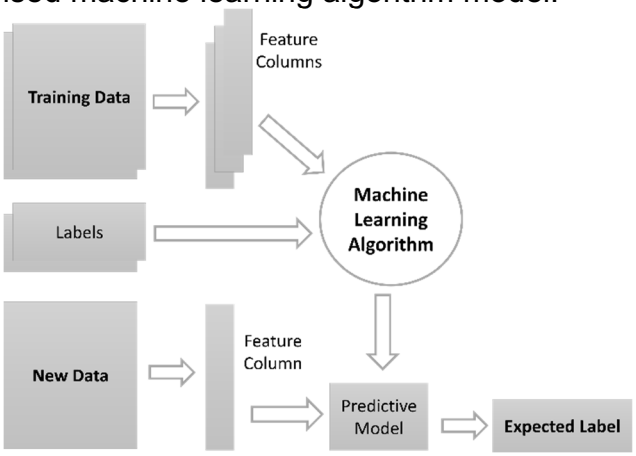

Source: Adapted from Nasteski (2017).

The objective is to build a model to generalize as accurately as possible without overfitting or underfitting the data. *Overfitting* occurs when a model fits too closely to the training set's particularities and cannot generalize to new data; the model is too complex for the amount of information. In contrast, *underfitting* occurs when the model cannot capture all the aspects of variability in the data (Müller; Guido, 2016). There are two major types of supervised machine-learning problems: *classification* and *regression*. In classification, the goal is to predict a class label, a choice from a predefined list of possibilities. At the same time, in regression, the expected output is a number from a continuous range rather than a discrete-valued class (Kubat, 2017).

3.4.4.1 K-Nearest Neighbours

The K-nearest neighbours (KNN) is a simple non-parametric method used for classification and regression. The algorithm "looks" at the K points in the training set

nearest to the test input x, counts how many members of each class are in this set, and returns that empirical fraction as the estimate (Murphy, 2012). The parameter k of neighbours can be an arbitrary number. So, for each test point, it is counted the number of neighbours which belong to class 0 and class 1; the more frequent class is assigned to that point or, in other words, the majority class among the k-nearest neighbours, as represented in Figure 13. By default, Euclidean distance is used to measure the distance between data points (Müller; Guido, 2016).

Figure 13 – The K-nearest neighbour algorithm representation. In the example, for k = 3, class A is more frequent; therefore, the tested data point (*i.e.*, star) is labelled as class A.

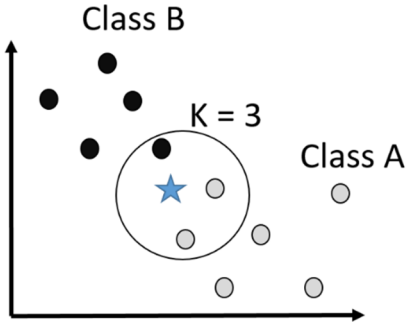

Source: Elaborated by the author.

3.4.4.2 Logistic Regression

Logistic regression (LR) models the probability (*i.e.*, a value between 0 and 1 exclusively) that a quantitative response variable belongs to a particular category. A logistic function is derived from a sigmoid function to ensure that the probability p(x) falls between 0 and 1, as represented in Equation (24). If there are multiple explanatory variables, the expression $\beta_0 + \beta_1 x$ can be revised to $\beta_0 + \beta_1 x + \beta_2 x_2 + \cdots + \beta_m x_m$.

$$p(x) = \frac{1}{1+ e^{-(\beta_0 + \beta_1 x)}} \quad (24)$$

For linear classification models, such as logistic regression, the decision boundary is a linear function of the input or, in other words, a linear classifier that separates two classes using a line, a plane, or a hyperplane. Thus, after the calculation of the linear model and mapping the result to the range of 0 to 1 with the logistic function, the prediction is interpreted by assigning a threshold to the probability (*i.e.*,

given two classes, if the probability is > 0.5, the output is predicted to class 1; otherwise, the prediction is for class 0, as represented in Figure 14. To make a good prediction, the algorithm needs to (a) optimize the parameters β to give the best possible reproduction of training set labels, which is usually done by numerical approximation of maximum likelihood or stochastic gradient descent, and (b) use some regularization parameter (Nasteski, 2017).

Figure 14 - Illustration of logistic regression algorithm concept.

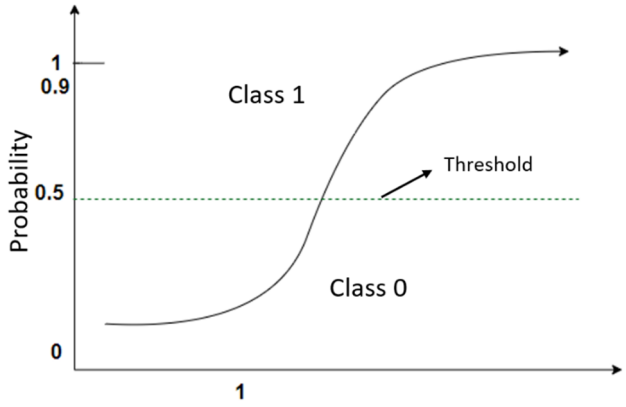

Source: Elaborated by the author.

3.4.4.3 Decision Trees

Decision trees are a non-parametric supervised learning method that aims to predict the value of a target variable by learning simple decision rules inferred from the data features. Essentially, DT learns a hierarchy of if/else questions, leading to a decision. These decision questions are called tests. In building a decision tree, the algorithm searches over all possible tests and finds the one that is more informative about the target variable (Nasteski, 2017). So, a binary tree of decisions is built, with each node containing a test, as shown in Figure 15.

Figure 15 – Representation of the decision tree algorithm. Each node contains a test or a conditional control statement, which leads to a decision.

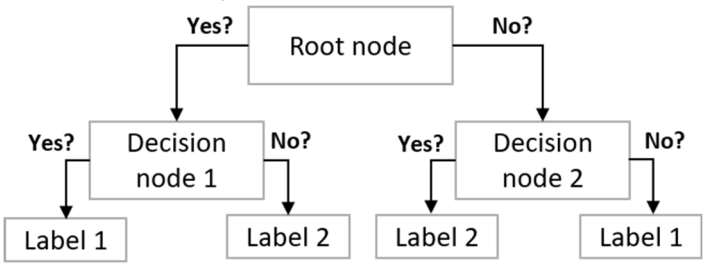

Source: Elaborated by the author.

3.4.4.4 Support Vector Machines

Support vector machines are supervised learning methods that can be used for regression and classification. Given labelled training data, the algorithm outputs an optimal hyperplane in N-dimensional space (N- the number of features) that distinctly classifies the data points, as represented in Figure 16 (a). This is known as the kernel trick, and it works by computing the distance (more precisely, the scalar products) of the data points for the expanded feature representation (Müller; Guido, 2016).

Many possible hyperplanes could be chosen, but the objective is to find a plane with the maximum margin (*i.e.*, the maximum distance between data points of both classes) since, in general, the larger the margin, the lower the generalization error of the classifier. Only a subset of training points matters for defining the hyperplane (or the decision boundary): the ones that lie on the border between the classes, namely, *support vectors*, as represented in Figure 16 (b) (Müller; Guido, 2016).

Figure 16 – (a) Representation of the support vector machine (SVM) algorithm. From the input space, the algorithm finds a line or hyperplane in multidimensional space that separates output classes. (b) Hyperplane representation of an SVM algorithm.

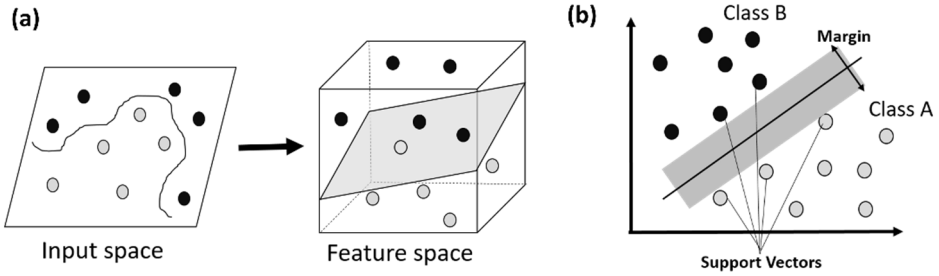

Source: Elaborated by the author.

In SVM, there are two main tuning parameters: the gamma and the C parameter. The *gamma* parameter determines how far the importance of a single training example reaches; with high values, only nearby points are considered, and with low values, far away points are also considered. The C parameter is a regularization parameter that controls how much to avoid misclassifying each training example. For large values of C, the optimization will choose a smaller-margin hyperplane if that hyperplane does a better job of getting all the training points classified correctly; conversely, a small value of C will cause the optimizer to look for a larger-margin separating hyperplane, even if that hyperplane misclassifies more points (Müller; Guido, 2016; Murphy, 2012).

3.4.5 Model Evaluation

Employing the same dataset for both training model parameters and evaluating its performance is a methodological error, as it can lead to overfitting—when a model fits the training data excessively and performs poorly on new, unseen data. The next sections introduce two distinct approaches to model evaluation.

3.4.5.1 Holdout Method

The simplest model evaluation approach is the holdout method, which divides a labelled dataset into two segments: a training set and a test set, as shown in Figure 17. Subsequently, a model is trained using the training data and used to predict the test set's labels. The dataset is partitioned through random subsampling, often allocating 70% of the samples to the training set and the remaining 30% to the test set. It is important to ensure stratified splitting, which retains the original class distribution within the resulting subsets (Kubat, 2017; Müller; Guido, 2016; Raschka, 2018).

In the context of the holdout method, holdout validation can be divided into the following stages: a) Partition the dataset into training and test sets; b) Select a suitable learning algorithm for the specific problem and train a model; c) Utilize the model on the test set to measure its generalization accuracy or error and; d) Evaluate the generalization performance using the entire dataset, operating under the assumption that the algorithm benefits from more data until its full capacity is reached (Raschka, 2018).

Figure 17 - Representation of the holdout method. The dataset is partitioned into a training set for constructing the model and a testing set for assessing model performance.

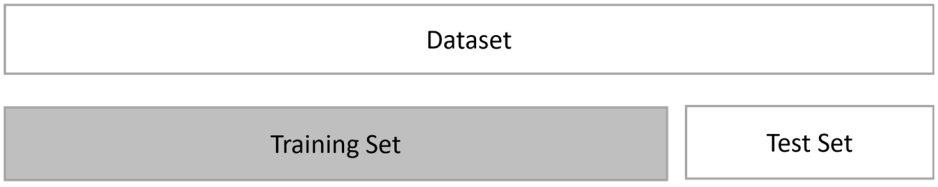

Source: Elaborated by the author.

3.4.5.2 Cross-Validation

When the dataset is partitioned into training and test sets, the number of samples for learning the model is reduced (especially in small datasets). One solution to this problem is to use the cross-validation (CV) technique. CV is a statistical method for evaluating generalization performance that is more stable and thorough than the subsampling of train-test sets. In this approach, the training set is split repeatedly, and multiple models are trained, with the most commonly used version being *k-fold cross-validation,* where *k* is a user-specified number (usually 5 or 10). The performance measure reported by *k-fold cross-validation* is the average of the values computed for each iteration (Hastie; Tibshirani; Friedman, 2009; James *et al.*, 2014; Müller; Guido, 2016). The CV method is exemplified in Figure 18.

Figure 18 - Illustration of k-fold cross-validation with k = 5. The training dataset is divided into k-subset (folds) and is used for test and training purposes for k iteration times so that each subsample will be used at least once as a test set and the remaining (k-1) as the training set. Once all the iterations are completed, the average prediction rate for each model is calculated.

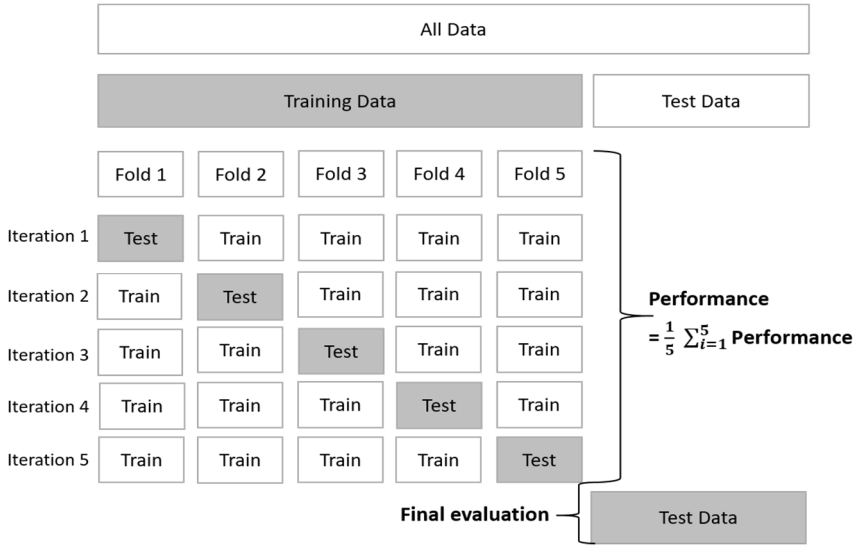

Source: Elaborated by the author.

There are some advantages of using CV instead of train-tests splits, such as: a) each model will be in training set precisely once, and each fold is the test set once; therefore, the model needs to generalize well to all of the samples in the dataset and the CV scores (and their mean) to be high; b) provides with an idea on how the model might perform in the worst-case and best-case scenarios when applied to new data

and; c) use of data more effectively which will usually result in more accurate models. The disadvantage of CV lies in the increased computational cost (Müller; Guido, 2016).

3.4.6 Model Evaluation Metrics

3.4.6.1 Correct and Incorrect Classification

When testing a classifier with known results classes, each sample classification encounters one of the four different outcomes: 1) the example is positive, and the classifier correctly recognizes it as such (*true positive* - *TP*); 2) the example is negative and the classifier correctly recognizes it as such (*true negative* - *TN*); 3) the example is positive, but the classifier labels it as negative (*false negative* - *FN*) and; 4) the example is negative, but the classifier labels it as positive (*false positive* – *FP*). So, the number of correct classifications is the number of TP plus TN, and the number of errors is the number of FP plus FN (Kubat, 2017). One way to represent the possible resulting outcomes is by using confusion matrices, as illustrated in Figure 19.

Figure 19 - Illustration of a confusion matrix for binary classification. TN – true negative, FP – false positive, FN – false negative, TP – true positive.

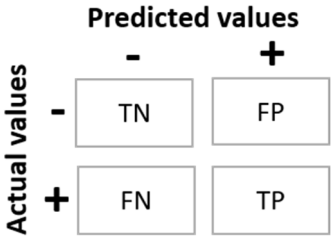

Source: Elaborated by the author.

3.4.6.2 Accuracy

Accuracy is a way to summarize the result in the confusion matrix and compute the model's accuracy, calculated as the number of correct predictions (TP and TN) divided by the number of all samples, detailed in Equation (25).

$$\text{Accuracy} = \frac{TP + TN}{TP + TN + FP + FN} \quad (25)$$

3.4.6.3 Precision

Precision is the probability that the classifier is right when labelling an example as positive, obtained by the number of true positives (TP) divided by the sum of positive predictions (TP and FP), as obtained in Equation (26). It is the frequency with which a model was correct when predicting the positive class. Precision is also known as *positive predictive value*.

$$\text{Precision} = \frac{TP}{TP+FP} \tag{26}$$

3.4.6.4 Recall

Measures the number of correct predictions, divided by the number of results that should have been predicted correctly, as detailed in Equation (27). Recall answers on how many the model correctly identified out of all the possible positive labels. It is the frequency with which a model is correct among all positive examples in the set. Recall is also known as sensitivity, hit rate, or true positive rate.

$$\text{Recall} = \frac{TP}{TP+FN} \tag{27}$$

3.4.6.5 Sensitivity and specificity

Sensitivity (Se) and Specificity (Sp) are the recall metrics measured on the positive and negative examples, respectively, as detailed in Equations (28) and (29).

$$\text{Se} = \frac{TP}{TP+ FN} \tag{28}$$

$$\text{Sp} = \frac{TN}{TN + FP} \tag{29}$$

3.4.6.6 F_1-score

F1-score is the combination of precision and recall, which can be a better measure than accuracy on imbalanced datasets, as demonstrated in Equation (30). It gives a score between 0 and 1, where 1 means the model is perfect (low false positives and low false negatives) and 0 means the model is useless.

$$F_1\text{-score} = 2 * \frac{Precision * Recall}{Precision + Recall} \quad (30)$$

3.4.6.7 The receiver operating curve and the area under the curve

Another tool commonly used to analyse the behaviour of classifiers at different thresholds is the *receiver operating characteristic curve*, or *ROC curve*. The ROC curve considers all possible thresholds for a given classifier, showing the *false positive rate* (FPR) against the *true positive rate* (TPR). The ideal curve for the ROC curve is close to the top left: a classifier that produces a high precision while keeping a low false-positive rate. The area under the curve (AUC) is a summary of the ROC curve represented by a single value between 0 (worst) and 1 (best). A meaningful interpretation of the AUC should be greater than 0.5, and values falling within the range of 0.7 to 0.8 are considered fair, while those between 0.8 and 0.9 are regarded as good, and values exceeding 0.9 are considered excellent. AUC is highly recommended to use when evaluating models on imbalanced data. (Kubat, 2017; Müller; Guido, 2016). Both concepts are illustrated in Figure 20.

Figure 20 – Representation of the receiver operating curve (ROC) and the area under the curve (AUC).

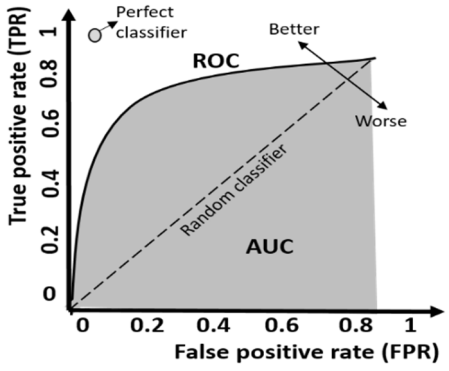

Source: Elaborated by the author.

4 HRV PROCESSING TOOL

This section describes the development of the heart rate variability analysis tool, which was used in the methodology of this work's first and second studies.

4.1 INTRODUCTION

Heart rate variability (HRV) analysis is a non-invasive method for autonomic modulation assessment (Billman, 2011; Karemaker, 2017). By examining variations in time intervals between successive heartbeats, HRV offers a unique perspective into the adaptability and resilience of the cardiovascular system (Shaffer; McCraty; Zerr, 2014). HRV analysis offers the potential to assist in monitoring diseases, categorizing risks, and providing crucial insights into individuals' health statuses. HRV analysis finds application in various clinical contexts besides cardiological conditions, such as mental health disorders, sleep health assessment, epilepsy management, diabetic neuropathy, and other medical scenarios (Faust *et al.*, 2022).

Due to the HRV's wide applicability in research, some HRV analysis tools have been developed such as the HRV toolkit available at Physionet (Vest *et al.*, 2018), the Kubios HRV software (Tarvainen *et al.*, 2014b), the R package RHRV (García Martínez *et al.*, 2017), the SinusCor (Bartels *et al.*, 2017), beside others. Although various analysis software packages are accessible, certain options are proprietary; some come pre-configured with limited settings, and others lack calculating all HRV features (with some only available in premium versions). Additionally, poor documentation and occasional lack of support from their authors further contribute to these software limitations. Thus, to facilitate accurate HRV assessment and analysis, the development of custom HRV software becomes indispensable.

Hence, this work aims to develop a specialized solution for HRV analysis that meets the specific needs of our research. Additionally, the goal is to incorporate modules for ECG, PPG, BRS, and EMD analysis while establishing integration with a database to centralize data and simplify further analysis procedures.

4.2 MATERIAL AND METHODS

4.2.1 Purpose and Overview

The main functionality of the tool includes an algorithm that extracts HRV signals from raw ECG signals and calculates various HRV-derived parameters. The extracted HRV signals encompass measures from the time domain, frequency domain, non-linear analyses, and empirical mode decomposition analysis. The tool also has an algorithm for PPG processing to estimate the blood pressure for the baroreflex analysis. Furthermore, the HRV processing tool has an MS Access (Microsoft, 2019) database connection for automated storage of the processed data.

The HRV processing tool was developed using MATLAB (R2018a, MathWorks, MA, USA). The algorithm implementation was built upon the open-source PhysioNet Cardiovascular Signal Toolbox (Vest *et al.*, 2018), utilizing the techniques described in Section 3. The overview of the developed HRV signal processing tool is presented in Figure 21.

Figure 21 – Diagram overview of the developed heart rate variability analysis tool. The electrocardiogram (ECG) signal is pre-processed to extract the heart rate variability (HRV) signal. HRV analysis includes measures from the time domain, frequency domain, non-linear, and empirical mode decomposition (EMD) analysis. The photoplethysmography (PPG) signal is processed and combined with the HRV signal for the baroreflex sensitivity (BRS) analysis. The HRV tool is connected to a database for storing the processed data.

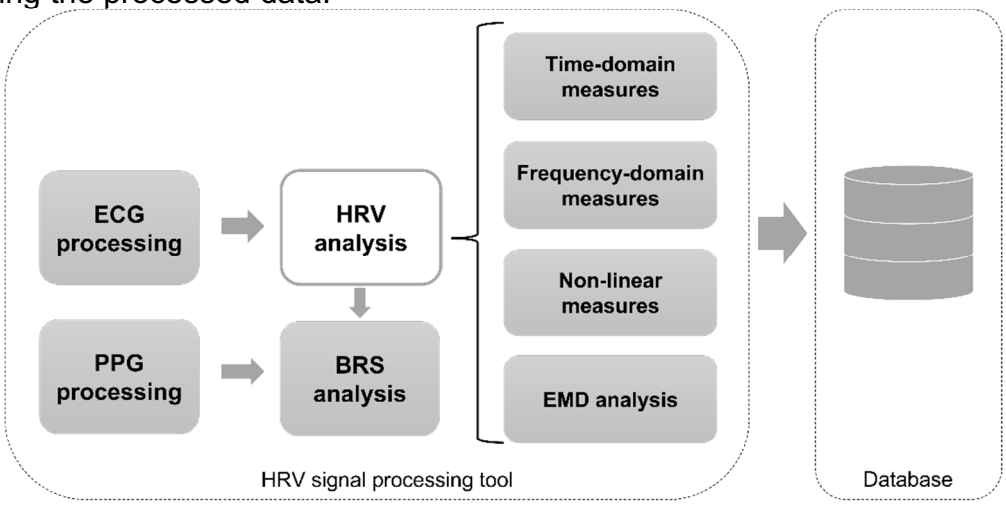

Source: Elaborated by the author.

4.2.2 Input and Data Pre-Processing

The HRV processing tool accepts ECG and PPG signals in .txt format. The signals' sampling frequency can be adjusted by setting one parameter (*e.g.*, 500 Hz or 1000 Hz).

The ECG pre-processing steps include: (a) baseline correction, mean subtraction to remove the DC offset from the signal and to centre the ECG waveform around the zero-axis, and (b) filtering, bandpass-filter (fourth-order Butterworth FIR filter, 0.5–40 Hz) to remove high-frequency noise, including power line interference and baseline wander.

The R peaks detection for extraction of the heart rate variability signal follows the ECG pre-processing. The RR intervals, characterized by the time between successive R peaks of the QRS complexes of the ECG signal, are detected and calculated based on Pan–Tompkin's algorithm (Pan; Tompkins, 1985). A specific RR interval (RR_n in seconds) within the ECG signal is defined as the interval of two successive QRS complexes determining the RR sequence: [RR_1, RR_2, …, RR_{n-1}] in seconds, and the heart rate (beats per minute) is given according to Equation 31.

$$\text{HR (bpm)} = \frac{60}{\text{RRn}} \tag{31}$$

The RR sequence is further processed to remove spurious peaks that are too close together (*i.e.*, gaps smaller than the sampling frequency) or too far (*i.e.*, gaps higher than 2 seconds) and RR intervals that change more than 20%, considering the median value of the previous five and next five intervals (Vest *et al.*, 2018). Finally, the corrected RR sequence (*i.e.*, the NN sequence) proceeds for HRV analysis (see section 4.2.3).

The PPG pre-processing steps are similar to the ECG including, (a) baseline correction, subtraction of the mean value from the PPG signal to remove baseline drift, and (b) filtering, bandpass-filter (fourth-order Butterworth FIR filter, 0.5–10 Hz). These pre-processing steps are essential to enhance the quality of both ECG and PPG signals, ensuring accurate and reliable data for further analysis. After pre-processing the PPG data, the next step involves detecting characteristic points in the PPG signal, such as the peaks and foot values. A sequence marking the foot values is then generated to be used as part of the BRS analysis (see section 4.2.4).

The ECG and PPG pre-processing algorithm is presented in the flowchart of Figure 22.

Figure 22 – The flowchart of the electrocardiogram (ECG) and photoplethysmogram (PPG) pre-processing steps.

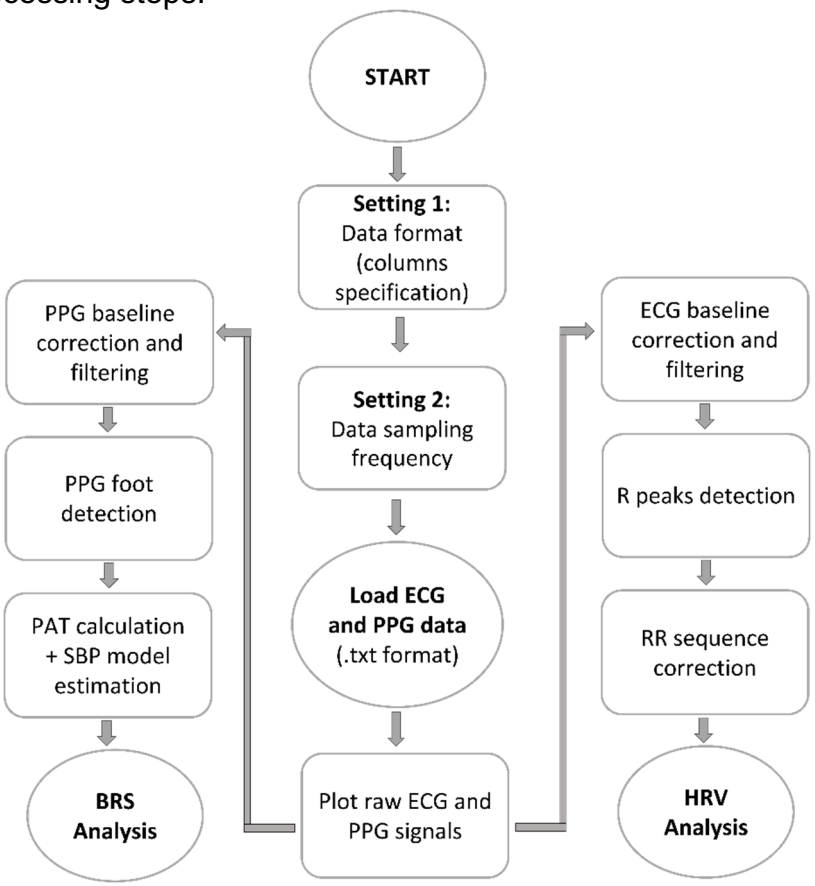

Abbreviations: HRV – heart rate variability, PAT – pulse arrival time, SBP – systolic blood pressure, and BRS – baroreflex sensitivity. Source: Elaborated by the author.

4.2.3 HRV Analysis

The HRV analysis comprises the computation of various HRV-based features. These include measures from both the time and frequency domains and nonlinear parameters. Additionally, it involves extracting features from the Empirical Mode Decomposition analysis.

From the time domain, some of the calculated parameters are the mean of NN intervals (NNmean), the standard deviation of all NN intervals (SDNN), root mean square of successive NN interval differences (RMSSD), number and percentage of differences between adjacent RR intervals that are longer than 50 ms (NN50 and pNN50, respectively), number and percentage of differences between adjacent RR

intervals that are longer than 20 ms (NN20 and pNN20, respectively), HRV triangular index (HTI), *i.e.*, integral of the density of the RR interval histogram divided by its height, triangular interpolation of NN interval histogram (TINN), *i.e.*, baseline width of the NN interval histogram and Baevsky's stress index (SI) (see section 3.1.1 for more details on HRV time-domain measures).

The frequency-domain measures rely on the power spectral density (PSD) estimation computed with Welch's and the Lomb-Scargle periodogram methods. The RR interval time series is an event time series, which can be interpreted as a hypothetical continuous function sampled unevenly in time at the moments of R peaks (Kamath; Watanabe; Upton, 2016). The Fourier transform assumes that the input data is sampled evenly in time; hence, FFT-based PSD estimate requires resampling to an evenly time series, and cubic spline interpolation is often preferred to linear interpolation because of the latter increases LF power (due to flattening) and HF power (due to sharp edges at each beat) (Vest *et al.*, 2018).

Welch's method is FFT-based so, the RR signal is resampled to 8 Hz, before applying Welch's method. The other parameters for Welch's method are the Hamming window function, window width of 300 points, 50% overlap between segments, and 1024 as the number of DFT points. On the other hand, the Lomb-Scargle periodogram can handle unevenly sampled data, making it a more appropriate analysis technique for the RR interval data since it provides a better PSD estimate (Clifford; Tarassenko, 2005).

After the PSD is calculated with the two cited methods, various frequency-domain HRV metrics will be calculated. The generalized frequency bands in the case of short-term HRV recordings are very low frequency (VLF, 0.003–0.04 Hz), low frequency (LF, 0.04–0.15 Hz), and high frequency (HF, 0.15–0.4 Hz). The frequency-domain measures extracted from the PSD estimated for each frequency band included absolute and relative powers of LF and HF bands, LF and HF band powers in normalized units, the LF/HF power ratio, and peak frequencies for each band (see section 3.1.2 for more details on the HRV frequency-domain measures).

In addition, the following methods were implemented to analyse the non-linear properties of HRV: Poincare plot (including the features SD1, SD2, S, SD1/SD2 or CSI and CVI), Correlation dimension (CD), Detrended fluctuation analysis (features $alpha_1$ and $alpha_2$), Approximate entropy (ApEn), Sample Entropy (SampEn), Multiscale entropy (MSE), Fuzzy entropy (FuzzyEn), Shannon entropy (ShEn), Permutation

entropy (PermEn) and Spectral entropy (SpEn) (see section 3.1.3 for more details on the HRV non-linear measures).

Finally, in the last module of the HRV processing tool, the HRV signals are decomposed using the EMD method, generating the intrinsic mode functions (IMFs). The processing tool analyses the HRV segments using the original EMD method outlined in (Huang *et al.*, 1998) with the official MATLAB code (R2018a, MathWorks, MA, USA). Custom code was implemented to compute the following features from the EMD-derived IMFs: the area of analytical signal representation (ASR_{area}), the second-order difference plot area ($SODP_{area}$), and the central tendency measure of the second-order difference plot ($SODP_{CTM}$). Furthermore, the features extracted after power spectral density estimation of the IMFs are peak amplitude (PSD_{pkamp}), band power (PSD_{bpow}), and mean frequency (PSD_{mfreq}) (see section 3.2 for more details on the EMD technique and its features).

Figure 23 illustrates a block diagram depicting the HRV and BRS analyses and outlining the feature extraction process.

Figure 23 – The block diagram of the heart rate variability (HRV) and baroreflex sensitivity (BRS).

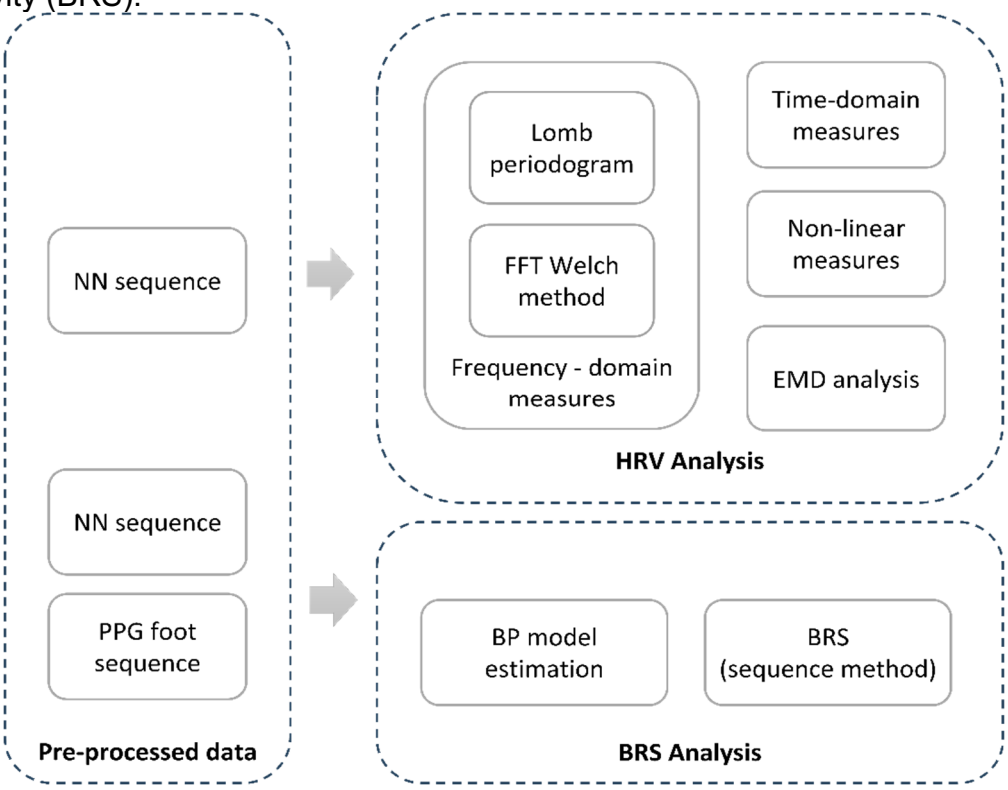

Abbreviations: NN sequence – RR interval corrected sequence. PPG – photoplethysmography, FFT – fast Fourier transform, EMD – empirical mode decomposition, BP – blood pressure.
Source: Elaborated by the author.

4.2.4 BRS Analysis

The BRS analysis includes two steps: (a) the blood pressure (BP) estimation obtained from the ECG (NN interval) and the PPG (foot sequence) and (b) the BRS calculated from the estimated systolic BP signal and the NN interval.

Firstly, the pulse arrival time is estimated (*i.e.*, the difference between the R peaks of the ECG and the PPG foot values – see Figure 8 in section 3.3), obtaining the PAT sequence. Secondly, the systolic blood pressure (SBP) model is estimated based on the study of Wong, Poon and Zhang (2009). Finally, from the estimated SBP model and the NN intervals, the BRS value is calculated using the sequence method, detailed in Figure 9 in section 3.3. From the accepted up-and-down sequences, some of the calculated parameters are the number of sequences selected, the number of up-and-down sequences, the mean and standard deviation of the up-and-down slopes, and the mean and standard deviation of all the sequences.

4.2.5 Database

A database is an organized collection of data, generally stored and accessed electronically from a computer system. The database management system (DBMS) is the software that interacts with end-users, applications, and the database to capture and analyse the data. Microsoft Access is a relational DBMS that models data as rows and columns in a series of tables, using SQL (structured query language) to write and query data.

The HRV processing tool in MATLAB is integrated with an Access Database, facilitating the transfer of processed data from MATLAB to the database. This centralized database is a repository for all participant-related data, encompassing clinical information, anthropometric measurements, questionnaire responses, and the various computed features extracted through the HRV processing tool.

The database is structured into several tables to manage and store the data efficiently. The main tables are:

- **Info Table -** contains information about each participant, such as their unique ID, name, age, gender, weight, height, DM type, age of DM diagnosis, DM duration, other relevant clinical details, and contact information;

- **Medications Table –** holds information regarding medications and their respective dosages;
- **Exams results Table –** holds information related to examination outcomes and blood test results;
- **Conditions Table –** stores information about the participant's medical conditions and associated complications;
- **DATA Table –** serves as the primary repository for all collected data information. It records which signals were collected, such as ECG, PPG, arterial blood pressure, and electromyography. Additionally, the table includes essential details such as the collection date, record time, and the sampling frequency for each data entry;
- **HRV Analysis –** contains information about all the calculated features derived from time and frequency domain measurements, as well as nonlinear measurements;
- **BRS Analysis –** comprises all the calculated features from the BRS analysis;
- **EMD Analysis –** comprises all the EMD extracted features.

The entity relationship diagram of the database's tables is demonstrated in Figure 24.

Figure 24 – The entity relationship diagram of the database.

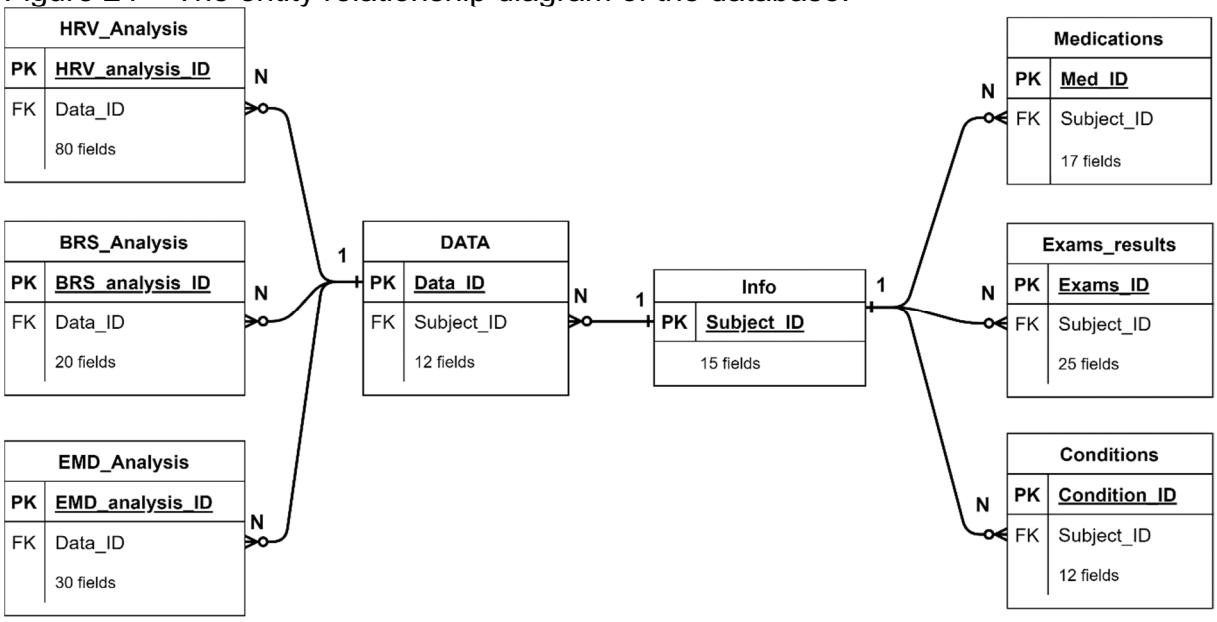

Abbreviations: PK – private key (unique identifier for each record in a database table); FK – foreign key (column in a database table that references the primary key of another table).
Source: Elaborated by the author.

During each analysis performed using the HRV processing tool in MATLAB, the calculated features for each sample are automatically written to their corresponding tables in the Access database, as represented in Figure 25. The processing tool maps the computed parameters to the appropriate entries in the database, ensuring that the data is accurately associated with the respective participant or sample. This integration between the processing tool and the database facilitates the efficient and accurate storage of HRV analysis results for further retrieval and analysis.

Figure 25 – The block diagram representing the connection between MATLAB's heart rate variability (HRV) processing tool and the Microsoft Access Database. The calculated parameters in MATLAB are inserted into the database table with an SQL function. Each data table column is a feature, and each line is a different sample.

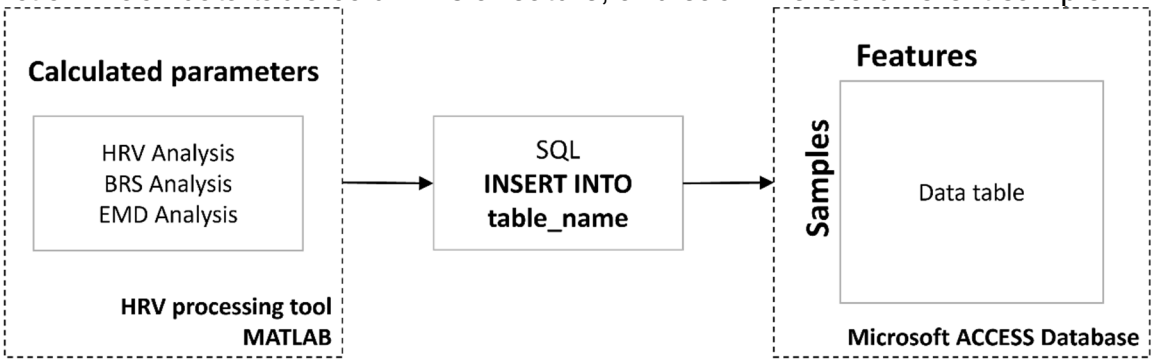

Source: Elaborated by the author.

4.2.6 Tool Validation

4.2.6.1 Participants

Twenty-five participants (10F / 15M) aged 32.2 ± 7.1 (mean ± SD) were recruited from the Professor Polydoro Ernany University Hospital of the Federal University of Santa Catarina—HU/UFSC/EBSERH. The inclusion criteria considered healthy individuals aged 18–75 years who exhibited no signs of any medical conditions. The institutional research ethics committee approved the study (protocol number 3.326.385), and participants only entered the study after informed consent. It is important to note that the researcher personally conducted the data collection process, ensuring a careful acquisition of information.

Initially, anthropometric data (including age, height, weight, and body mass index) were collected, along with administering a questionnaire to identify potential

medical conditions. Subsequently, resting ECG signals were acquired from participants for 10 minutes, during which they maintained a supine position. These ECG signals were captured using a custom-built acquisition system developed by the Institute of Biomedical Engineering at the Federal University of Santa Catarina. The system operates at a sampling rate of 500 Hz and employs a bipolar three-lead configuration. This setup utilizes disposable adhesive electrodes (3M, Red Dot, 2560) for electrode placement.

4.2.6.2 Statistical Analysis

The HRV processing tool was validated to ensure its accuracy and reliability. This validation was performed by comparing nineteen of the calculated HRV measurements with those obtained from Kubios HRV Standard 3.5.0, a scientifically validated HRV analysis software (Tarvainen et al., 2014).

After the HRV signals were extracted from the twenty-five collected ECG recordings, the subsequent features were derived: (a) from time-domain: NN mean, SDNN, RMSSD, pNN50, HTI, and TINN; (b) from frequency-domain: VLF power, LF power, HF power, LF/HF, LF norm and HF norm and; (c) from the non-linear analyses: SD1, SD2, SD2/SD1, SampEN, ApEN, DFA α_1 and DFA α_2. These features are explained in section 3.1. Both software used Welch's power spectrum estimation method for frequency domain analysis, with segment size set to 300s and 50% overlap. No artefact correction nor any preprocessing method was applied to the signals. The validation included statistical analyses with the Intraclass Correlation Coefficient (ICC) calculation and Bland-Altman plots.

When measuring continuous data, the ICC assesses the consistency or agreement between multiple raters or methods. It considers systematic variation (*i.e.*, biases) and random variations (*i.e.*, errors or uncertainties) between the measurement methods. ICC values range from 0 to 1, with higher values indicating better agreement (Koo; Li, 2016; Liljequist; Elfving; Roaldsen, 2019). According to Koo and Li (2016), an ICC interpretation is presented in Table 7.

Table 7 – The intraclass correlation coefficient (ICC) interpretation.

ICC	Interpretation
<0.5	Poor agreement
0.5 to 0.75	Moderate agreement
0.75 to 0.9	Good agreement
0.9 to 1.0	Excellent agreement

Source: KOO; LI (2016).

The Bland-Altmann method is a method to assess the agreement between two continuous measurement methods by constructing limits of agreement. This method involves plotting the difference between measurements against their average, allowing for visualization of any systematic bias or variability (Bland; Altman, 1999; Karun; Puranik, 2021; Sedgwick, 2013). The steps to construct a Bland-Altmann plot, according to Karun and Puranik (2021), include (1) calculation of the difference between the measurements of method one and method two (*e.g.*, the developed HRV tool and the Kubios software); (2) calculation of the mean of the measurements of method one and method two and; (3) calculation of the lower and upper limits of agreement as mean of difference ± 1.96 x standard deviation of difference. An example of a Bland-Altmann plot is presented in Figure 26.

Figure 26 – The Bland-Altmann plot.

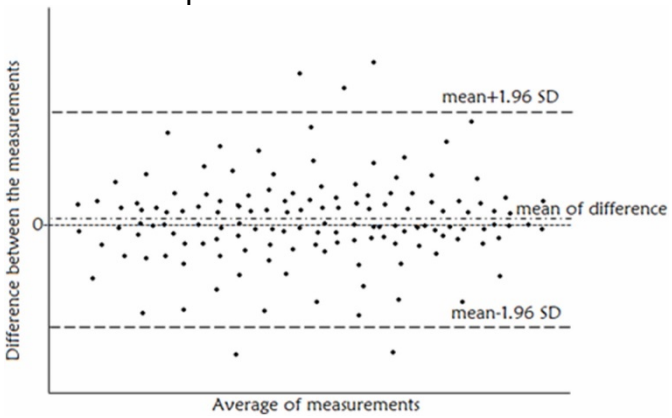

Source: Elaborated by the author.

The calculation of Intraclass Correlation Coefficients (ICC) and their corresponding 95% confidence intervals followed an absolute-agreement model for a single measure (*i.e.*, when systematic differences between methods are relevant and where a single measure of a single method is considered). The Bland-Altmann method

was calculated based on an R function (*i.e.*, BA.plot) provided by Karun and Puranik (2021). The statistical analyses were performed using R 4.2.0 (R Core Team, 2022).

4.3 RESULTS

This section presents some of the results (data and graphs) generated by the developed HRV processing tool and its validation results.

4.3.1 HRV Analysis

Figures 27 to 31 present the HRV initial analysis steps: (a) the ECG pre-processed with the baseline corrected and filtered (Figure 27); (b) the R peaks detection (Figure 28); (c) the heart rate obtained from the RR intervals (Figure 29); (d) the RR correction obtaining the NN sequence (Figure 30), and; (e) the NN intervals histogram (Figure 31).

Figure 27 – The electrocardiogram (ECG) signal after detrending and filtering using a finite impulse response (FIR) bandpass filter with cut-off frequencies set at 0.5 and 45 Hz.

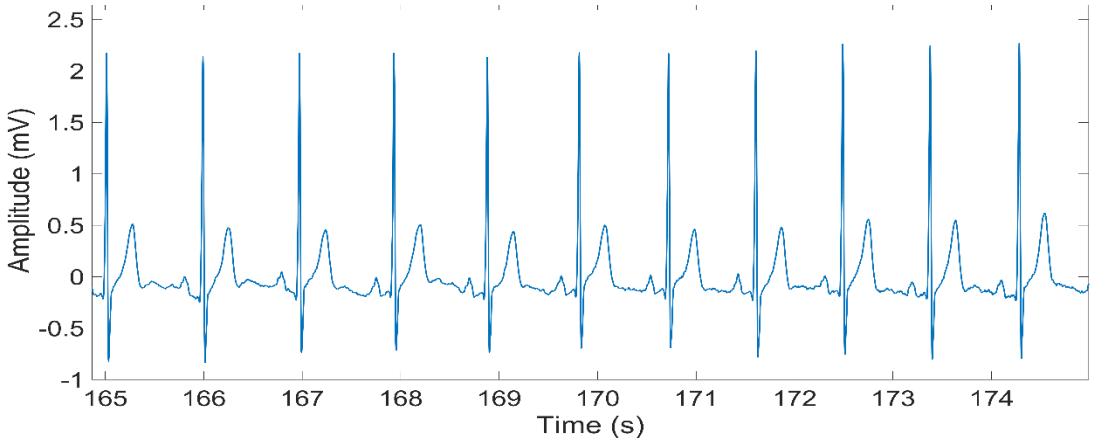

Source: Elaborated by the author.

Figure 28 – The electrocardiogram (ECG) signal with the identified R peaks.

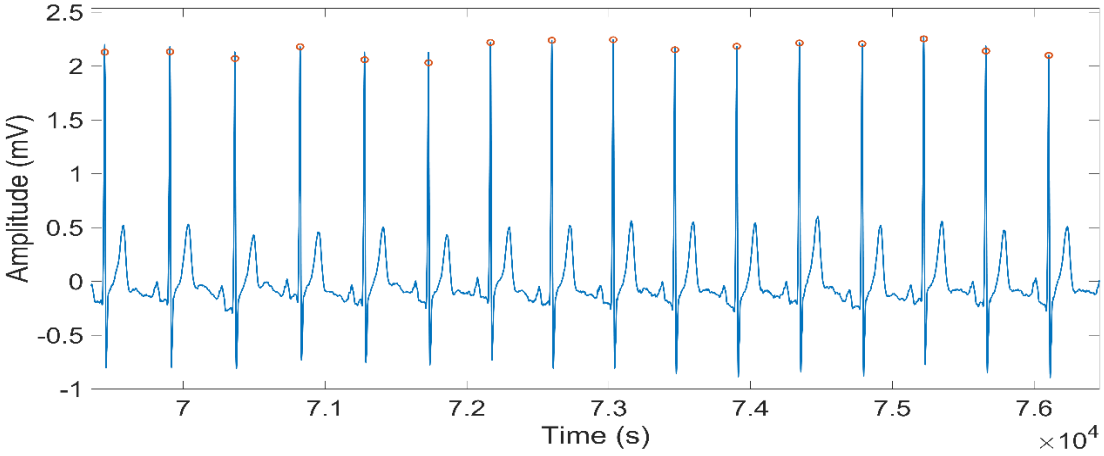

Source: Elaborated by the author.

Figure 29 – The heart rate, measured in beats per minute (bpm), derived from the calculated RR intervals.

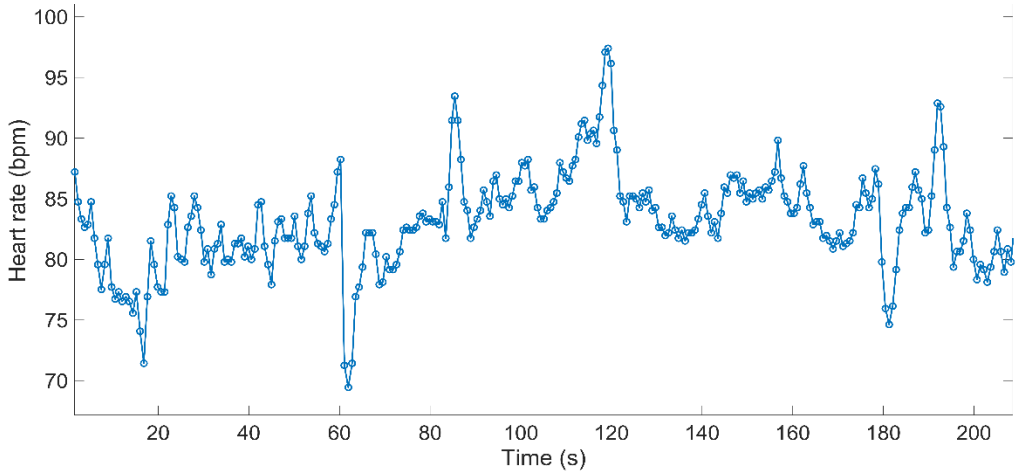

Source: Elaborated by the author.

Figure 30 – The original RR interval (blue line) and the corrected RR interval or NN sequence (red line).

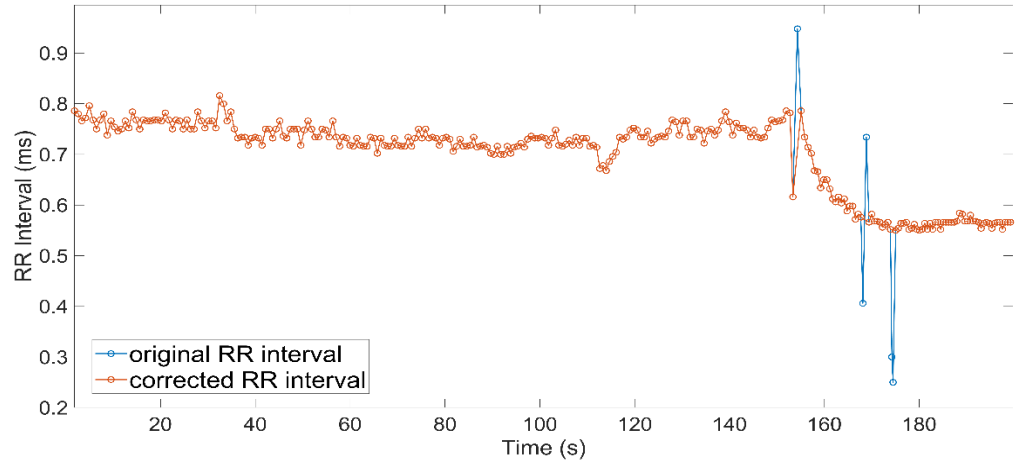

Source: Elaborated by the author.

Figure 31 – The NN intervals histogram.

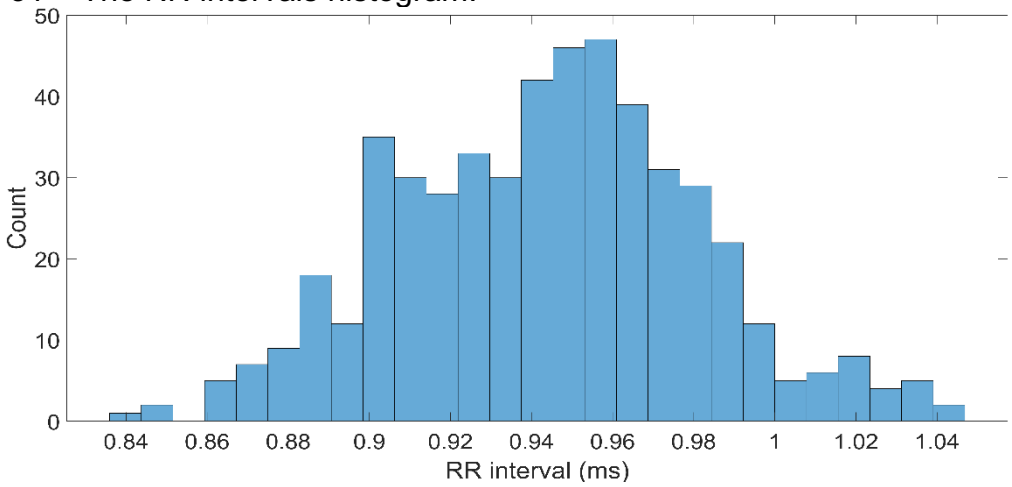

Source: Elaborated by the author.

Figures 32 to 36 present the subsequent HRV analysis steps: (a) Spectral analysis of HRV using the FFT-based Welch's periodogram method (Figure 32); (b) Spectral analysis of HRV using the Lomb periodogram method (Figure 33); (c) the Poincaré plot (Figure 34); (d) the result of the EMD applied to HRV signals (Figure 35) and; (e) the power spectral density of the EMD-derived components (Figure 36).

Figure 32 - Spectral analysis of HRV using the FFT-based Welch's periodogram method.

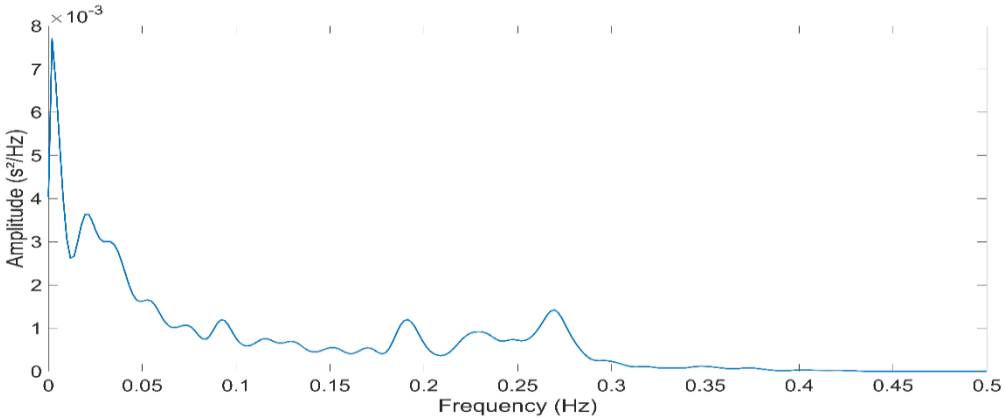

Source: Elaborated by the author.

Figure 33 - Spectral analysis of HRV using the Lomb periodogram method

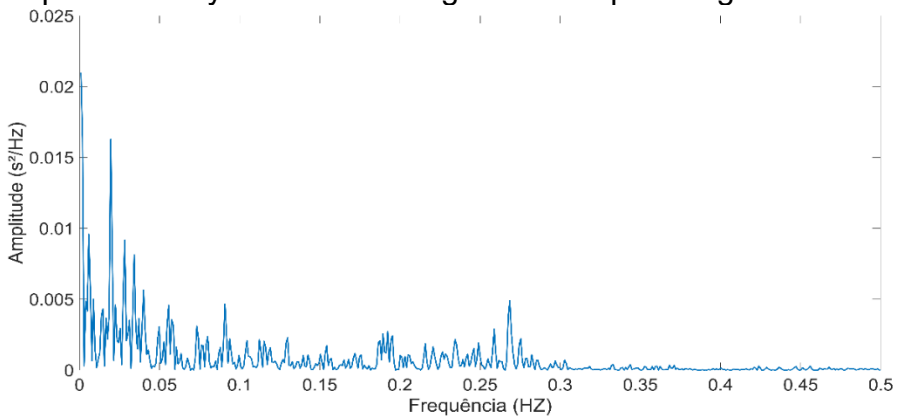

Source: Elaborated by the author.

Figure 34 – The Poincaré plot.

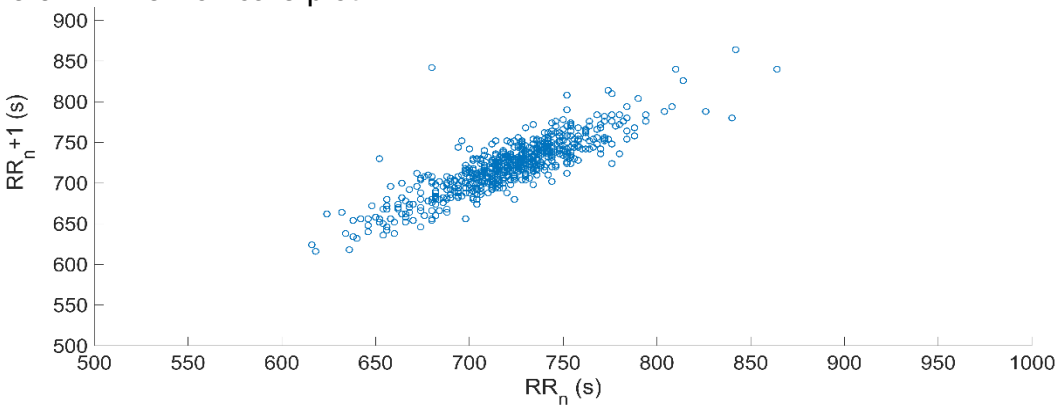

Source: Elaborated by the author.

Figure 35 - The first four intrinsic mode functions (IMFs) and the residual derived from the empirical mode decomposition applied to a heart rate variability signal. The plot at the top depicts the original RR interval data. In all plots, the x-axis denotes time in seconds, while the y-axis represents the amplitude of RR intervals.

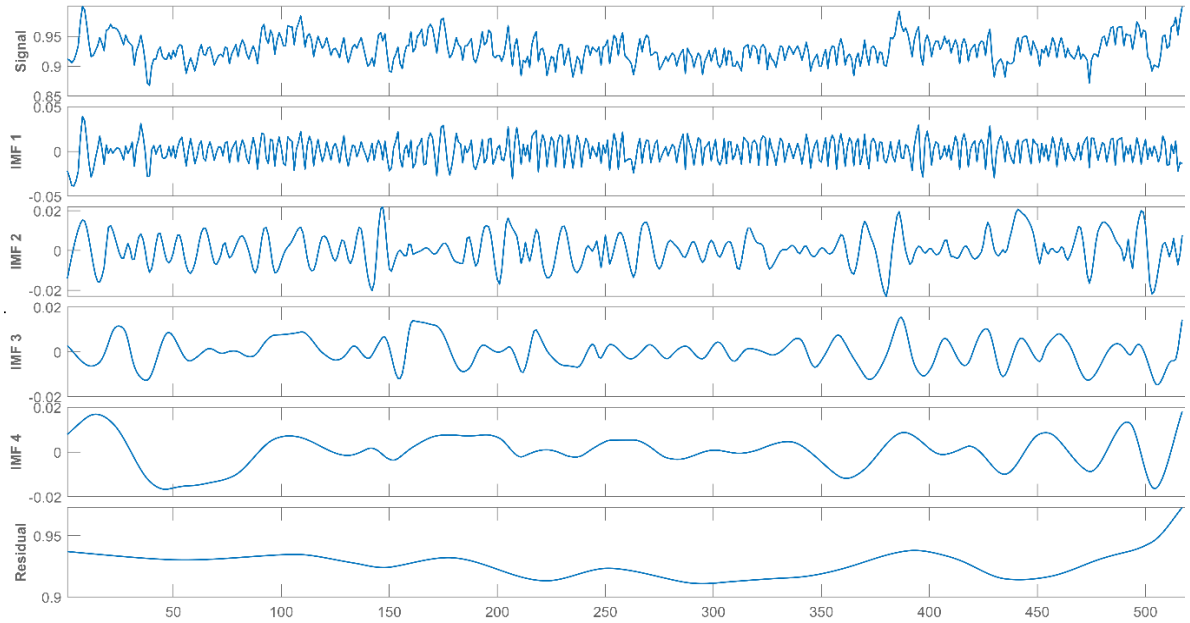

Source: Elaborated by the author.

Figure 36 – The power spectral density estimation of the intrinsic mode functions (IMFs) derived from the empirical mode decomposition of a heart rate variability signal.

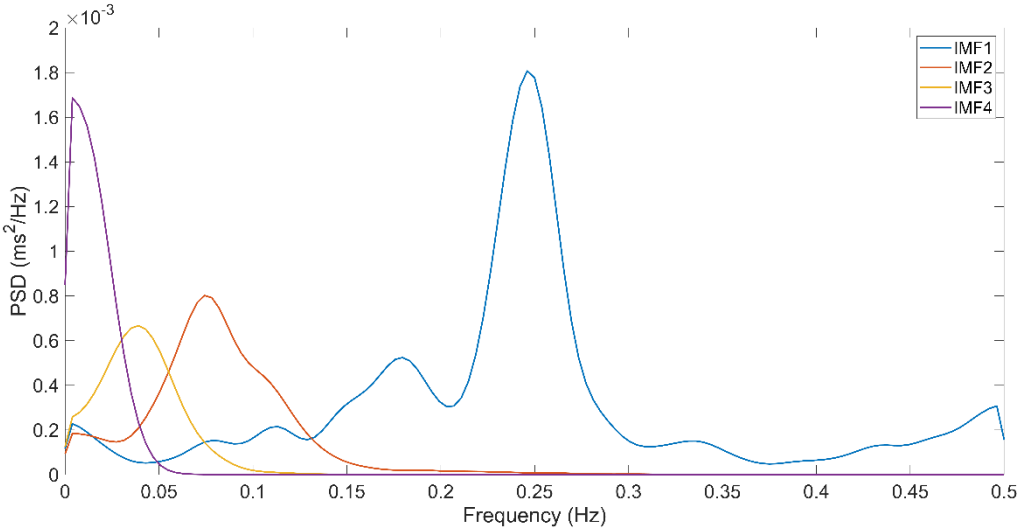

Source: Elaborated by the author.

4.3.2 BRS Analysis

Figures 37, 38, and 39, respectively, present the BRS analysis steps: (a) the ECG and PPG pre-processing obtaining the NN sequence and the PPG foot sequence for calculation of the pulse arrival time; (b) the estimation of blood pressure variations over time and; (c) the BRS calculation which relies on the up and down sequences derived from the NN interval and systolic blood pressure variations.

Figure 37 – Plot of the electrocardiogram (ECG) and photoplethysmogram (PPG) filtered signals, along with the marked ECG peaks and PPG feet points used to calculate the pulse arrival time.

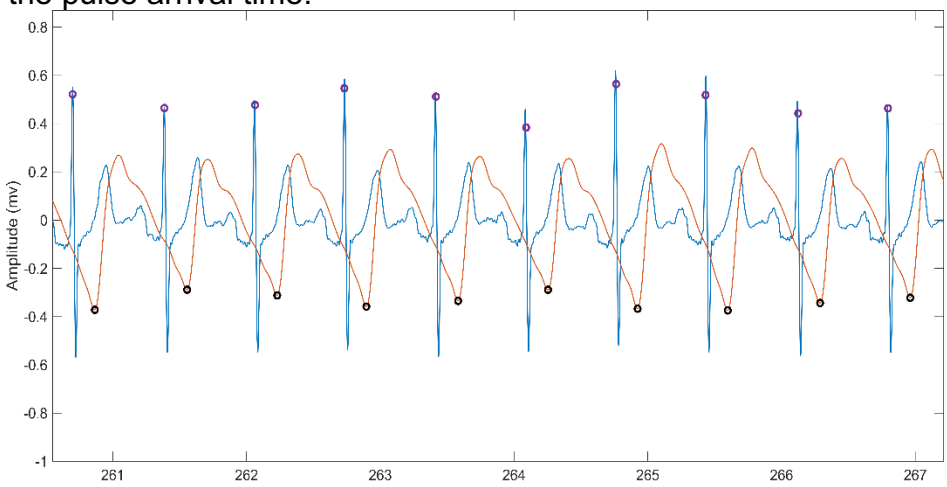

Source: Elaborated by the author.

Figure 38 - The model generated the blood pressure (BP) variation over time. The upper line (blue) represents the systolic BP, while the middle line (black) represents the diastolic BP. The bottom line corresponds to the mean arterial pressure.

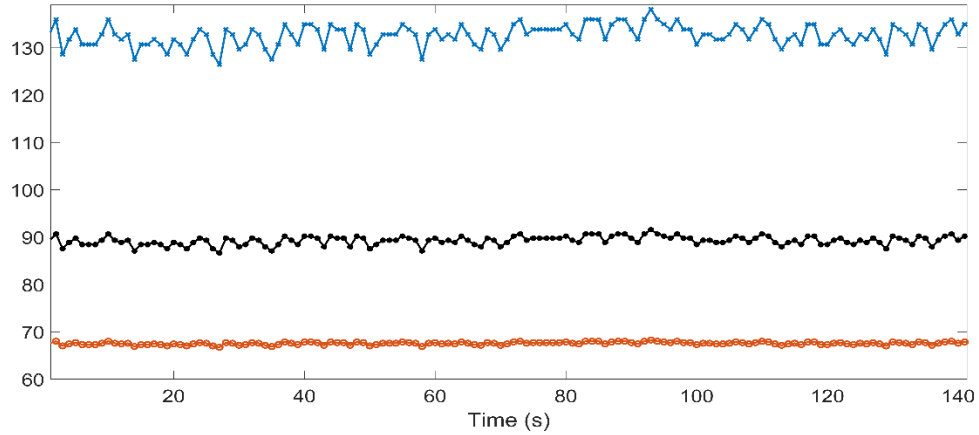

Source: Elaborated by the author.

Figure 39 – Measurement of baroreflex sensitivity (BRS) from positive sequences (red lines with increasing systolic blood pressure and RR interval) and negative sequences (blue lines with decreasing systolic blood pressure and RR interval).

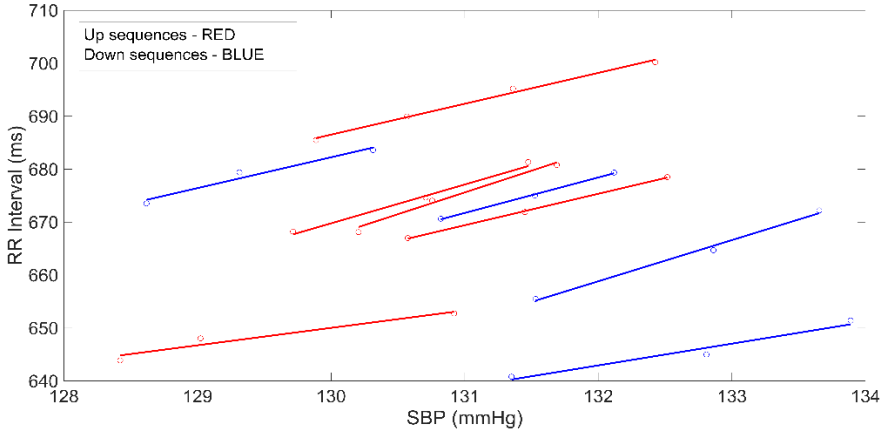

Source: Elaborated by the author.

4.3.3 Tool Validation

The ICC results are presented in Table 8. It is worth highlighting that most of the calculated HRV features exhibited ICC values above 0.9, with two features (TINN and LF power) above 0.8 and one feature (DFA α_2) resulting in an ICC of 0.67.

Table 8 – The intraclass correlation coefficient (ICC) results for the HRV analysis features measured using both the developed HRV tool and Kubios software.

		F test with true value 0			
Measurement	**ICC** (95% C.I.)	Value	*df1*	*df2*	**p-value**
NN mean	**1** (1-1)	2.3e+08	24	25	<0.001
SDNN	**1** (1-1)	3.98e+08	24	25	<0.001
RMSSD	**1** (1-1)	1.46e+08	24	25	<0.001
pNN50	**0.995** (0.99 – 0.998)	433	24	25	<0.001
HTI	**0.935** (0.86 – 0.971)	29.8	24	25	<0.001
TINN	**0.846** (0.686 – 0.929)	12	24	25	<0.001
VLF power	**0.956** (0.903 – 0.98)	44.2	24	25	<0.001
LF power	**0.852** (0.696 – 0.932)	12.5	24	25	<0.001
HF power	**0.982** (0.959 – 0.992)	108	24	25	<0.001
LF/HF	**0.994** (0.986 – 0.997)	324	24	25	<0.001
LF norm	**0.969** (0.932 – 0.986)	63.3	24	25	<0.001
HF norm	**0.969** (0.932 – 0.986)	63.4	24	25	<0.001
SD1	**1** (1-1)	1.42e+08	24	25	<0.001
SD2	**0.994** (0.986 – 0.997)	309	24	25	<0.001
SD2/SD1	**0.999** (0.998 – 1)	2752	24	25	<0.001
SampEN	**0.947** (0.884 – 0.976)	36.5	24	25	<0.001
ApEN	**0.906** (0.802 – 0.957)	20.4	24	25	<0.001
DFA α_1	**0.957** (0.905 – 0.98)	45	24	25	<0.001
DFA α_2	**0.677** (0.397 – 0.843)	5.19	24	25	<0.001

Source: Elaborated by the author.

The Bland-Altman method was used to plot the difference in the HRV features for each participant (the HRV processing tool measurement minus Kubios HRV measurement) against the mean of the two measurements. Figures 40, 41, and 42 showcase Bland-Altmann plots for various features across time domain, frequency domain, and non-linear analysis. Notably, upon observing the graphs, it becomes evident that a significant proportion of data points within the Bland-Altman plots depicting HRV features keep to the limits of agreement.

Figure 40 – The Bland-Altman plots comparing heart rate variability features extracted from the time domain, measured using the developed HRV tool and Kubios software. (a) NN mean (the mean of NN intervals), (b) SDNN (the standard deviation of NN intervals), (c) HTI (HRV triangular index; integral of the density of the RR interval histogram divided by its height), and (d) TINN (Triangular interpolation; baseline width of the NN interval histogram).

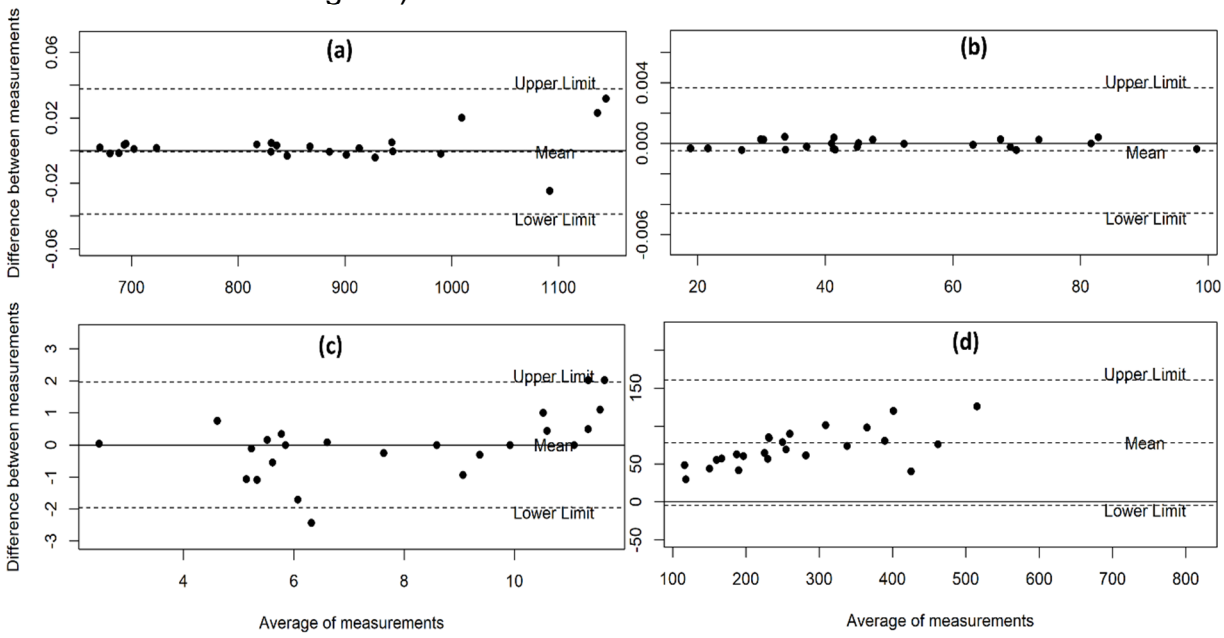

Source: Elaborated by the author.

Figure 41 – The Bland-Altman plots comparing heart rate variability features extracted from the frequency domain, measured using the developed HRV tool and Kubios software. (a) VLF power (the absolute power of the very-low-frequency band – 0.003 to 0.04 Hz), (b) LF power (the absolute power of the low-frequency band – 0.04 to 0.15 Hz), (c) HF power (the absolute power of the high-frequency band – 0.15 to 0.40 Hz), and (d) LF/HF (the ratio of LF to HF power).

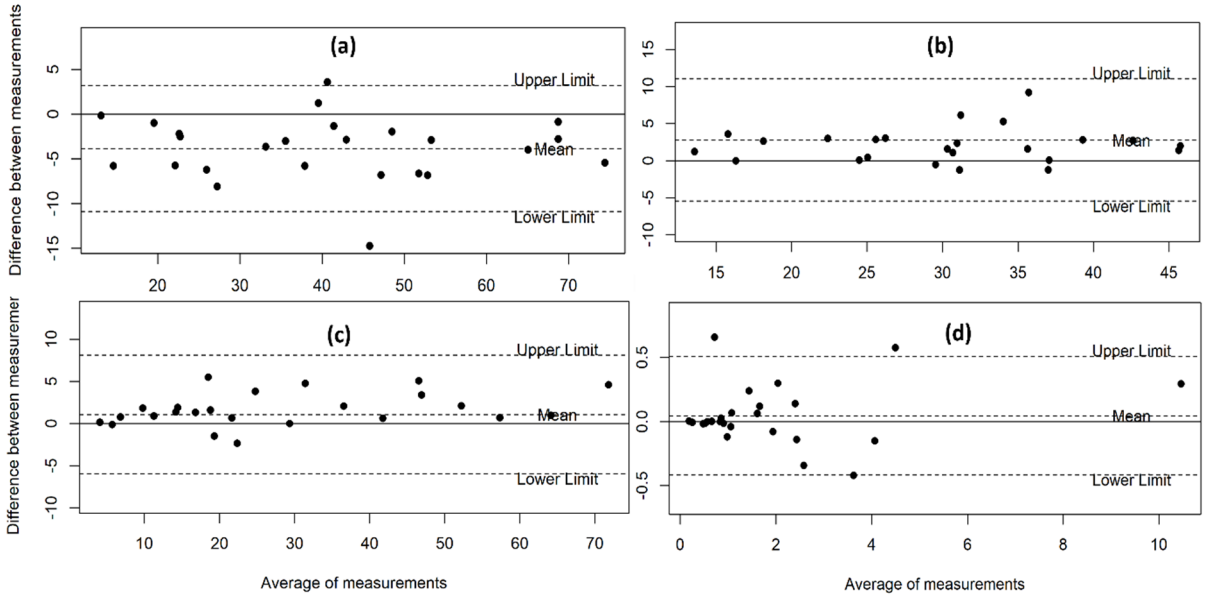

Source: Elaborated by the author.

Figure 42 – The Bland-Altman plots comparing nonlinear heart rate variability features measured with the developed HRV tool and Kubios software. (a) SD2/SD1 (Poincaré plot ratio), (b) SampEN (sample entropy), (c) ApEN (approximate entropy), and (d) DFA α_1 (slope α_1 from the detrended fluctuation analysis).

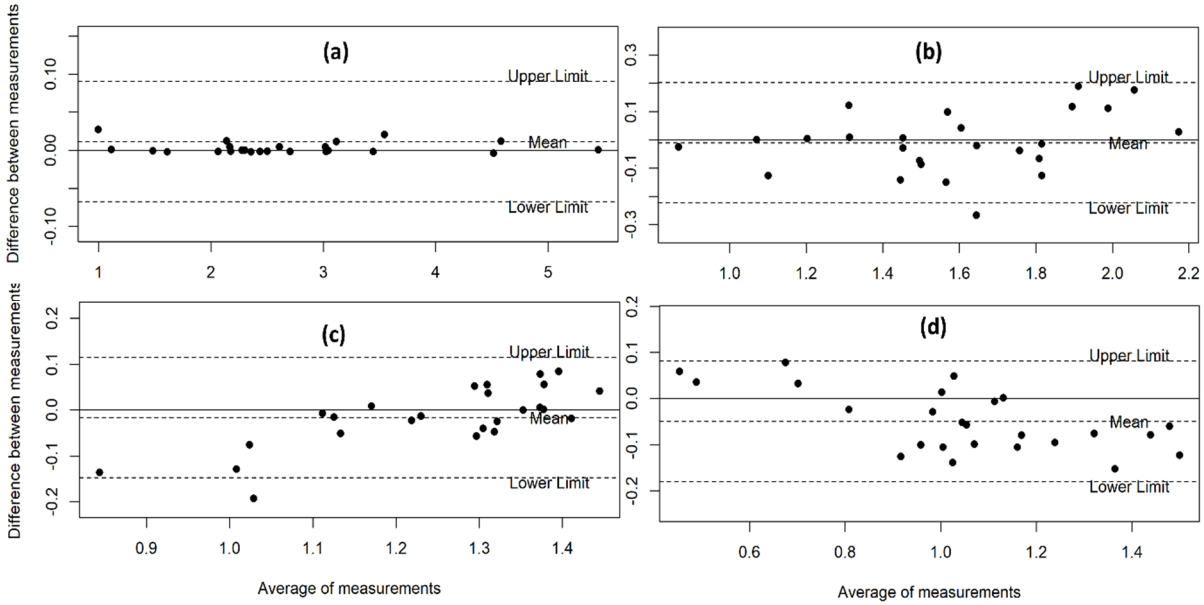

Source: Elaborated by the author.

4.4 DISCUSSION AND CONCLUSION

The HRV tool demonstrated in this section was primarily developed as a custom solution for ECG analysis. It includes the computation of essential HRV features and integrates PPG analysis to facilitate the BRS assessment. Additionally, the tool features a module for the empirical mode decomposition analysis and is connected to a database, facilitating data analysis. The studies outlined in this work (sections 5 and 6) utilized the developed HRV tool, demonstrating its usability and adaptability. This includes the flexibility to adjust feature units, include new features or methods, and format data outputs according to the study requirements.

Regarding the validation of the software, the interpretation of the Bland-Altmann plots provides an understanding of the agreement between the two measurement methods, namely the developed HRV tool and the Kubios software, for assessing heart rate variability features. Most data points on the Bland-Altman plots fall within the limits of agreement, indicating a strong consistency between the two measurement methods.

This is reflected in the high ICC values, predominantly exceeding 0.9, indicating an excellent agreement between the two approaches. Notably, for two features (the LF

power and TINN), the ICC values were above 0.8, still indicating a good agreement between the methods. Lastly, one feature (DFA α_2) exhibited an ICC of 0.67, which suggests a moderate level of agreement. While still indicating an acceptable level of agreement, this result warrants further investigation to understand potential sources of variability or measurement differences specific to this feature extracted from the detrended fluctuation analysis.

To conclude, the Bland-Altman plots, in conjunction with the ICC values, demonstrated the overall consistency between the developed HRV tool and Kubios software across various HRV features. These results suggest that the developed software is accurate and reliable for computing HRV-based features.

5 FIRST STUDY

This section presents the first study of this work entitled **"The Use of Empirical Mode Decomposition on Heart Rate Variability Signals to Assess Autonomic Neuropathy**" (Cossul *et al.*, 2023).

5.1 OBJECTIVE

This research investigated the relevance of the EMD-based features extracted from HRV signals to differentiate between progression levels of cardiovascular autonomic neuropathy among type 2 DM patients (*i.e.*, no CAN, subclinical CAN, and established CAN).

5.2 MATERIAL AND METHODS

A block diagram of our proposed methodology for CAN investigation based on the EMD method applied to HRV signals is presented in Figure 43 and will be further explained in the following sections.

5.2.1 Participants

An a priori sample size estimation was performed in G*Power (Erdfelder *et al.*, 2009), assuming a statistical power of 0.80 and a significance level of 0.05. For a one-way ANOVA with three groups and a moderate effect size (Cohen's d = 0.05), the study required a minimum sample size of 42 participants. However, to ensure robustness and address potential limitations, sixty participants diagnosed with type 2 DM were recruited from Professor Polydoro Ernany University Hospital of the Federal University of Santa Catarina—HU/UFSC/EBSERH (see Table 9). The inclusion criteria specified that participants were 18–75 years old and of any gender. The exclusion criteria included the diagnosis of retinopathy, chronic infectious or inflammatory diseases, use of an implantable electronic device (*e.g.*, a cardiac pacemaker), and use of drugs that can affect cardiovascular function (*e.g.*, beta-blockers). The institutional research ethics committee approved the study (protocol number 3.326.385 – Attachment A), and participants only entered the study after informed consent. It is important to note

that the researcher personally conducted the data collection process, ensuring a careful acquisition of information.

Figure 43 - A block diagram illustrating the proposed methodology for investigating cardiovascular autonomic neuropathy (CAN) in individuals with type 2 diabetes mellitus (T2DM) through the application of empirical mode decomposition (EMD) to heart rate variability (HRV) signals. The participants' electrocardiogram (ECG) and photoplethysmography (PPG) signals were collected. In the pre-processing stage, the ECG signals underwent bandpass filtering, followed by the derivation of the HRV signals. The feature extraction stage involved applying EMD to the HRV signals to obtain the first four intrinsic mode functions (IMFs) components. From these IMFs, the following features were calculated: ASR_{area} - area of the analytical signal; $SODP_{area}$ - area of the second-order difference plot; $SODP_{CTM}$ - the central tendency measure of the second-order difference plot; PSD_{pkamp} - peak amplitude of the power spectral density estimation; PSD_{bpow} - band power of the power spectral density estimation; and PSD_{mfreq} - mean frequency of the power spectral density estimation. The final stage involved conducting the statistical analysis to compare the mean differences of all the features among the different CAN severity level groups: noCAN - individuals with T2DM without CAN; subCAN - individuals with T2DM and subclinical CAN; and estCAN - individuals with T2DM and established CAN. The PPG signal was used for CAN classification purposes.

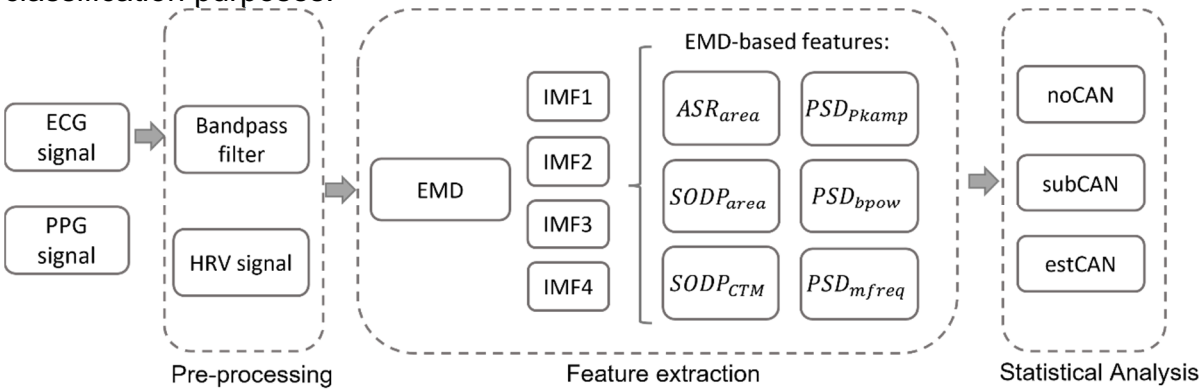

Source: Data from (Cossul *et al.*, 2023).

Table 9 – Demographic and clinical data of the participants.

	noCAN	**subCAN**	**estCAN**
n	20	20	20
Age (yrs)	60.1 ± 4.5	62.0 ± 7.0	57.0 ± 8.4
Gender	7F/13M	12F/8M	10F/10M
DM duration (yrs)	13.2 ± 9.5	13.9 ± 9.8	17.6 ± 9.3
HbA1c (mmol/mol)	89 ± 22	71 ± 31	99 ± 19

Note: Values are presented as mean ± SD. Abbreviations: DM - diabetes mellitus; noCAN - individuals with type 2 DM without cardiac autonomic neuropathy; subCAN - individuals with type 2 DM with subclinical cardiac autonomic neuropathy; estCAN - individuals with type 2 DM and established cardiac autonomic neuropathy; HbA1c - glycated haemoglobin. Source: Data from (Cossul *et al.*, 2023).

The anthropometric and clinical data (*e.g.*, age, DM duration, use of medications, presence of complications, and the last results of the glycated haemoglobin (HbA1c) test—a blood test that shows the average blood sugar (glucose) level over the past two to three months) were obtained from previous ECG and photoplethysmography (PPG) data. The participants were given cardiac autonomic reflex tests (CARTs) and baroreflex sensitivity (BRS) analyses to classify them into three levels of CAN (*i.e.*, noCAN—no presence of CAN, subCAN—subclinical CAN, and estCAN—established CAN). The CARTs comprised tests for heart rate response, including the RR interval to paced breathing, the Valsalva manoeuvre, and postural change from lying to standing (Fisher; Tahrani, 2017). The standardized CARTs used in this study are the gold standard method recommended for CAN assessment in patients with diabetes (Vinik *et al.*, 2018). Furthermore, BRS is a quantitative description of the arterial baroreflex, a critical determinant of the neural regulation of the cardiovascular system, relying on the analysis of spontaneous fluctuations of beat-by-beat arterial pressure and cardiac interval (Borowik *et al.*, 2015). BRS is a sensitive indicator of CAN in type 2 DM (Borowik *et al.*, 2015; Kück *et al.*, 2020) and an accurate screening tool for staging CAN, even in the subclinical phase when the usual clinical tests do not detect alteration due to the absence of overt symptoms (Petry; Marques; Marques, 2020). Further details about the BRS analysis can be obtained in section 3.3.

The CARTs were performed according to the O'Brien tests (O'Brien; O'Hare; Corrall, 1986), based on Ewing (Ewing; Campbell; Clarke, 1980), and incorporated a composite score (CS). The CARTs were evaluated as normal (*i.e.*, CS up to 1) or abnormal (*i.e.*, CS greater than 2). For the BRS analysis, two steps were performed: (i) an estimation of systolic blood pressure (SBP) from ECG and PPG signals based on a model proposed by Rajala, Lindholm, and Taipalus (2018) and (ii) a BRS value estimation from the estimated SBP and the RR intervals based on the sequence method (Kuusela, 2013). The mean values of BRS were compared against age-adjusted reference values to determine normal or abnormal results (Kardos *et al.*, 2001; Tank *et al.*, 2000). Subsequently, the noCAN group was defined when the CARTs and BRS analysis were considered normal, and the subCAN group was defined when the CARTs were normal and the BRS analysis was abnormal. Finally, estCAN was defined when the CART and BRS results were abnormal.

5.2.2 ECG and PPG Recording and Processing

The participants were asked to lie in a comfortable position. Three disposable adhesive electrodes (3M, Red Dot, 2560) were positioned following the bipolar derivation for ECG recording. The PPG sensor was positioned on the index finger, and the cuff for measuring blood pressure (model Omron HEM-712) was placed on the left arm, opposite the PPG sensor, as illustrated in Figure 44.

Figure 44 – The protocol illustration for ECG, PPG, and blood pressure data collection.

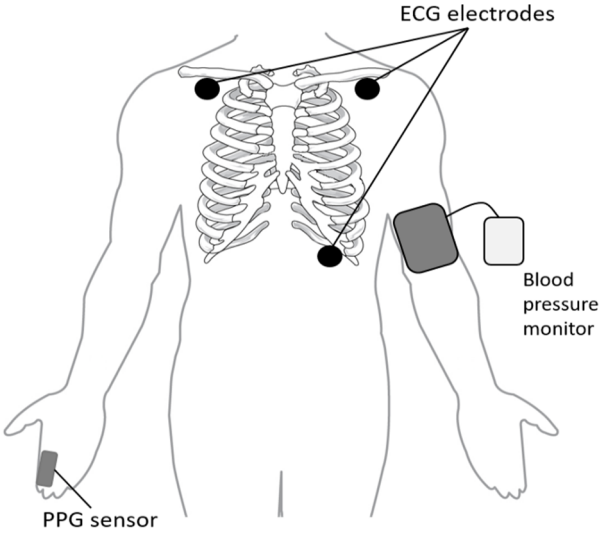

Source: Elaborated by the author.

The ECG and PPG signals were recorded using a custom-made acquisition system developed by the Federal University of Santa Catarina's Institute of Biomedical Engineering with a sampling frequency of 500 Hz. The data collection protocol started allowing the subject to rest for ten minutes. This initial phase establishes a baseline assessment unaffected by motion or external factors, ensuring a dependable basis for consistently comparing subjects. Following this, the data collection proceeded as follows, according to the CARTs protocol described in section 2.4.1:

1. **Resting**

   The participant lies supine quietly, without sleeping, for 10 minutes while ECG and PPG signals are recorded.

2. **Blood Pressure measurement**

   The blood pressure was measured with the participant lying.

3. **HR response to Deep Breathing**

The participant was instructed to breathe deeply at six breaths a minute (*i.e.*, five seconds in and five seconds out). The data collection software emits informative and correctly paced sounds to help the participant regulate breathing.

4. **HR response to Valsalva Manoeuvre**

The participant was asked to blow into a mouthpiece connected to a manometer (digital), hold a pressure of 40 mmHg for 15 seconds, and then breathe normally for 45 seconds.

5. **Immediate HR response to Standing**

With the participant lying, the PPG and ECG signals were continuously measured for approximately 10 seconds; the participant was then asked to stand up unaided, and the recording continued for one more minute.

6. **Blood Pressure measurement**

The blood pressure was measured about a minute after the participant stood.

After data collection, the ECG signal proceeded to data processing. The ECG signals were bandpass-filtered (fourth-order Butterworth FIR filter, 0.5–40 Hz) to remove high-frequency noise, including power line interference and baseline wander. Subsequently, the RR intervals between successive R peaks of QRS complexes were detected and calculated based on Pan-Tompkin's algorithm (Pan; Tompkins, 1985). Lastly, the RR sequence was inspected to remove spurious RR peaks where the RR intervals changed more than 20% within a median value window of the following five and the previous five RR intervals (Vest *et al.*, 2018). The corrected HRV signals proceeded for analysis (see section 4, which describes the HRV signal processing tool).

5.2.3 Feature Extraction

The HRV segments were analysed using the original EMD method outlined in Huang et al. (1998) with the official MATLAB (R2018a, MathWorks, MA, USA) EMD algorithm for the component's derivation. Then, custom software was created in MATLAB to extract features from the EMD modes, including the area of the analytical signal (ASR_{area}), the area of the second-order difference plot ($SODP_{area}$), the central

tendency measure of the second-order difference plot ($SODP_{CTM}$), and the features extracted after power spectral density estimation: peak amplitude (PSD_{pkamp}), band power (PSD_{bpow}), and mean frequency (PSD_{mfreq}).

Further details of the EMD technique and the extracted features are delineated in Section 3 – Methods, while the developed MATLAB HRV Processing Tool is described in Section 4 – HRV signal Processing Tool.

5.2.4 Statistical Analysis

A one-way analysis of variance (ANOVA) was conducted to compare mean differences between CAN severity level groups (*i.e.*, noCAN, subCAN, and estCAN). The homogeneity of variances and the normality assumptions were verified through Levene's test and Shapiro–Wilks's test, respectively. As a result of the non-normal distribution, variables were log-transformed to perform the analysis. Pairwise multiple comparisons were performed with Tukey (equal variances assumed) or the Games–Howell test for unequal variances. The results are shown as mean ± standard deviation, and the significance level of 0.05 was adopted. The statistical analysis was performed with R 4.2.0 (R Core Team, 2022).

5.3 RESULTS

The results of the Shapiro–Wilk test of normality indicate that the distributions were non-normal for the variables ASR_{area}, $SODP_{area}$, $PSD_{pkamp,}$ and PSD_{bpow} while the variables $SODP_{CTM}$ and PSD_{mfreq} were normally distributed. The same results were observed for the four IMF components of each feature. The results of Levene's homogeneity of variances test indicate equal variances for all features except for the $SODP_{CTM}$ of the 1st, 2nd, and 4th IMF components.

A representative illustration of the resulting EMD applied to decompose the RR interval signal in a subject with no diagnosis of CAN is illustrated in Figure 45. The top row shows the original RR interval signal. The following rows demonstrate the first four IMFs and the residual component. As expected, the higher the IMF index, the lower its frequency content.

Figure 45 - The first row represents the original RR interval signal, followed by its first four intrinsic mode functions and the residual obtained after empirical mode decomposition from a subject with no diagnosis of cardiovascular autonomic neuropathy.

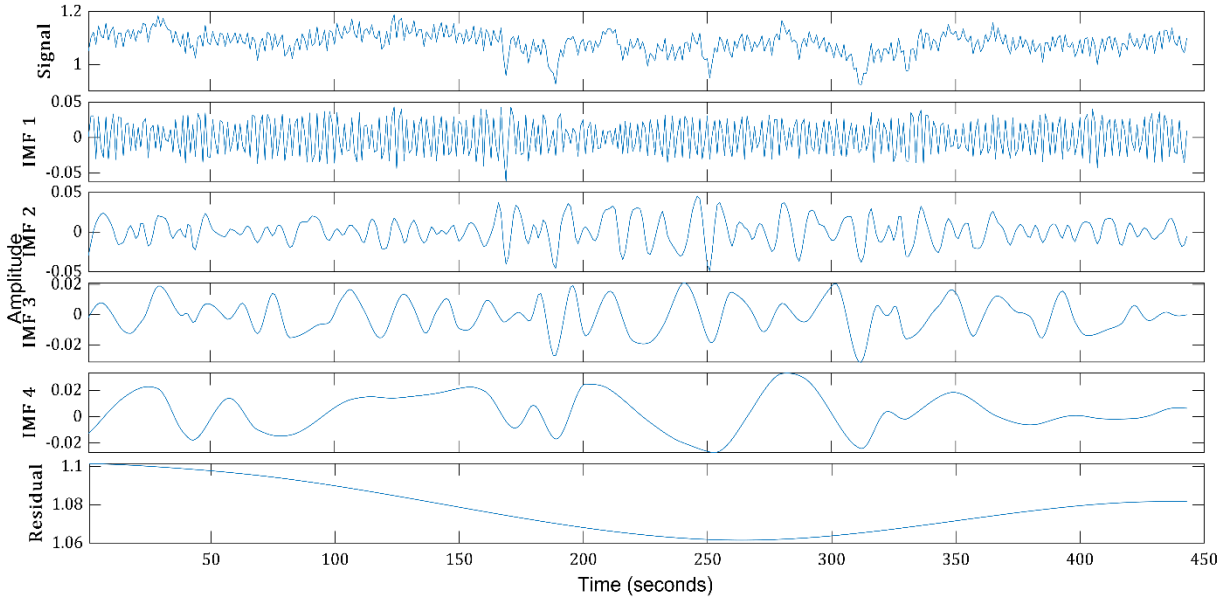

Source: Data from (Cossul *et al.*, 2023).

The univariate ANOVA shows a significant difference between the CAN groups for the variables $\log(ASR_{area})$, $\log(SODP_{area})$, $\mathrm{SODP}_{\mathrm{CTM}}$, $\log(PSD_{bpow})$, and $\log(PSD_{pkamp})$ and their components (*i.e.*, IMF_1, IMF_2, IMF_3, and IMF_4) ($p < 0.01$). In contrast, there was no significant difference between the CAN groups for the PSD_{mfreq} variable and its EMD components. The feature values are presented in Table 10.

Table 10 - Feature values (mean ± standard deviation) for $\mathrm{ASR}_{\mathrm{area}}$ - the area of the analytical signal; $SODP_{area}$ - the area of the second-order difference plot (SODP); $SODP_{CTM}$ - the central tendency measure of SODP; PSD_{bpow} - the power spectral density (PSD) band power; PSD_{pkamp} - the PSD peak amplitude; and PSD_{mfreq} - the PSD mean frequency for the four intrinsic mode functions decomposed from the empirical mode decomposition technique of each group; noCAN - individuals with type 2 DM without cardiac autonomic neuropathy; subCAN - individuals with type 2 DM with subclinical cardiac autonomic neuropathy; and estCAN - individuals with type 2 DM and established cardiac autonomic neuropathy. Significance levels are [a] $p < 0.05$ when comparing noCAN to subCAN, [b] $p < 0.05$ when comparing noCAN to estCAN, and [c] $p < 0.05$ when comparing subCAN to estCAN.

Feature	Group	$\mathbf{IMF_1}$	$\mathbf{IMF_2}$	$\mathbf{IMF_3}$	$\mathbf{IMF_4}$
log (ASR_{area})	noCAN	−6.777 ± 0.770 [b]	−7.399 ± 0.338 [b]	−7.424 ± 0.287 [b]	−7.300 ± 0.432 [ab]
	subCAN	−7.199 ± 0.540 [c]	−7.580 ± 0.282	−7.609 ± 0.204	−7.616 ± 0.263 [a]
	estCAN	−7.655 ± 0.382 [bc]	−7.739 ± 0.268 [b]	−7.694 ± 0.450 [b]	−7.712 ± 0.224 [b]
log ($SODP_{area}$)	noCAN	−0.654 ± 0.665 [b]	−1.878 ± 0.609 [b]	−2.810 ± 0.488 [ab]	−3.598 ± 0.527 [ab]
	subCAN	−1.957 ± 0.802 [c]	−2.374 ± 0.740 [c]	−3.294 ± 0.584 [a]	−4.071 ± 0.557 [ac]
	estCAN	−1.086 ± 0.759 [bc]	−2.963 ± 0.703 [bc]	−3.733 ± 0.733 [b]	−4.551 ± 0.621 [bc]
$\mathrm{SODP}_{\mathrm{CTM}}$	noCAN	0.773 ± 0.268 [b]	0.887 ± 0.173 [b]	0.317 ± 0.180 [ab]	0.694 ± 0.234 [ab]
	subCAN	0.887 ± 0.209	0.941 ± 0.105	0.531 ± 0.276 [ac]	0.868 ± 0.143 [ac]
	estCAN	0.981 ± 0.037 [b]	0.987 ± 0.029 [b]	0.750 ± 0.253 [bc]	0.947 ± 0.089 [bc]
log (PSD_{bpow})	noCAN	−3.480 ± 0.574 [b]	−3.839 ± 0.432 [b]	−3.921 ± 0.370 [ab]	−3.912 ± 0.390 [ab]
	subCAN	−3.897 ± 0.668 [c]	−4.166 ± 0.564 [c]	−4.288 ± 0.388 [ac]	−4.314 ± 0.382 [ac]
	estCAN	−4.492 ± 0.654 [bc]	−4.749 ± 0.622 [bc]	−4.687 ± 0.612 [bc]	−4.655 ± 0.527 [bc]
log (PSD_{pkamp})	noCAN	−2.562 ± 0.617 [b]	−2.771 ± 0.435 [b]	−2.613 ± 0.379 [ab]	−2.392 ± 0.403 [ab]
	subCAN	−3.028 ± 0.692 [c]	−3.094 ± 0.570 [c]	−2.975 ± 0.368 [ac]	−2.793 ± 0.391 [ac]
	estCAN	−3.667 ± 0.724 [bc]	−3.741 ± 0.626 [bc]	−3.349 ± 0.644 [bc]	−3.106 ± 0.551 [bc]
PSD_{mfreq}	noCAN	0.290 ± 0.051	0.097 ± 0.019	0.041 ± 0.010	0.018 ± 0.003
	subCAN	0.266 ± 0.054	0.090 ± 0.029	0.039 ± 0.121	0.019 ± 0.006
	estCAN	0.285 ± 0.0463	0.098 ± 0.031	0.039 ± 0.008	0.017 ± 0.004

Source: Data from (Cossul *et al.*, 2023).

The analytic signal and the second-order difference plots of the IMFs for the three groups (noCAN, subCAN, and estCAN) are demonstrated in Figures 46 and 47, respectively. From Figure 46, it can be observed that the spread of the analytic signal is lower for the estCAN group in all IMFs, resulting in a larger number of points inside the radius and, therefore, a larger ASR_{area}. Similarly, Figure 47 reveals that the second-order difference plot exhibits a greater dispersion in the noCAN group but becomes progressively more clustered in the subCAN group and even more in the estCAN

group. This result is reflected by the decrease in the $SODP_{area}$ and an increase in the $\mathrm{SODP_{CTM}}$, which calculates the ellipse area and the grouping of points around the origin.

Figure 46 - The analytic signal representation (ASR) of the first four intrinsic mode functions obtained after the empirical mode decomposition analysis of the RR interval signals for the three groups: noCAN - individuals with type 2 diabetes (T2DM) without cardiovascular autonomic neuropathy (CAN); subCAN - individuals with T2DM with subclinical CAN; and estCAN - with T2DM with established CAN. Note: The zoomed plots of the estCAN group are presented in the top corner of each IMF plot.

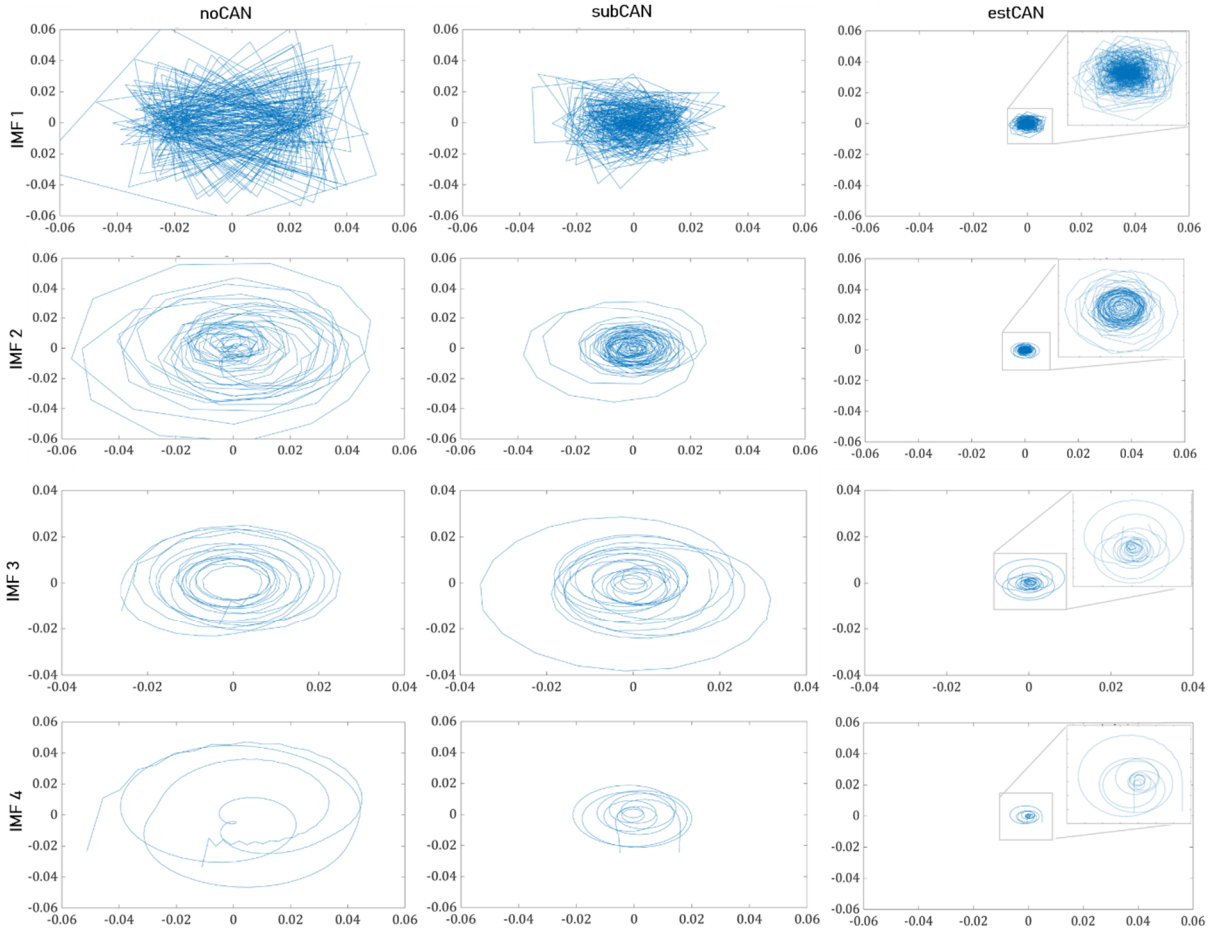

Source: Data from (Cossul *et al.*, 2023).

Figure 47 - The second-order difference plots for the first four intrinsic mode functions (IMFs) obtained after empirical mode decomposition analysis of the RR interval signal for the three groups are as follows: noCAN - individuals with type 2 diabetes (T2DM) without cardiovascular autonomic neuropathy (CAN); subCAN - individuals with T2DM with subclinical CAN; and estCAN - individuals with T2DM with established CAN. Note: The zoomed plots of the estCAN group are presented in the top corner of each IMF plot.

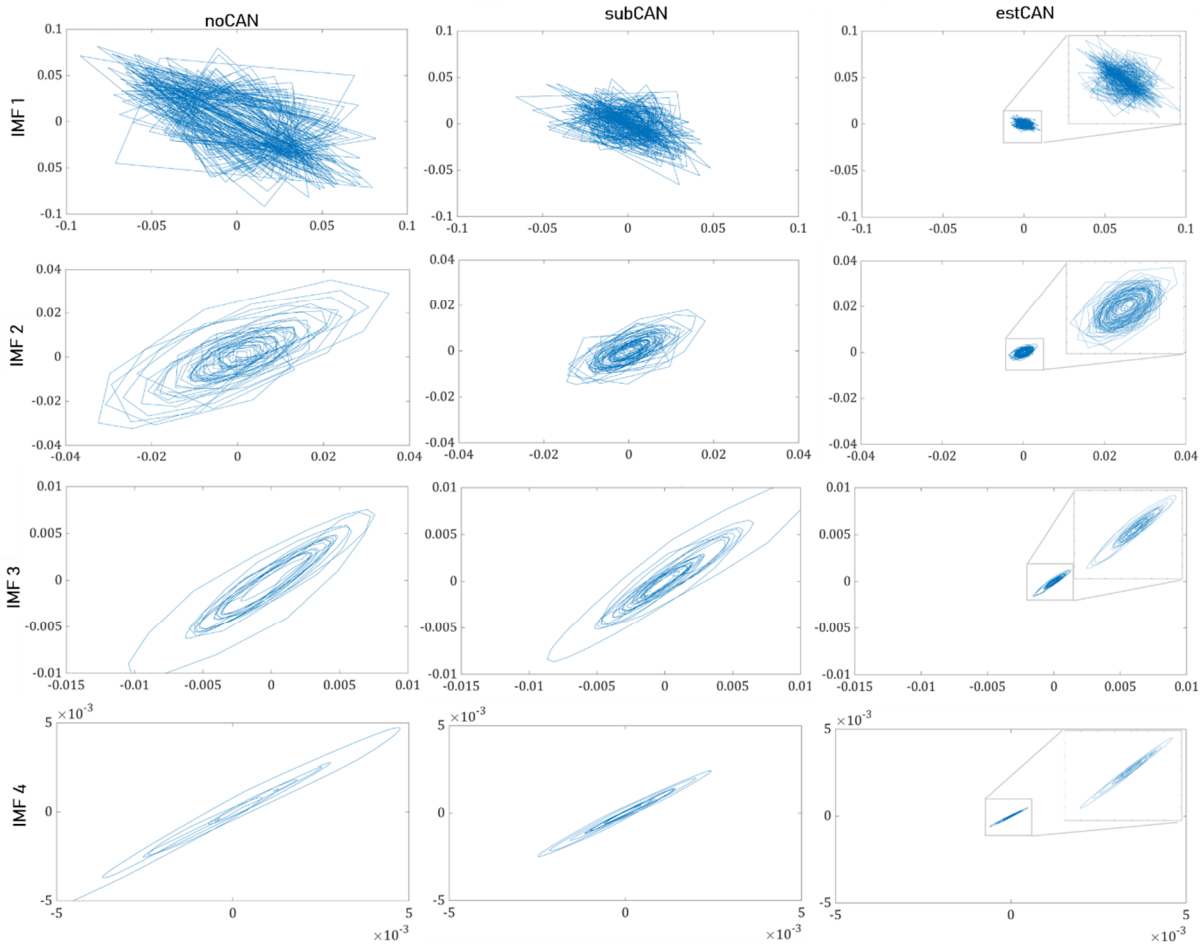

Source: Data from (Cossul *et al.*, 2023).

Welch's power spectral density estimation plots of the intrinsic mode functions for the three groups (noCAN, subCAN, and estCAN) are demonstrated in Figure 48; the frequency content decreases as the IMF index increases. The power of all IMF shows a decreasing trend from the noCAN group to the subCAN group and further to the estCAN group. When examining each group's IMFs individually, the noCAN group exhibits a higher power in IMF_1, while the subCAN and estCAN groups show higher powers in IMF_3 and IMF_4.

Figure 48 - The power spectral density (PSD) estimation for the first four intrinsic mode functions (IMFs) was obtained after the empirical mode decomposition analysis of the RR interval signals for the three groups: noCAN - individuals with type 2 diabetes (T2DM) without cardiovascular autonomic neuropathy (CAN); subCAN - individuals with T2DM with subclinical CAN; and estCAN - individuals with T2DM with established CAN. Note: The plots have different scales on the y-axis for better visualization.

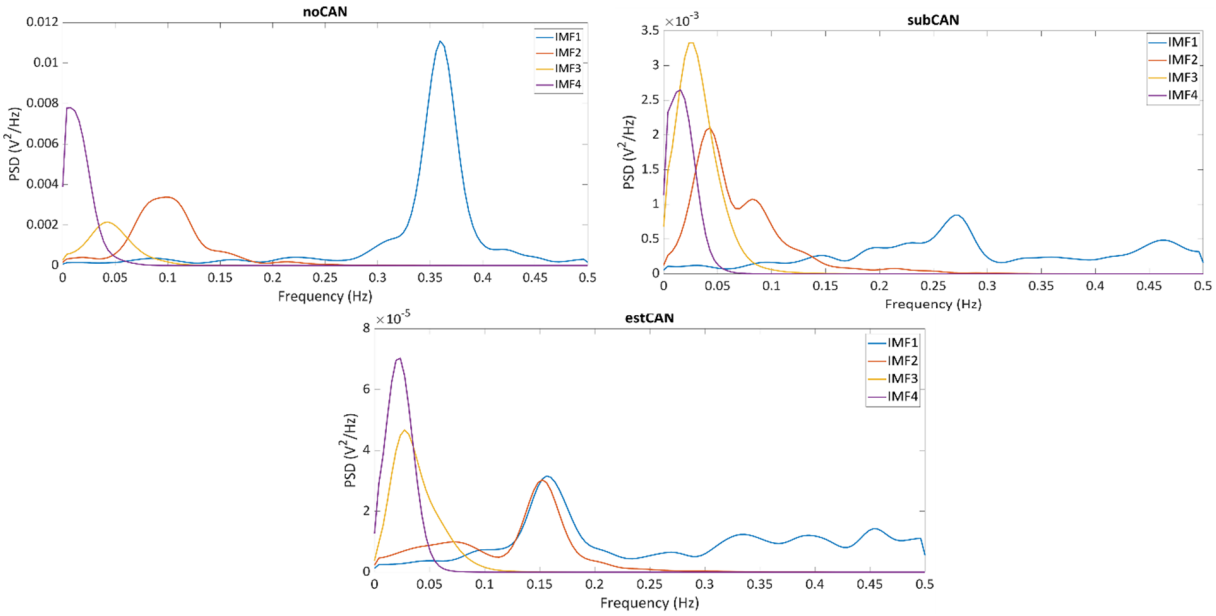

Source: Data from (Cossul *et al.*, 2023).

All features derived from the four EMD-extracted IMF components exhibited significant differences between the extreme groups (noCAN and estCAN). When comparing the noCAN and subCAN groups, the third and fourth components were particularly effective in distinguishing between them. Furthermore, for the subCAN and estCAN groups, certain EMD components of each feature presented a significant ability to distinguish between the groups. The following paragraphs provide a more detailed description of these results.

Regarding the $\log(ASR_{area})$ of the four EMD components of each group, the posthoc analysis demonstrates that there was a significant difference between the noCAN and estCAN groups ($p < 0.01$) for all components, a significant difference between the subCAN and estCAN groups ($p < 0.05$) in the fourth component, and a significant difference between the noCAN and subCAN groups ($p < 0.05$) in the first component (see Table 10 and Figure 49a).

Figure 49 - The comparison of parameters for cardiovascular autonomic neuropathy (CAN) groups for the four IMFs of the RR interval signals (mean ± standard error of the mean): noCAN - individuals with type 2 diabetes (T2DM) without CAN; subCAN - individuals with T2DM with subclinical CAN; and estCAN - individuals with T2DM with established CAN. (**a**) ASR_{area} - the area of analytic signal representation. (**b**) $SODP_{area}$ - the area of the second-order difference plot (SODP). (**c**) $SODP_{CTM}$ - the central tendency measure of SODP. (**d**) PSD_{bpow} - the power spectral density (PSD) band power. (**e**) PSD_{pkamp} - the PSD peak amplitude. * $p < 0.05$ - significant group difference.

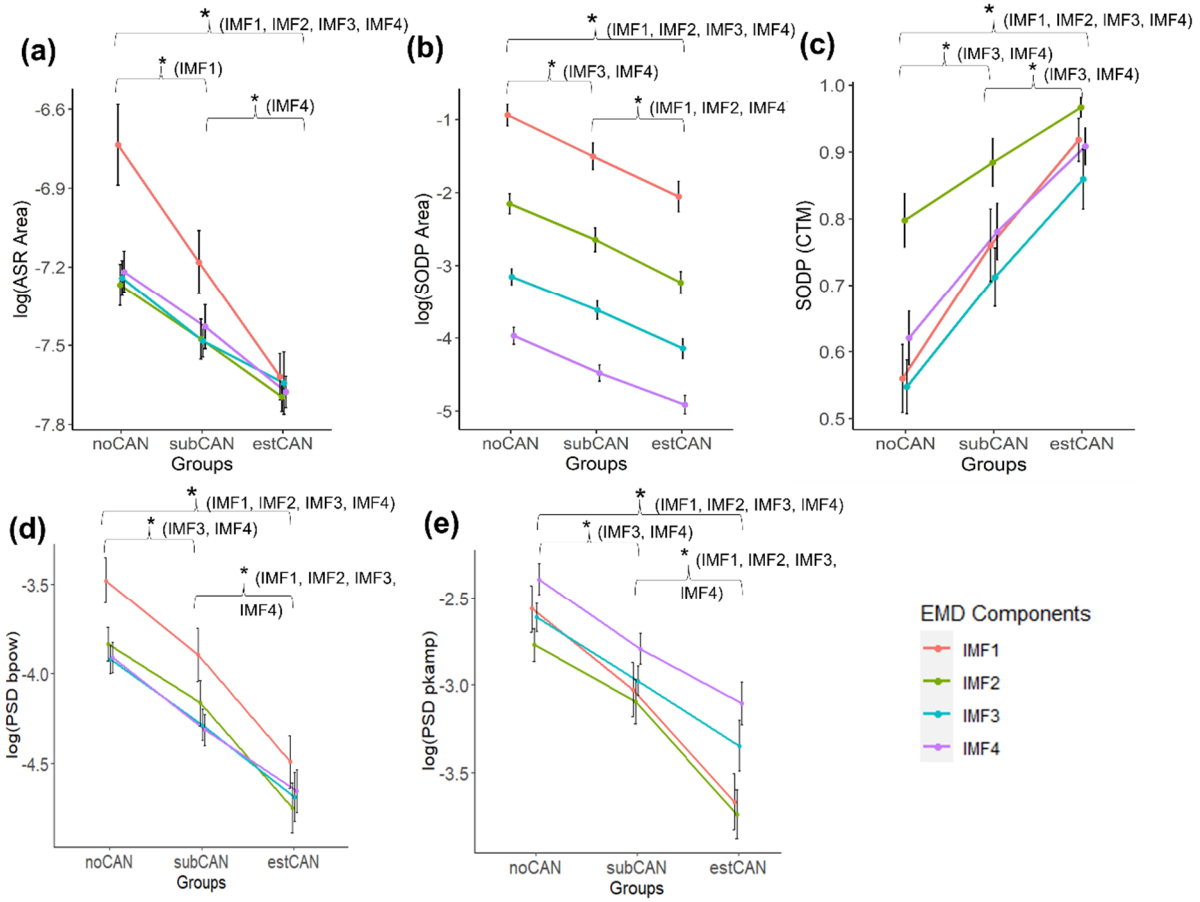

Source: Data from (Cossul *et al.*, 2023).

Considering the $\log(SODP_{area})$, the posthoc analysis of the four EMD components of each group also revealed a significant difference between the noCAN and estCAN groups ($p < 0.01$) for all components. Additionally, a significant difference between the noCAN and subCAN ($p < 0.05$) groups was found for the $\log(SODP_{area})$ of the third and fourth IMFs, and a significant difference between subCAN and estCAN ($p < 0.05$) for all components, except for the third one ($p < 0.09$) (see Table 10 and Figure 49b).

The estCAN group shows a significantly higher $SODP_{CTM}$ mean value ($p < 0.01$) for all components compared to the noCAN group, as well as a significantly higher

mean value ($p < 0.05$) for the 3rd and 4th IMF components compared to the subCAN group. Similarly, the estCAN group exhibited a significantly higher $SODP_{CTM}$ mean value ($p < 0.05$) for the third and fourth components compared to the subCAN group (see Table 10 and Figure 49c).

Lastly, the post hoc analysis of PSD-derived features demonstrates significantly reduced log (PSD_{bpow}) ($p < 0.05$) and log (PSD_{pkamp}) ($p < 0.05$) mean values for the estCAN group compared to the noCAN and subCAN groups for all IMFs. Similarly, the subCAN group presented significantly reduced mean values for the log (PSD_{bpow}) ($p < 0.05$) and log (PSD_{pkamp}) ($p < 0.05$) parameters compared to the noCAN group for the 3rd and 4th IMF components (see Table 10, Figure 49d, e).

5.4 DISCUSSION

In summary, it was observed that all features (except the PSD_{mfreq}) calculated from the four EMD-extracted IMF components differed significantly between the extreme groups (*i.e.*, noCAN and estCAN). More importantly, the specific IMF components of each feature could effectively distinguish individuals without a CAN diagnosis or with an established CAN from those with subclinical CAN (refer to Figure 49).

This research explores a new approach for analysing the RR interval signals acquired from type 2 DM individuals at different stages of cardiovascular autonomic neuropathy. We used the EMD method, which decomposes non-stationary and nonlinear signals into IMFs. The findings of this study suggest that employing the nonlinear EMD method enables the extraction of several parameters from heart rate variability that hold promise in identifying changes associated with the manifestation and progression of CAN. Specifically, the complex plane plots from the analytical signal representation and the second-order difference plot of the first four IMFs were used to extract the $\mathrm{ASR_{area}}$, $\mathrm{SODP_{area}}$ and $\mathrm{SODP_{CTM}}$ features, while the power spectral density of the IMFs was used to obtain the PSD_{bpow}, $\mathrm{PSD_{pkamp}}$ and PSD_{mfreq} features. These parameters were compared across subjects at distinct stages of CAN (noCAN, subCAN, and estCAN). The main results were as follows: (a) decreased IMF variability and (b) decreased IMF power distribution, according to CAN progression.

The autonomic nervous system (ANS) maintains homeostasis by regulating arterial pressure and all significant cardiovascular variables through the sympathetic and parasympathetic divisions (Orini *et al.*, 2017). The ANS imbalance manifesting as CAN in the diabetic population is an important predictor of cardiovascular events (Vinik *et al.*, 2018), as reflected in the abnormal HRV indices. The nonlinear analysis methods of HRV allow a more subtle characterization of autonomic balance and are reliable markers of morbidity and mortality in patients with cardiovascular disease (Vinik *et al.*, 2018). Furthermore, nonlinear HRV indices in diabetic populations may have diagnostic and prognostic potential for identifying asymptomatic CAN and cardiovascular events (Khandoker; Jelinek; Palaniswami, 2009). A recent study found that prediabetes and T2DM patients were independently associated with lower HRV (both in the time and frequency domains), strongly suggesting that the HRV indices could help identify subclinical CAN (Coopmans *et al.*, 2020). In another study, T2DM patients presented an overall decrease in HRV and decreased sympathetic and parasympathetic activity (Benichou *et al.*, 2018). Correspondingly, BRS is also a sensitive indicator of CAN in DM patients (Frattola *et al.*, 1997) and can be associated with cardiovascular events (Spallone, 2019).

Previous studies (Chen *et al.*, 2019; Pan *et al.*, 2019) have demonstrated a correlation between the first four IMFs extracted by EMD and the HRV frequency components (VHF, HF, LF, and VLF, respectively). The HRV oscillatory components are usually divided into the following spectral profiles: (a) very-high-frequency (VHF, 0.4 to 1 Hz); (b) high-frequency (HF, 0.15 to 0.40 Hz); (c) low-frequency (LF, 0.04 to 0.15 Hz); (d) very-low-frequency (VLF, <0.04 Hz) bands (Shaffer; Ginsberg, 2017). However, in short-term recordings (5–10 min), the spectral analysis of HRV holds three main frequency bands: HF, LF, and VLF (Shaffer; Ginsberg, 2017). By examining the power spectrum density of the HRV signal's EMD components (Figure 48), we could observe the energy distribution according to the different frequency components and associate IMF_1 with the HF component, IMF_3 with the LF component, and IMF_4 with the VLF band. IMF_2 is not clearly defined between the LF and HF components. Importantly, each frequency component can be related to the different activities of the autonomic nervous system. The HF band reflects parasympathetic activity and is a marker of cardiac vagal modulation. In contrast, the LF band modifies the parasympathetic and sympathetic nervous systems and indicates baroreceptor activity during resting conditions (Shaffer; Ginsberg, 2017). We noticed that the mean values

of PSD_{bpow} and $\mathrm{PSD}_{\mathrm{pkamp}}$ decrease as CAN progresses. This effect was more evident when comparing the estCAN group to the noCAN or subCAN groups, as all EMD components were significant. This reduction was less noticeable when comparing the noCAN group to the subCAN group, as only the 3rd and 4th IMFs were significant. These results demonstrated reduced sympathetic and parasympathetic activity and baroreceptor activity as the disease progressed.

In the subCAN group, the sympathetic activity (IMF_2, IMF_3, and IMF_4) had a higher amplitude than the parasympathetic activity (mainly IMF_1). In contrast, in the noCAN group, the parasympathetic modulation was higher. This result was expected since autonomic nerves are affected in a length-dependent manner (Balcıoğlu, 2015; Vinik; Ziegler, 2007). The first manifestation of CAN often occurs due to damage in the vagus nerve, the longest nerve of the ANS, disrupting the parasympathetic activity and increasing the sympathetic tone (Balcıoğlu, 2015; Pop-Busui, 2010). This fact is reflected in the results, where the HF components of HRV, represented by IMF_1 and partly by IMF_2, were not significantly different between the noCAN and subCAN groups, while the LF components represented by IMF_3 and IMF_4 were significantly different. Therefore, for the CAN subclinical assessment, it would be more important to use parameters derived from the lower frequency contents of the HRV.

Considering the features obtained from the analytical signal representation and the second-order difference plot, we evaluated the presence and extent of variability in the IMFs of RR intervals in the CAN groups. It was observed that the $\mathrm{ASR}_{\mathrm{area}}$ and $\mathrm{SODP}_{\mathrm{area}}$ values decreased in the IMFs of the subCAN group compared to noCAN and decreased further in the IMFs of the estCAN group compared to the others, indicating a pattern of decreasing variability according to CAN progression. In contrast, the $\mathrm{SODP}_{\mathrm{CTM}}$ values increase in the noCAN group compared to subCAN, and a further increase in the estCAN group. The lower values of the $\mathrm{SODP}_{\mathrm{CTM}}$ indicate higher dispersion as the signal is spread and the number of points within the same radius is reduced. Thus, similar to $\mathrm{ASR}_{\mathrm{area}}$ and $\mathrm{SODP}_{\mathrm{area}}$, the $\mathrm{SODP}_{\mathrm{CTM}}$ parameter is associated with decreased variability in IMFs for more severe levels of CAN. The heart rate response test is still preserved in the subclinical stage, and symptoms are absent. However, baroreflex sensitivity tests present alterations and could explain why only the $\mathrm{ASR}_{\mathrm{area}}$, $\mathrm{SODP}_{\mathrm{area}}$, and $\mathrm{SODP}_{\mathrm{CTM}}$ metrics of some IMFs could distinguish subtle changes in the RR interval of the subCAN group.

Several studies (Alkhodari *et al.*, 2021; Carricarte Naranjo *et al.*, 2017b; Cornforth; Jelinek; Tarvainen, 2015; Faust *et al.*, 2012; Jelinek *et al.*, 2019; Khandoker *et al.*, 2010; Khandoker; Jelinek; Palaniswami, 2009a; Lin *et al.*, 2017; Pachori *et al.*, 2015; Roy; Ghatak, 2013; Selvan *et al.*, 2022) have demonstrated the effectiveness of nonlinear HRV methods in evaluating the progression of CAN. However, many of these approaches have addressed CAN as a binary classification problem, distinguishing only between no CAN and CAN (Alkhodari *et al.*, 2021; Carricarte Naranjo *et al.*, 2017b; Khandoker; Jelinek; Palaniswami, 2009a). Others have examined cardiovascular function in healthy individuals and those with DM (Faust *et al.*, 2012; Pachori *et al.*, 2015; Roy; Ghatak, 2013). As a result, they fail to capture the distinct stages of disease progression. Nonetheless, some works (Cornforth; Jelinek; Tarvainen, 2015; Jelinek *et al.*, 2019; Khandoker *et al.*, 2010; Selvan *et al.*, 2022) evaluated CAN as a multiclass problem, separating the groups by levels of severity, which aligns with the approach proposed in our work. For example, SELVAN *et al*. (2022) evaluated time segments of ECG recordings from individuals with different disease severities and healthy individuals using complexity analysis, specifically computing the fractal dimension. Similarly, Cornforth; Jelinek; Tarvainen (2015), and Jelinek *et al*. (2019) categorized the participants into three CAN groups (*i.e.*, without, early, and definite) and applied techniques such as multiscale entropy, multifractal detrended fluctuation analysis, and Renyi entropy to sets of RR intervals. Khandoker *et al*. (2010) also introduced a novel HRV parameter named tone-entropy, which demonstrated the ability to differentiate between stages of CAN progression. In contrast to our study, these studies have certain limitations. Firstly, they relied solely on CARTs to classify participants, whereas we employed CARTs and BRS measurements. Secondly, they had relatively small or disproportional sample sizes, potentially impacting the generalizability of their findings. Lastly, there was a lack of diabetes clinical data available (*e.g.*, DM type and duration) for the participants, which restricts further analysis possibilities.

5.5 CONCLUSION

In this work, we investigated the relevance of EMD-based features extracted from RR intervals to identify changes between different levels of CAN severity. We observed a gradual reduction in the IMF variability and power distribution over the frequency correlated to the stages of CAN severity, indicating the loss of complexity and decrease in autonomic nervous system tones as CAN progressed. All the features, except PSD_{mfreq}, could distinguish between individuals with no CAN and those with either subclinical or established CAN. We highlight that the specific IMF components of each feature could effectively distinguish individuals without a CAN diagnosis or with established CAN from those with subclinical CAN. Subclinical CAN detection is essential for timely interventions to improve prognostics and potentially reverse disease progression. Thus, this study's findings suggest that EMD-based outcome measures are promising in characterizing changes associated with CAN progression in individuals with T2DM.

A limitation of this study is that we did not compare the proposed features with the standard HRV features to determine whether they offer superior performance or contribute to better differentiation between the groups. Nonetheless, this method can be further developed by combining a larger sample size with other HRV-based indices and user-independent classification algorithms. Future studies could also explore the progression of CAN in individuals with type 1 DM and gestational DM. These could contribute to developing diagnostic tools for a more accurate assessment of CAN progression.

6 SECOND STUDY

This section presents the second study of this work entitled "**Classifying Cardiovascular Autonomic Neuropathy in Diabetic Subjects: A Machine Learning Multiclass Approach using Heart Rate Variability and Empirical Mode Decomposition**".

6.1 OBJECTIVE

To assess the performance of machine learning models in the multiclass classification of CAN severity levels (*i.e.*, no CAN, subclinical CAN, and established CAN) using a combination of HRV features and EMD-derived features.

6.2 MATERIAL AND METHODS

The diagram of the methodology for CAN classification using machine learning models is presented in Figure 50 and will be further explained in the following sections.

The data pre-processing and feature extraction were performed using the developed HRV signal processing tool in MATLAB (R2018a, MathWorks, MA, USA), which were described in Section 4. The next steps, including feature selection, model training, and evaluation, were conducted using Python 3.9.7 and Jupyter Notebook 6.4.5. The libraries imported and used within the project were *scikit-learn* (Pedregosa *et al.*, 2011), *pandas,* and *numpy*.

Figure 50 – General overview diagram of the methodology. The data collected from multiple studies involving individuals with diabetes mellitus (DM) includes the electrocardiogram (ECG) and photoplethysmography (PPG) signals, blood pressure measurements, questionnaires about signs and symptoms of cardiovascular autonomic neuropathy (CAN) and glycated haemoglobin (HbA1C) test results. The heart rate variability signal (HRV) processing tool is used for data pre-processing and feature extraction, including the HRV, empirical mode decomposition (EMD), and baroreflex sensitivity analysis (BRS) (see section 4). The participants were classified into three levels of CAN: "noCAN" (absence of CAN), "subCAN" (subclinical CAN), and "estCAN" (established CAN). The dataset, containing all features, was partitioned into three distinct feature sets. Subsequently, feature selection techniques were applied, including SelectKBest, Recursive Feature Elimination (RFE), and Principal Component Analysis (PCA). Following this feature selection process, various classification models, such as SVM (Support Vector Machine), KNN (K-Nearest Neighbours), LDA (Linear Discriminant Analysis), QDA (Quadratic Discriminant Analysis), logistic regression, decision tree, and AdaBoost (Adaptive Boosting), were employed on the data. Lastly, the models were evaluated to assess their classification performance.

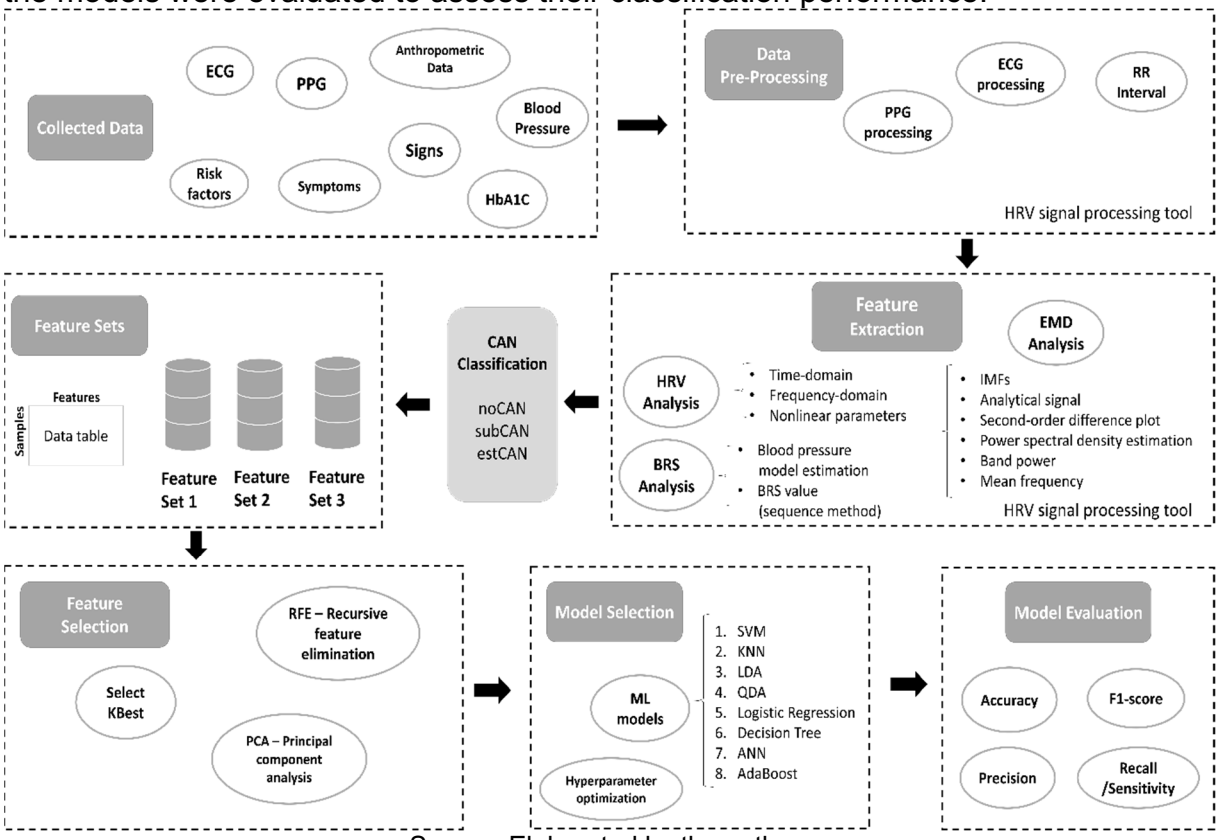

Source: Elaborated by the author.

6.2.1 Dataset Description

The dataset employed in this study comprises ECG and PPG data collected from 250 participants diagnosed with either type 1 or type 2 DM.

All data were collected at the Professor Polydoro Ernany University Hospital of the Federal University of Santa Catarina—HU/UFSC/EBSERH, as part of previous

studies conducted by the research group at the Federal University of Santa Catarina's Institute of Biomedical Engineering. The institutional research ethics committee approved the studies (protocol numbers 3.326.385, 120.103, and 4.982.983), and participants only entered the study after informed consent.

The study data included in the dataset were collected under the same conditions and using a similar protocol. The ECG and PPG data were collected during a resting state of five to eight minutes and sampled at 500 Hz. Additionally, CARTs were performed, and blood pressure measurements were recorded for BRS evaluations for each participant. The dataset also contained additional demographic and clinical information about the participants, including their age, gender, duration of DM, and HbA1c levels. With the collected dataset, participants were classified into three levels of CAN: "noCAN" (absence of CAN), "subCAN" (subclinical CAN), and "estCAN" (established CAN). The data collection protocol and participants' classification criteria are the same as those in the first study (refer to section 5.2). Table 11 presents a detailed overview of the dataset, detailing its classes.

Table 11 – Dataset description.

	noCAN	**subCAN**	**estCAN**
n	127	75	50
Age (yrs)	42.0 ± 15.0	46.0 ± 15.0	50.5 ± 12.0
Gender	59 F / 68 M	38 F / 37M	28 F / 22 M
DM duration (yrs)	14.9 ± 10.3	16.2 ± 10.4	17.5 ± 10.5
HbA1c (%)	8.4 ± 1.7	8.5 ± 1.7	10.0 ± 1.88

Note: Values are presented as mean ± SD. Abbreviations: DM - diabetes mellitus; noCAN - individuals with type 2 DM without cardiac autonomic neuropathy; subCAN - individuals with type 2 DM with subclinical cardiac autonomic neuropathy; estCAN - individuals with type 2 DM and established cardiac autonomic neuropathy; HbA1c - glycated haemoglobin. Source: Elaborated by the author.

6.2.2 Data Pre-processing and Feature Extraction

The data pre-processing includes the ECG and PPG data filtering for noise and interference removal. The ECG is further processed for the detection of RR peaks and the extraction of the HRV signal. The PPG data is used for predicting the blood pressure model, allowing for the BRS analysis. The data pre-processing and feature

calculation were accomplished using the developed HRV processing tool explained and validated in Section 4.

6.2.3 Feature Sets

For data analysis, three distinct sets of features were derived from the same original dataset as follows:

- **Feature Set One -** a feature set comprising HRV parameters obtained through time, frequency domain, and non-linear analysis;

The parameters included in this feature set are: the mean of NN intervals (*NN mean*), the standard deviation of NN intervals (*SDNN*), the coefficient of variation of NN intervals (*CV*), root mean square of successive NN interval differences (*RMSSD*), percentage of successive NN intervals that differ by more than 50 ms (*pNN50*), HRV triangular index (*HTI*), the absolute power of the very-low-frequency band (*VLF power*), the absolute power of the low-frequency band (*LF power*), the absolute power of the high-frequency band (*HF power*), the sum of energy in the VLF, LF and HF bands (*Total power*), ratio of LF to HF power bands (*LF/HF*), Poincaré plot features (*SD1*, *SD2*, *SD1/SD2, ellipse area*), approximate entropy (*ApEN*), sample entropy (*SampEN*), fuzzy entropy (*FuzzyEn*), cardiac sympathetic and vagal index (*CSI, CVI*) and features from the detrended fluctuation analysis (*DFA* α_1 and *DFA* α_2) (see section 3.1 for features description).

- **Feature Set Two** - a feature set derived from EMD analysis of HRV signals; features were calculated for each of the first four intrinsic mode functions (IMFs) components obtained from the EMD method.

The parameters included in this feature set are the area of the analytical signal (ASR_{area}), the area of the second-order difference plot ($SODP_{area}$), the central tendency measure of the second-order difference plot ($SODP_{CTM}$), peak amplitude (PSD_{pkamp}) extracted after power spectral density estimation, approximate entropy (*ApEN*), and the coefficient of variation (*CV*) (see section 3.2 for features description).

- **Feature Set Three (composite)** - a set combining all features from the preceding feature sets (feature set one and feature set two).

6.2.4 Feature Scaling

Given the differences in feature ranges, feature normalization was employed for the classification input features to prevent potential biases (S. B. Kotsiantis; D. Kanellopoulos; P. E. Pintelas, 2006). The methods considered for feature scaling included standardization, min-max normalization, and mean normalization, as detailed in Section 3.4.3.

6.2.5 Feature Selection

Feature selection (FS) helps to choose the most discriminative features from a given feature set and avoid overfitting (S. B. Kotsiantis; D. Kanellopoulos; P. E. Pintelas, 2006). Initially, a correlation analysis was conducted, and in cases where the correlation between features exceeded 0.9, one of them was subsequently eliminated.

Afterwards, various FS techniques and their respective variations were used for further feature refinement: (a) SelectKBest, employing both ANOVA F-value and mutual information score functions; (b) Recursive feature elimination (RFE) with four different estimators: Support Vector Classification (with a linear kernel), Logistic Regression, Decision Treen, and Gradient Boosting Classifier; and (c) Principal component analysis (PCA) with the option to retain either five or ten components. Three different feature set sizes were considered for each FS method, considering 10, 15, and 20 features (see section 3.4.1 for more details about the FS methods). The FS methods and their variations are summarized in Table 12.

Table 12 – Summary of employed feature selection methods and their variations.

ID	Method	Score function/Estimator	Number of features /components to select
1	SelectKBest	ANOVA F-value	10
2	SelectKBest	ANOVA F-value	15
3	SelectKBest	ANOVA F-value	20
4	SelectKBest	Mutual info	10
5	SelectKBest	Mutual info	15
6	SelectKBest	Mutual info	20
7	RFE	SVC linear	10
8	RFE	SVC linear	15
9	RFE	SVC linear	20
10	RFE	Logistic regression	10
11	RFE	Logistic regression	15
12	RFE	Logistic regression	20
13	RFE	Decision tree	10
14	RFE	Decision tree	15
15	RFE	Decision tree	20
16	RFE	Gradient boosting	10
17	RFE	Gradient boosting	15
18	RFE	Gradient boosting	20
19	PCA	-	5
20	PCA	-	10

Note: SVC – support vector classification; RFE – recursive feature elimination; PCA – principal component analysis. Source: Elaborated by the author.

6.2.5.1 Classification

The methodology included testing supervised machine learning models in the three feature sets, where the classes were noCAN, subCAN, and estCAN. This study used various machine learning models and their variations for the multiclass classification of HRV-based features. The models employed were: (a) SVM – support vector machine with four different kernels: linear, rbf, poly, and sigmoid; (b) KNN – K nearest neighbours with the number of neighbours equal to five, ten and fifteen; (c) LDA and QDA - linear and quadratic discriminant analysis; (d) LR – logistic regression with three solvers: lbfgs, liblinear and newton-cg; (e) AdaBoost Classifier with both 1.0 and 0.2 learning rates and; (f) DT – Decision tree (see section 3.4.4 for further model-specific details). The employed ML models and their variations are summarized in Table 13.

Table 13 - Summary of employed machine learning models and their variations.

Machine learning model	Parameters
SVM	kernels = linear, rbf, poly, sigmoid
KNN	number of neighbours = 5, 10, 15
LDA	solver = svd
QDA	default
LR	solver = lbfgs, liblinear, newton-cg
AdaBoost	learning rate = 1.0, 0.2
DT	default

Note: SVM – support vector machine; KNN – K-nearest neighbours; LDA – linear discriminant analysis; QDA – quadratic discriminant analysis; LR – logistic regression; DT – decision tree.

Source: Elaborated by the author.

6.2.6 Model Evaluation

This study used a ten-fold cross-validation method to evaluate the classifiers. This method involved partitioning the dataset into ten subsets, and in each iteration, nine subsets were used for training while the remaining one was held out for testing. The classifier performance was quantified by calculating the average value across these ten folds (section 3.4.5). The ML models were evaluated using various performance metrics, including accuracy, F1-score, and the area under the ROC curve (AUC) (section 3.4.6).

6.3 RESULTS

A summary of some of the feature values used in the classification models for the three classes of CAN is presented in Table 14. Notably, a reduction in certain features is noticeable, specifically "HTI," "power_lf_welch," "power_hf_welch," and all "Peak_amplitude_db" when comparing the noCAN group to the subCAN and estCAN groups. On the contrary, a decrease is observed in some variables, including "alpha2" and all "CTM_r."

Table 14 – Feature values (mean ± standard deviation) for the three classes: noCAN - individuals without cardiac autonomic neuropathy (CAN), subCAN - individuals with subclinical CAN, and estCAN – individuals with established CAN.

Feature	Method	noCAN	subCAN	estCAN
NNmean	TD	893.62 ± 130.99	765.38 ± 123.32	765.75 ± 128.56
HTI	TD	10.35 ± 4.13	6.62 ± 3.47	4.27 ± 1.74
CVI	TD	3.10 ± 0.43	2.61 ± 0.52	2.18 ± 0.51
power_lf_welch	FD	34.17 ± 12.61	30.87 ± 11.66	22.22 ± 12.43
power_hf_welch	FD	29.44 ± 15.41	26.06 ± 17.71	27.60 ± 22.06
alpha1	NL	0.98 ± 0.23	1.03 ± 0.28	0.92 ± 0.33
alpha2	NL	0.80 ± 0.19	0.89 ± 0.18	0.94 ± 0.20
CTM_r1	EMD	0.29 ± 0.16	0.53 ± 0.26	0.71 ± 0.21
CTM_r2	EMD	0.51 ± 0.22	0.76 ± 0.23	0.90 ± 0.15
CTM_r3	EMD	0.76 ± 0.21	0.90 ± 0.17	0.97 ± 0.95
CTM_r4	EMD	0.69 ± 0.21	0.86 ± 0.15	0.94 ± 0.09
Peak_amplitude_db1	EMD	-23.10 ± 6.25	-29.94 ± 6.99	-35.22 ± 6.87
Peak_amplitude_db2	EMD	-25.18 ± 4.69	-30.51 ± 6.06	-37.58 ± 6.78
Peak_amplitude_db3	EMD	-24.61 ± 4.03	-29.73 ± 4.81	-34.77 ± 6.90
Peak_amplitude_db4	EMD	-23.16 ± 4.59	-28.02 ± 4.60	-32.63 ± 6.35

Note: TD – time domain; FD – frequency domain; NL – nonlinear and EMD – empirical mode decomposition. Source: Elaborated by the author.

The top features selected by the FS methods are demonstrated in Tables 15, 16, and 17, corresponding to the first, second, and third feature sets, respectively. In Table 15, representing feature set one, the selected features vary and encompass elements from time, frequency, and nonlinear domains. In Table 16, which represents feature set two, a mixture of features from all EMD components is observed, with only the RFE including the IMFs' coefficient of variation. Finally, in the third feature set, as seen in Table 17, the selected features are predominantly derived from the time and nonlinear domains combined with EMD-based features.

Table 15 – The most significant features identified through selectKbest and recursive feature elimination (RFE) feature selection methods for feature set one (combining time, frequency, and non-linear domain features extracted from heart rate variability signals).

Feature Selection Method	Top Selected Features
SelectKBest (ANOVA f-value)	'TypeDM', 'NNmean', 'SDNN', 'CV', 'RMSSD', 'pNN50_pr', 'HTI', 'power_vlf_welch', 'power_lf_welch', 'ellipse_area', 'CVI', 'alpha2', 'Ent_Fuzzy', 'CTM_r1', 'CTM_r2'
SelectKBest (mutual info)	'NNmean', 'SDNN', 'CV', 'RMSSD', 'pNN50_pr', 'HTI', 'power_lf_welch','power_hf_welch','lf_nu_welch', 'ellipse_area', 'CVI', 'alpha1', 'alpha2', 'CTM_r1', 'CTM_r2'
RFE (SVC linear and gradient boosting)	'NNmean', 'SDNN', 'CV', 'RMSSD', 'HTI', 'power_lf_welch', 'lf_nu_welch', 'SD1_SD2_ratio', 'alpha1', 'alpha2', 'ApEN', 'Ent_Amostra', 'Ent_Fuzzy', 'CTM_r1', 'CTM_r2'

Source: Elaborated by the author.

Table 16 - The most significant features identified through selectKbest and recursive feature elimination (RFE) feature selection methods for feature set two (combining EMD-based features from heart rate variability signals).

Feature Selection Method	Top Selected Features
SelectKBest (ANOVA f-value)	'log_Asr1', 'CTM_r1', 'log_Asodp_abs1', 'log_Asr2', 'log_Asodp_abs2', 'log_Asr3', 'CTM_r3', 'log_Asodp_abs3', 'log_Asr4', 'CTM_r4', 'log_Asodp_abs4', 'Peak_amplitude_db1', 'Peak_amplitude_db2', 'Peak_amplitude_db3', 'Peak_amplitude_db4'
SelectKBest (mutual info)	'log_Asr1', 'log_Asodp_abs1', 'log_Asr2', 'CTM_r2', 'log_Asodp_abs2', 'log_Asr3', 'CTM_r3', 'log_Asodp_abs3', 'log_Asr4', 'CTM_r4', 'log_Asodp_abs4', 'Peak_amplitude_db1', 'Peak_amplitude_db2', 'Peak_amplitude_db3', 'Peak_amplitude_db4'
RFE (SVC linear and gradient boosting)	'log_Asr1', 'log_Asodp_abs1', 'log_Asr2', 'CTM_r3', 'CTM_r4', 'Peak_amplitude_db1', 'Peak_amplitude_db2', 'Peak_amplitude_db3', 'Peak_amplitude_db4, 'ap_entr2', 'ap_entr3', 'cv_imf1', 'cv_imf2', 'cv_imf3', 'cv_imf4'

Source: Elaborated by the author.

Table 17 - The most significant features identified through selectKbest and recursive feature elimination (RFE) feature selection methods for feature set three (combining time, frequency, non-linear domain, and EMD-based features from heart rate variability signals – all features from feature sets one and two).

Feature Selection Method	Top Selected Features
SelectKBest (ANOVA f-value)	'SDNN', 'HTI', 'CVI', 'CTM_r1', 'CTM_r2', 'log_Asr1', 'log_Asr2', 'log_Asodp_abs2', 'CTM_r3', 'log_Asodp_abs3', 'log_Asodp_abs4', 'Peak_amplitude_db1', 'Peak_amplitude_db2', 'Peak_amplitude_db3', 'Peak_amplitude_db4'
SelectKBest (mutual info)	'SDNN', 'HTI', 'ellipse_area', 'CVI', 'CTM_r1', 'CTM_r2', 'log_Asr1', 'log_Asodp_abs2', 'log_Asr3', 'CTM_r3', 'log_Asodp_abs3', 'CTM_r4', 'Peak_amplitude_db2', 'Peak_amplitude_db3', 'Peak_amplitude_db4'
RFE (SVC linear and gradient boosting)	'NNmean', 'HTI', 'power_hf_welch', 'alpha1', 'CTM_r1', 'CTM_r3', 'CTM_r4', 'Peak_amplitude_db1', 'Peak_amplitude_db2', 'Peak_amplitude_db3', 'Peak_amplitude_db4', 'ap_entr1', 'cv_imf1', 'cv_imf4'

Source: Elaborated by the author.

The classification results of the ML models are summarized in Tables 18, 19, and 20, corresponding to the first, second, and third feature sets, respectively. Within each feature set, the tables highlight the ten best results from all models and their variations, accounting for all feature selection methods and their corresponding variations.

In Table 18, representing feature set one, the classification performances ranged from 68.6% to 72.5%. The SVM model with a linear kernel achieved the highest classification accuracy. This model was built using the ten initial features selected through RFE with a decision tree estimator (accuracy = 72.5%, F1-score = 73.0%, and AUC = 0.856). As shown in Table 19, the classification performances varied from 68.6% to 76.5% within feature set two. The best classifier in this set was the SVM model with a linear kernel, utilizing fifteen features chosen through RFE with a gradient boosting estimator (accuracy = 76.5%, F1-score = 72.6%, and AUC = 0.842).

Lastly, classification performances improved for feature set three, as represented in Table 20, ranging from 82.5% to 88.4%. The most successful classifier was the KNN model with five neighbours, employing ten selected features from RFE with support vector classification and a linear score function (accuracy = 88.4%, F1-score = 87.9%, and AUC = 0.881).

Table 18 – Evaluation of multiclass classification performance for cardiovascular autonomic neuropathy using feature set one (combining time, frequency, and non-linear domain features extracted from heart rate variability signals).

Classifier	FS method	Accuracy (%)	F1-score (%)	AUC
SVM linear	SelectKBest (6)	72.5	71.2	0.827
	RFE (13)	**72.5**	**73.0**	**0.856**
	RFE (17)	72.5	72.4	0.824
KNN (n = 15)	SelectKBest (1)	70.6	67.9	0.807
LDA	SelectKBest (1)	68.6	68.5	0.794
	SelectKBest (4)	68.6	68.5	0.795
	RFE (14)	70.6	70.7	0.809
LR (liblinear)	SelectKBest (2)	71.6	69.8	0.805
	RFE (14)	70.6	70.5	0.833
AdaBoost (LR = 0.2)	RFE (18)	68.6	68.0	0.758

Notes: Machine learning classifier models = support vector machine with linear kernel (SVM linear); K-nearest neighbours (KNN) model with fifteen neighbours n; linear discriminant analysis (LDA); logistic regression (LR) with 'liblinear' solver; AdaBoosting classifier with learning rate (LR) equal to 0.2; *Feature selection (FS) method* = recursive feature elimination (RFE). The numbers in parenthesis correspond to the FS methods' specifics, as detailed in Table 12.
Source: Elaborated by the author.

Table 19 - Evaluation of multiclass classification performance for cardiovascular autonomic neuropathy using feature set two (combining EMD-based features from heart rate variability signals).

Classifier	FS method	Accuracy (%)	F1-score (%)	AUC
SVM linear	SelectKBest (6)	68.6	68.0	0.837
	RFE (14)	72.6	72.3	0.815
	RFE (17)	**76.5**	**72.6**	**0.842**
SVM rbf	RFE (9)	71.6	69.9	0.789
KNN (n = 5)	SelectKBest (4)	70.6	70.0	0.800
LDA	SelectKBest (6)	70.6	70.6	0.835
QDA	RFE (9)	72.5	71;0	0.788
LR liblinear	SelectKBest (6)	73.5	73.6	0.825
	SelectKBest (18)	70.6	70.0	0.815
AdaBoost (LR = 1.0)	RFE (12)	68.6	68.0	0.788

Notes: Machine learning classifier models = support vector machine with linear and rbf kernels (SVM linear, SVM rbf); K-nearest neighbours (KNN) model with five neighbours n; linear discriminant analysis (LDA); quadratic discriminant analysis (QDA), logistic regression (LR) with 'liblinear' solver; AdaBoosting classifier with learning rate (LR) equal to 1.0; *Feature selection (FS) method* = recursive feature elimination (RFE). The numbers in parenthesis correspond to the FS methods' specifics, as detailed in Table 12.
Source: Elaborated by the author.

Table 20 – Evaluation of multiclass classification performance for cardiovascular autonomic neuropathy using feature set three (combining time, frequency, non-linear domain, and EMD-based features from heart rate variability signals – all features from feature sets one and two).

Classifier	FS method	Accuracy (%)	F1-score (%)	AUC
SVM linear	SeleckKbest (6)	80.6	79.9	0.858
	RFE (9)	82.5	82.2	0.845
	RFE (18)	84.5	84.3	0.861
	PCA (20)	84.5	83.4	0.851
KNN (n = 5)	SelectKBest (1)	82.5	81.3	0.842
	RFE (7)	**88.4**	**87.9**	**0.881**
LDA	RFE (1)	86.5	86.1	0.878
	RFE (16)	86.5	86.0	0.822
LR (liblinear)	RFE (18)	86.5	86.3	0.834
AdaBoost (LR = 0.2)	RFE (9)	82.5	82.0	0.810

Notes: Machine learning classifier models = support vector machine with linear kernel (SVM linear); K-nearest neighbours (KNN) model with five neighbours n; linear discriminant analysis (LDA); logistic regression (LR) with 'liblinear' solver; AdaBoosting classifier with learning rate (LR) equal to 0.2; *Feature selection (FS) method* = recursive feature elimination (RFE); principal component analysis (PCA). The numbers in parenthesis correspond to the FS methods' specifics, as detailed in Table 12.
Source: Elaborated by the author.

6.4 DISCUSSION

This study evaluated several machine learning methods, including SVM, KNN, LDA, QDA, LR, AdaBoost, and DT, along with different feature selection techniques such as SelectKBest, RFE, and PCA. The main objective was to perform a multiclass classification focusing on CAN severity levels using features derived from HRV. Additionally, the aim was to assess the performance of applying EMD to calculating HRV signal parameters within the classification process. For this purpose, three feature sets were considered: one containing conventional HRV features (including time, frequency domains, and nonlinear parameters), another consisting solely of EMD-based features derived from HRV, and the last incorporating all these HRV-derived features. The study utilized a dataset comprising clinical information, ECG, and PPG data collected from 250 individuals with DM. Participants were categorized into three groups: those with no presence of CAN, those with early or subclinical CAN, and those with severe or established CAN.

The main findings of the current study revealed that: a) the combination of traditional HRV measures with EMD-based features (*i.e.*, feature set three), in

conjunction with the KNN classifier, resulted in the highest classification accuracy, achieving a value of 88.4% (see Table 20); b) the features from all HRV analysis methods contributed to this result, considering the top selected features determined through the RFE technique within the third feature set (see Table 17); c) the classification models using individual features, whether conventional or computed from decomposed components of the HRV signal (*i.e.*, feature sets one and two), did not achieve a classification accuracy exceeding 76.5%.

Recently, several studies have proposed the use of machine learning algorithms for CAN classification based on HRV features (Abdalrada *et al.*, 2017; Alkhodari *et al.*, 2021; Carricarte Naranjo *et al.*, 2017b; Cornforth; Tarvainen; Jelinek, 2013, 2014; Hassan *et al.*, 2022; Khandoker; Jelinek; Palaniswami, 2009b; Nedergaard *et al.*, 2023; Wehler *et al.*, 2021). The summary of the methodology and performance of these studies is presented in Table 21.

Most existing approaches have successfully identified CAN through binary classification, primarily focusing on distinguishing between patients with CAN and without CAN. One example is the study of (Alkhodari *et al.*, 2021), which investigated the feasibility of using HRV features over 24 hours for screening the presence of CAN, achieving an accuracy of 98.3%. In another approach, the study of (Wehler *et al.*, 2021) investigated the reliability of HRV analysis of ultra shorts HRV to classify definite CAN, achieving good results (AUC > 0.8). Other examples of binary CAN classification studies include the studies of (Carricarte Naranjo *et al.*, 2017c; Cornforth; Tarvainen; Jelinek, 2013, 2014; Khandoker; Jelinek; Palaniswami, 2009b) that explore nonlinear techniques in the HRV analysis. Nevertheless, this binary methodology has constraints when it comes to categorization, as it cannot detect patients with early CAN alterations.

To address this limitation, developing multiclass classification methods that can differentiate among various CAN severity levels can enhance diagnostic accuracy, providing opportunities for early diagnosis and timely interventions (Williams *et al.*, 2022). In the literature, the most relevant study in this context is the study by Hassan *et al*. (2022), which uses parameters collected from Ewing tests, QT analysis, HRV features, demographic, and other clinical data to perform a multiclass classification of CAN stages, achieving excellent results with an accuracy of 88.959% and an AUC of 0.933. Nedergaard *et al*. (2023)' study also assessed CAN at three levels of classification using clinical measures, clinical biochemistry, and certain features from HRV in the time and frequency domains. The best result was achieved with the random

forest classifier, which returned an F1-score of 60%, indicating a result that may be considered less substantial. This study does not evaluate the impact of nonlinear variability measures on classification. Another study, conducted by Abdalrada *et al*. (2017), also adopted a multiclass approach for CAN assessment, using HRV features from time, frequency, and nonlinear methods, and achieved good classification results. However, this study lacks important information about the dataset employed, such as the number of participants, identification of individuals with DM, types of DM, and demographic and clinical features.

In summary, the methodology presented in this study differs from other studies in the literature in two significant ways. Firstly, it employs a multiclass approach to account for different levels of CAN. Secondly, it combines the EMD method for nonlinear HRV analysis, a technique not explored in prior studies on CAN assessment. It is also worth mentioning that the DM type was included in the models as a feature. Despite the distinct differences between DM types 1 and 2, the effects of CAN have similar impacts on cardiovascular autonomic control (Chowdhury *et al.*, 2021; Pop-Busui, 2012).

Table 21 - Studies conducted on cardiovascular autonomic neuropathy (CAN) classification based on HRV features.

Authors	Methods	Classifier	Type	Performance
(Hassan *et al.*, 2022)	Ewing tests results QT interval Time, frequency domain, and nonlinear	DT	multiclass	Accuracy: 88.959% AUC: 0.933
(Nedergaard *et al.*, 2023)	Clinical measures and biochemistry Time and frequency domain	SVM, DT, and RF	multiclass	F1-score: 60% (RF)
(Abdalrada *et al.*, 2017)	Ewing tests results Time and frequency domain and nonlinear	ensemble classifiers	multiclass	Accuracy: 95% ROC: 0.978
(Alkhodari *et al.*, 2021)	Time and frequency domain and nonlinear	SVM	binary	Accuracy: 98.3%
(Wehler *et al.*, 2021)	Time and frequency domain (ultra short ECG time series)	ROC curves	binary	AUC: 0.892 (low-frequency FFT – 300s) AUC: 0.833 (SDNN – 300s)
(Carricarte Naranjo *et al.*, 2017c)	Time and frequency domain Shannon and Permutation entropy	LDA	binary	Accuracy: 75%
(Cornforth; Tarvainen; Jelinek, 2014)	Time and frequency domain and nonlinear	NB, SMO, KNN, and DT	binary	Accuracy: 71% (SMO)
(Cornforth; Tarvainen; Jelinek, 2013)	Time and frequency domain and nonlinear Renyi entropy	1 - PCA with NB 2 – GA with KNN	binary	1 – Accuracy: 64.5% AUC: 0.713 2 – Accuracy: 68.1% AUC: 0.734
(Khandoker; Jelinek; Palaniswami, 2009b)	Time and frequency domain Poincaré plot and Sample entropy	DT	binary	Accuracy: 88.24% Se: 100% Spe: 75%

Note: SVM – support vector machine; DT – decision tree; RF – random forest; LDA – linear discriminant analysis; NB – Naïve Bayes classifier; SMO – sequential minimal optimisation classifiers based on the support vector machine; KNN – K nearest neighbours; PCA – principal component analysis; GA – genetic algorithm.
Source: Elaborated by the author.

6.5 CONCLUSION

In conclusion, this study indicated that combining HRV-based features derived from the decomposed HRV components using the EMD method with traditional HRV features (involving time, frequency, and nonlinear analysis) leads to improved accuracy in distinguishing between different levels of CAN severity in comparison to the methods assessed individually, resulting in a classification accuracy of 88.4% (AUC = 0.881). The importance of this study is further highlighted by its application of a multiclass classification method to identify and diagnose three levels of CAN: absence, subclinical, and established. This allows for the potential use of this method as an additional screening tool for cardiovascular complications arising from DM, allowing for the identification of asymptomatic patients in the early stages of the disease, during which CAN is still reversible.

One limitation of this study is the imbalance in class distribution, where the representation of participants across various CAN severity levels may not be proportionate. The F1 score was chosen as an evaluation metric due to its consideration of this class imbalance. Nevertheless, future research could involve larger, more balanced datasets or the implementation of techniques to address class imbalance, such as employing oversampling approaches.

7 FINAL CONSIDERATIONS

This thesis's main objective was to evaluate initial alterations in cardiac autonomic function among diabetic individuals. This assessment was performed using metrics obtained from conventional HRV analysis techniques and metrics calculated from decomposed HRV signals following the Empirical Mode Decomposition method. Considering this, two studies were proposed: the first one investigated the relevance of EMD-based parameters to differentiate among levels of CAN progression, while the second one assessed the performance of machine learning models in the multiclass classification of CAN.

The main contributions of this thesis are as follows: (a) the significant relevance of EMD-based features extracted from HRV signals for distinguishing between progression levels of CAN, as demonstrated through statistical analysis and further supported by (b) the promising classification results achieved by machine learning models in multiclass CAN classification. The results of the studies also indicated that (c) the combination of conventional HRV measures with EMD-based features outperforms individual features in the classification of CAN; (d) features obtained from all HRV domain analyses, including time, frequency, nonlinear analyses, and EMD based are significant in CAN characterization, and; (e) as CAN progresses, a decrease in variability and power distribution is observed in the EMD decomposed components of the HRV signal. Additional contributions include (f) developing a signal processing tool for ECG and PPG data preprocessing, HRV-derived feature calculation, BRS and EMD analysis, and (g) developing a database to facilitate data management and subsequent analyses.

CAN is widely acknowledged as a form of diabetic autonomic neuropathy that results in disruptions in heart rate control, as well as changes in central and peripheral vascular dynamics (Fisher; Tahrani, 2017). The autonomic nervous system imbalance occurs early in the progression of CAN and is associated with an elevated cardiovascular risk before the development of definitive CAN (Vinik *et al.*, 2018). CAN is a condition characterized by a gradual deterioration, emphasizing the importance of assessing it in its early progressive stages and, ideally, identifying the initial alterations before symptoms become present, where autonomic balance can still be reversed (Vinik, 2012). The cardiovascular reflex tests measure heart rate and BP response to provocative physiological manoeuvres and still represent the gold standard in

autonomic testing and CAN diagnosis. Nevertheless, the most widely used diagnostic tests in clinical research are the conventional HRV indices derived from time- and frequency-domain and BRS (Spallone, 2019). The HRV signal is determined by combined inputs of the sympathetic and parasympathetic branches of the autonomic nervous system, divided as follows: the very low-frequency component representing the SNS, the low-frequency component representing a combination of SNS and PNS, and the high-frequency band corresponding to the function of the PNS (Williams *et al.*, 2022). Thus, introducing the EMD technique into HRV analysis can improve CAN assessment. Firstly, because the extracted components can be correlated with HRV frequency components (Chen *et al.*, 2019; Pan *et al.*, 2019) and secondly, because this enables an individual assessment of the responses of the ANS branches, allowing the visualization and characterization of intrinsic changes that may not be apparent when analysing the composite HRV signal.

To conclude, the results showed a promising use of the nonlinear EMD technique applied to HRV signals in evaluating the dynamic changes occurring in subclinical stages of DM patients with CAN. While this technique has been employed in other biomedical signals for assessing various conditions, it has not been employed in CAN assessment. Furthermore, most studies that evaluated CAN with other methods based on HRV have been limited by their binary methodology. In contrast, the methodology employed in this thesis adopted a multiclass approach, demonstrating the significance of EMD-based features in characterizing CAN and achieving a noteworthy classification accuracy of 88.4%. These results are consistent with the findings of a few relevant studies in the literature that also adopted a multiclass classification based on other HRV features. Given this perspective of CAN evaluation, a multidomain and multivariate approach is more appropriate for obtaining a comprehensive understanding of cardiac autonomic regulation.

Future works can involve conducting a more thorough CAN analysis with more patients to enhance the study's statistical power and overall reliability. Additionally, including more samples for machine learning models can further improve the accuracy and generalizability of the results. One important aspect of future studies evaluating CAN progression would be the continuous collection and analysis of data over time. This would enable more effective screening and help to identify which parameters have been altered and which ones have not, as well as assess whether treatment interventions have improved or even reversed CAN progression.

REFERENCES

ABDALRADA, Ahmad Shaker *et al.* Meta learning ensemble technique for diagnosis of cardiac autonomic neuropathy based on heart rate variability features. **30th International Conference on Computer Applications in Industry and Engineering, CAINE 2017**, [*s. l.*], n. June 2019, p. 169–175, 2017.

ABDULRAHMAN, Awf; BAYKARA, Muhammet; ALAKUS, Talha Burak. A Novel Approach for Emotion Recognition Based on EEG Signal Using Deep Learning. **Applied Sciences 2022, Vol. 12, Page 10028**, [*s. l.*], v. 12, n. 19, p. 10028, 2022.

ACHARYA, U. Rajendra *et al.* Application of empirical mode decomposition (EMD) for automated identification of congestive heart failure using heart rate signals. **Neural Computing and Applications**, [*s. l.*], v. 28, n. 10, p. 3073–3094, 2017.

ACHARYA, U. Rajendra *et al.* Application of entropies for automated diagnosis of epilepsy using EEG signals: A review. **Knowledge-Based Systems**, [*s. l.*], v. 88, p. 85–96, 2015.

ACHARYA, U. Rajendra *et al.* Automated diagnosis of epileptic EEG using entropies. **Biomedical Signal Processing and Control**, [*s. l.*], v. 7, n. 4, p. 401–408, 2012.

ACHARYA, U Rajendra; KANNATHAL, N; KRISHNAN, S M. Comprehensive analysis of cardiac health using heart rate signals. **Physiological Measurement**, [*s. l.*], v. 25, n. 5, p. 1139–1151, 2004.

AHLUWALIA, Tarunveer S. *et al.* Editorial: Novel Biomarkers for Type 2 Diabetes. **Frontiers in Endocrinology**, [*s. l.*], v. 10, n. SEP, p. 1–3, 2019.

ALKHODARI, Mohanad *et al.* Screening Cardiovascular Autonomic Neuropathy in Diabetic Patients with Microvascular Complications Using Machine Learning: A 24-Hour Heart Rate Variability Study. **IEEE Access**, [*s. l.*], v. 9, p. 119171–119187, 2021.

AMERICAN DIABETES ASSOCIATION. 2. Classification and Diagnosis of Diabetes: Standards of Medical Care in Diabetes—2021. **Diabetes Care**, [*s. l.*], v. 44, n. Supplement_1, p. S15–S33, 2021.

AMIN, Noha; DOUPIS, John. Diabetic foot disease: From the evaluation of the “foot at risk” to the novel diabetic ulcer treatment modalities. **World Journal of Diabetes**, [*s. l.*], v. 7, n. 7, p. 153–64, 2016.

ANDERSEN, Signe T. *et al.* Risk factors for the presence and progression of cardiovascular autonomic neuropathy in type 2 diabetes: Addition-Denmark. **Diabetes Care**, [*s. l.*], v. 41, n. 12, p. 2586–2594, 2018.

ANG, Lynn *et al.* Cardiovascular autonomic neuropathy: A silent killer with long reach. **Autonomic Neuroscience**, [*s. l.*], v. 225, p. 102646, 2020.

ASGHARZADEH-BONAB, Akbar; AMIRANI, Mehdi Chehel; MEHRI, Alaeddin. Spectral entropy and deep convolutional neural network for ECG beat classification. **Biocybernetics and Biomedical Engineering**, [*s. l.*], v. 40, n. 2, p. 691–700, 2020.

BAJAJ, V.; PACHORI, R. B. Classification of Seizure and Nonseizure EEG Signals Using Empirical Mode Decomposition. **IEEE Transactions on Information Technology in Biomedicine**, [*s. l.*], v. 16, n. 6, 2012.

BALCIOĞLU, Akif Serhat. Diabetes and cardiac autonomic neuropathy: Clinical manifestations, cardiovascular consequences, diagnosis and treatment. **World Journal of Diabetes**, [*s. l.*], v. 6, n. 1, p. 80, 2015.

BARNOVA, Katerina *et al.* A novel algorithm based on ensemble empirical mode decomposition for non-invasive fetal ECG extraction. **PLOS ONE**, [*s. l.*], v. 16, n. 8, 2021.

BARTELS, Rhenan *et al.* SinusCor: An advanced tool for heart rate variability analysis. **BioMedical Engineering Online**, [*s. l.*], v. 16, n. 1, p. 1–15, 2017.

BAUTISTA, Centeno *et al.* Electrocardiogram Analysis by Means of Empirical Mode Decomposition-Based Methods and Convolutional Neural Networks for Sudden Cardiac Death Detection. **Applied Sciences 2023, Vol. 13, Page 3569**, [*s. l.*], v. 13, n. 6, p. 3569, 2023.

BENICHOU, Thomas *et al.* Heart rate variability in type 2 diabetes mellitus: A systematic review and meta-analysis. **PLoS ONE**, [*s. l.*], v. 13, n. 4, p. 1–19, 2018.

BERNARDI, Luciano *et al.* Methods of investigation for cardiac autonomic dysfunction in human research studies. **Diabetes/Metabolism Research and Reviews**, [*s. l.*], v. 27, n. 7, p. 654–664, 2011.

BIAGGIONI, Italo *et al.* (org.). **Primer on the Autonomic Nervous System**. 4th. ed. Cambridge, EUA: Academic Press, 2022.

BILLMAN, George E. Heart rate variability - A historical perspective. **Frontiers in Physiology**, [*s. l.*], v. 2 NOV, p. 16984, 2011.

BLAND, J Martin; ALTMAN, Douglas G. Measuring agreement in method comparison studies. **http://dx.doi.org/10.1177/096228029900800204**, [*s. l.*], v. 8, n. 2, p. 135–160, 1999.

BOROWIK, Emila *et al.* Clinical usefulness of baroreflex sensitivity test in the detection of cardiovascular autonomic neuropathy in patients with type 2 diabetes mellitus. **Polski merkuriusz lekarski : organ Polskiego Towarzystwa Lekarskiego**, [*s. l.*], v. 39, n. 233, 2015.

BOROWSKA, Marta. Entropy-based algorithms in the analysis of biomedical signals. **Studies in Logic, Grammar and Rhetoric**, [*s. l.*], v. 43, n. 56, p. 21–32, 2015.

BOTE, José M.; RECAS, Joaquín; HERMIDA, Román. Evaluation of blood pressure estimation models based on pulse arrival time. **Computers and Electrical Engineering**, [*s. l.*], v. 84, p. 106616, 2020.

BOULTON, A J; GRIES, F A; JERVELL, J A. Guidelines for the diagnosis and outpatient management of diabetic peripheral neuropathy. **Diabetic medicine: a journal of the British Diabetic Association**, [*s. l.*], v. 15, n. 6, p. 508–14, 1998.

BRANDT, Christoph; POMPE, Bernd. Permutation entropy - a natural complexity measure for time series. **Physical Review Letters**, [*s. l.*], v. 88, n. 17, p. 1–5, 2002.

BRAVI, Andrea; LONGTIN, André; SEELY, Andrew Je. **Review and classification of variability analysis techniques with clinical applications**. [*S. l.: s. n.*], 2011.

CALLAGHAN, Brian C. *et al.* Diabetic neuropathy: what does the future hold? **Diabetologia**, [*s. l.*], v. 63, n. 5, p. 891–897, 2020.

CARDINALI, Daniel Pedro. **Autonomic nervous system: Basic and clinical aspects**. [*S. l.: s. n.*], 2017.

CARDOSO, Claudia R.L. *et al.* Prognostic importance of cardiovascular autonomic neuropathy on cardiovascular and mortality outcomes in individuals with type 2 diabetes: The Rio de Janeiro type 2 diabetes cohort. **Diabetes Research and Clinical Practice**, [*s. l.*], v. 196, p. 110232, 2023.

CARRICARTE NARANJO, Claudia *et al.* Permutation entropy analysis of heart rate variability for the assessment of cardiovascular autonomic neuropathy in type 1 diabetes mellitus. **Computers in Biology and Medicine**, [*s. l.*], v. 86, n. 409, p. 90–97, 2017a.

CASTIGLIONI, Paolo *et al.* Heart Rate Variability for the Early Detection of Cardiac Autonomic Dysfunction in Type 1 Diabetes. **Frontiers in Physiology**, [*s. l.*], v. 13, p. 1319, 2022.

CAVALHEIRO, Guilherme L *et al.* Study of age-related changes in postural control during quiet standing through Linear Discriminant Analysis. **BioMedical Engineering OnLine**, [*s. l.*], v. 8, n. 1, 2009.

CHA, Seon Ah *et al.* Time- and frequency-domain measures of heart rate variability predict cardiovascular outcome in patients with type 2 diabetes. **Diabetes Research and Clinical Practice**, [*s. l.*], v. 143, p. 159–169, 2018.

CHEN, Mingjing *et al.* Empirical mode decomposition as a novel approach to study heart rate variability in congestive heart failure assessment. **Entropy**, [*s. l.*], v. 21, n. 12, 2019.

CHEN, Weiting *et al.* Measuring complexity using FuzzyEn, ApEn, and SampEn. **Medical Engineering and Physics**, [*s. l.*], v. 31, n. 1, p. 61–68, 2009.

CHOWDHURY, Mahin *et al.* Cardiac autonomic neuropathy and risk of cardiovascular disease and mortality in type 1 and type 2 diabetes: a meta-analysis. **BMJ Open Diab Res Care**, [*s. l.*], v. 9, p. 2480, 2021.

CICHOSZ, Simon Lebech; JOHANSEN, Mette Dencker; HEJLESEN, Ole. Toward Big Data Analytics: Review of predictive models in management of Diabetes and its complications. **Journal of Diabetes Science and Technology**, [*s. l.*], v. 10, n. 1, p. 27–34, 2016.

CLIFFORD, Gari D.; TARASSENKO, Lionel. Quantifying errors in spectral estimates of HRV due to beat replacement and resampling. **IEEE Transactions on Biomedical Engineering**, [*s. l.*], v. 52, n. 4, p. 630–638, 2005.

COHEN, M.E.; HUDSON, D.L.; DEEDWANIA, P.C. Applying continuous chaotic modelling to cardiac signal analysis. **IEEE Engineering in Medicine and Biology Magazine**, [*s. l.*], v. 15, n. 5, 1996.

COOPMANS, Charlotte *et al.* Both Prediabetes and Type 2 Diabetes Are Associated With Lower Heart Rate Variability: The Maastricht Study. **Diabetes Care**, [*s. l.*], p. dc192367, 2020.

CORNFORTH, David; JELINEK, Herbert F.; TARVAINEN, Mika. A Comparison of Nonlinear Measures for the Detection of Cardiac Autonomic Neuropathy from Heart Rate Variability. **Entropy 2015, Vol. 17, Pages 1425-1440**, [*s. l.*], v. 17, n. 3, p. 1425–1440, 2015.

CORNFORTH, David; TARVAINEN, Mika P.; JELINEK, Herbert F. Automated selection of measures of heart rate variability for detection of early cardiac autonomic neuropathy | IEEE Conference Publication | IEEE Xplore. *In*: , 2014. **Computing in Cardiology**. [*S. l.: s. n.*], 2014.

CORNFORTH, David; TARVAINEN, Mika; JELINEK, Herbert F. Computational intelligence methods for the identification of early Cardiac Autonomic Neuropathy. **Proceedings of the 2013 IEEE 8th Conference on Industrial Electronics and Applications, ICIEA 2013**, [*s. l.*], p. 929–934, 2013.

COSSUL, Sandra *et al.* The Use of Empirical Mode Decomposition on Heart Rate Variability Signals to Assess Autonomic Neuropathy Progression in Type 2 Diabetes. **Applied Sciences 2023, Vol. 13, Page 7824**, [*s. l.*], v. 13, n. 13, p. 7824, 2023.

COSTA, Madalena; GOLDBERGER, Ary L.; PENG, C. K. Multiscale entropy analysis of biological signals. **Physical Review E - Statistical, Nonlinear, and Soft Matter Physics**, [*s. l.*], v. 71, n. 2, p. 1–18, 2005.

DA SILVA, Anne Kastelianne França *et al.* Application of Heart Rate Variability in Diagnosis and Prognosis of Individuals with Diabetes Mellitus: Systematic Review. **Annals of Noninvasive Electrocardiology**, [*s. l.*], v. 21, n. 3, p. 223–235, 2016.

DAGLIATI, Arianna *et al.* Machine Learning Methods to Predict Diabetes Complications. **Journal of Diabetes Science and Technology**, [*s. l.*], v. 12, n. 2, p. 295–302, 2018.

DILLINGHAM, Timothy *et al.* Establishing high-quality reference values for nerve conduction studies: A report from the normative data task force of the American Association of Neuromuscular & Electrodiagnostic Medicine. **Muscle and Nerve**, [*s. l.*], v. 54, n. 3, p. 366–370, 2016.

DING, Xiao Rong *et al.* Continuous Cuffless Blood Pressure Estimation Using Pulse Transit Time and Photoplethysmogram Intensity Ratio. **IEEE Transactions on Biomedical Engineering**, [*s. l.*], v. 63, n. 5, p. 964–972, 2016.

DORCELY, Brenda *et al.* **Novel biomarkers for prediabetes, diabetes, and associated complications**. [*S. l.*]: Dove Medical Press Ltd., 2017.

DUBEY, Rahul *et al.* Automated diagnosis of muscle diseases from EMG signals using empirical mode decomposition-based method. **Biomedical Signal Processing and Control**, [*s. l.*], v. 71, 2022.

ECHEVERRIA, J C *et al.* Application of empirical mode decomposition to heart rate variability analysis. **Medical & Biological Engineering & Computing**, [*s. l.*], v. 39, 2001.

EGAN, Aoife M.; DINNEEN, Seán F. **What is diabetes?**. [*S. l.*]: Elsevier Ltd, 2019.

ERDFELDER, Edgar *et al.* Statistical power analyses using G*Power 3.1: Tests for correlation and regression analyses. **Behavior Research Methods**, [*s. l.*], v. 41, n. 4, p. 1149–1160, 2009.

EWING, D. J. *et al.* The value of cardiovascular autonomic function tests: 10 years' experience in diabetes. **Diabetes Care**, [*s. l.*], v. 8, n. 5, p. 491–498, 1985.

EWING, D. J.; CAMPBELL, I. W.; CLARKE, B. F. Assessment of Cardiovascular Effects in Diabetic Autonomic Neuropathy and Prognostic Implications. **Annals of Internal Medicine**, [*s. l.*], v. 92, n. 2_Part_2, 1980.

FAGHERAZZI, G.; RAVAUD, P. Digital diabetes: Perspectives for diabetes prevention, management and research. **Diabetes and Metabolism**, [*s. l.*], v. 45, n. 4, p. 322–329, 2019.

FAUST, Oliver *et al.* Heart rate variability for medical decision support systems: A review. **Computers in Biology and Medicine**, [*s. l.*], v. 145, p. 105407, 2022.

FAUST, Oliver *et al.* Linear and non-linear analysis of cardiac health in diabetic subjects. **Biomedical Signal Processing and Control**, [*s. l.*], v. 7, n. 3, 2012.

FELDMAN, Eva L. *et al.* Diabetic neuropathy. **Nature Reviews Disease Primers**, [*s. l.*], v. 5, n. 1, 2019.

FISHER, Victoria L; TAHRANI, Abd A. Cardiac autonomic neuropathy in patients with diabetes mellitus: current perspectives. **Diabetes, Metabolic Syndrome and Obesity: Targets and Therapy**, [*s. l.*], v. Volume 10, p. 419–434, 2017.

FRATTOLA, A. *et al.* Time and frequency domain estimates of spontaneous baroreflex sensitivity provide early detection of autonomic dysfunction in diabetes mellitus. **Diabetologia**, [*s. l.*], v. 40, n. 12, p. 1470–1475, 1997.

GARCÍA MARTÍNEZ, Constantino Antonio *et al.* Heart Rate Variability Analysis with the R package RHRV. Cham, Use R, 2017.

GERRITSEN, Jeanet *et al.* Impaired autonomic function is associated with increased mortality, especially in subjects with diabetes, hypertension, or a history of cardiovascular disease: The hoorn study. **Diabetes Care**, [*s. l.*], v. 24, n. 10, p. 1793–1798, 2001.

GOLDBERGER, Ary L.; GOLDBERGER, Zachary D.; SHVILKIN, Alexei. **Goldberger's Clinical Electrocardiography**. 8th. Ed. [*S. l.*]: Elsevier, 2013-. ISSN 0267-6591. v. 32

HADOUSH, Hikmat; ALAFEEF, Maha; ABDULHAY, Enas. Automated identification for autism severity level: EEG analysis using empirical mode decomposition and second order difference plot. **Behavioural Brain Research**, [*s. l.*], v. 362, n. December 2018, p. 240–248, 2019.

HASAN, Nahian Ibn; BHATTACHARJEE, Arnab. Deep Learning Approach to Cardiovascular Disease Classification Employing Modified ECG Signal from Empirical Mode Decomposition. **Biomedical Signal Processing and Control**, [*s. l.*], v. 52, 2019.

HASSAN, Md Rafiul *et al.* Early detection of cardiovascular autonomic neuropathy: A multi-class classification model based on feature selection and deep learning feature fusion. **Information Fusion**, [*s. l.*], v. 77, p. 70–80, 2022.

HASTIE, Trevor; TIBSHIRANI, Robert; FRIEDMAN, Jerome. **The elements of statistical learning: Data Mining, Inference and Prediction**. [*S. l.: s. n.*], 2009.

HILLIS, G. S. *et al.* Resting heart rate and the risk of death and cardiovascular complications in patients with type 2 diabetes mellitus. **Diabetologia**, [*s. l.*], v. 55, n. 5, p. 1283–1290, 2012.

HO, Yi Lwun *et al.* The prognostic value of non-linear analysis of heart rate variability in patients with congestive heart failure-a pilot study of multiscale entropy. **PLoS ONE**, [*s. l.*], v. 6, n. 4, p. 4–9, 2011.

HOSHI, Rosangela A. *et al.* Decreased heart rate variability as a predictor for diabetes—A prospective study of the Brazilian longitudinal study of adult health. **Diabetes/Metabolism Research and Reviews**, [*s. l.*], v. 35, n. 7, p. 1–8, 2019.

HSU, Che Hao *et al.* Poincaré plot indexes of heart rate variability detect dynamic autonomic modulation during general anesthesia induction. **Acta Anaesthesiologica Taiwanica**, [*s. l.*], v. 50, n. 1, p. 12–18, 2012.

HUANG, Norden E. *et al.* The empirical mode decomposition and the Hilbert spectrum for nonlinear and non-stationary time series analysis. **Proceedings of the Royal Society of London. Series A: Mathematical, Physical and Engineering Sciences**, [*s. l.*], v. 454, n. 1971, p. 903–995, 1998.

INTERNATIONAL DIABETES FEDERATION. **IDF Diabetes Atlas**. 10th. ed. [*S. l.: s. n.*], 2021. Available on: www.diabetesatlas.org.

ISLER, Yalcin *et al.* Multi-stage classification of congestive heart failure based on short-term heart rate variability. **Chaos, Solitons and Fractals**, [*s. l.*], v. 118, p. 145–151, 2019.

JAISWAL, Mamta *et al.* Reduced heart rate variability among youth with type 1 diabetes: The SEARCH CVD study. **Diabetes Care**, [*s. l.*], v. 36, n. 1, p. 157–162, 2013.

JAMES, Gareth *et al.* **An Introduction to Statistical Learning with Applications in R**. [*S. l.: s. n.*], 2014.

JELINEK, Herbert F. *et al.* Association of cardiovascular risk using non-linear heart rate variability measures with the Framingham risk score in a rural population. **Frontiers in Physiology**, [*s. l.*], v. 4, 2013.

JELINEK, Herbert F. *et al.* Investigation of Linear and Nonlinear Properties of a Heartbeat Time Series Using Multiscale Rényi Entropy. **Entropy 2019, Vol. 21, Page 727**, [*s. l.*], v. 21, n. 8, p. 727, 2019.

JELINEK, Herbert F. *et al.* Using meta-regression data mining to improve predictions of performance based on heart rate dynamics for Australian football. **Applied Soft Computing Journal**, [*s. l.*], v. 14, n. PART A, p. 81–87, 2014.

JUSTER-SWITLYK, Kelsey; SMITH, A. Gordon. Updates in diabetic peripheral neuropathy. **F1000Research**, [*s. l.*], v. 5, n. 0, p. 738, 2016.

KAMATH, Markad V.; WATANABE, Mari A.; UPTON, Adrian R.M. **Heart rate variability (HRV) signal analysis: Clinical applications**. [*S. l.*]: CRC Press, 2016.

KARDOS, Attila *et al.* Determinants of Spontaneous Baroreflex Sensitivity in a Healthy Working Population. **Hypertension**, [*s. l.*], v. 37, n. 3, p. 911–916, 2001.

KAREMAKER, John M. An introduction into autonomic nervous function. **Physiological Measurement**, [*s. l.*], v. 38, n. 5, p. R89, 2017.

KARUN, Kalesh M.; PURANIK, Amitha. BA.plot: An R function for Bland-Altman analysis. **Clinical Epidemiology and Global Health**, [*s. l.*], v. 12, p. 100831, 2021.

KAVAKIOTIS, Ioannis *et al.* Machine Learning and Data Mining Methods in Diabetes Research. **Computational and Structural Biotechnology Journal**, [*s. l.*], v. 15, p. 104–116, 2017.

KHANDOKER, Ahsan H. *et al.* Association of cardiac autonomic neuropathy with alteration of sympatho-vagal balance through heart rate variability analysis. **Medical Engineering & Physics**, [*s. l.*], v. 32, n. 2, p. 161–167, 2010.

KHANDOKER, Ahsan H.; JELINEK, Herbert F.; PALANISWAMI, Marimuthu. Identifying diabetic patients with cardiac autonomic neuropathy by heart rate complexity analysis. **BioMedical Engineering Online**, [*s. l.*], v. 8, p. 1–12, 2009.

KIM, Hye Geum *et al.* Stress and heart rate variability: A meta-analysis and review of the literature. **Psychiatry Investigation**, [*s. l.*], v. 15, n. 3, p. 235–245, 2018.

KOO, Terry K.; LI, Mae Y. A Guideline of Selecting and Reporting Intraclass Correlation Coefficients for Reliability Research. **Journal of Chiropractic Medicine**, [*s. l.*], v. 15, n. 2, p. 155–163, 2016.

KÖREI, Anna *et al.* Why Not to Use the Handgrip Test in the Assessment of Cardiovascular Autonomic Neuropathy Among Patients with Diabetes Mellitus. **Current Vascular Pharmacology**, [*s. l.*], v. 15, n. 1, p. 66–73, 2017.

KUBAT, Miroslav. **An Introduction to Machine Learning**. [*S. l.: s. n.*], 2017.

KÜCK, Jana-Luise *et al.* Impairment in Baroreflex Sensitivity in Recent-Onset Type 2 Diabetes Without Progression Over 5 Years. **Diabetes**, [*s. l.*], v. 69, n. 5, 2020.

KUEHL, Michael; STEVENS, Martin J. Cardiovascular autonomic neuropathies as complications of diabetes mellitus. **Nature Reviews Endocrinology**, [*s. l.*], v. 8, n. 7, p. 405–416, 2012.

KUMAR, Shailesh; PANIGRAHY, Damodar; SAHU, P.K. Denoising of Electrocardiogram (ECG) signal by using empirical mode decomposition (EMD) with non-local mean (NLM) technique. **Biocybernetics and Biomedical Engineering**, [*s. l.*], v. 38, n. 2, 2018.

KUUSELA, Tom. Methodological Aspects of Baroreflex Sensitivity Analysis. *In*: KAMATH, Markad V.; WATANABE, Mari A.; UPTON, Adrian R.M. (org.). **Heart Rate Variability (HRV) Signal Analysis: Clinical Applications**. [*S. l.: s. n.*], 2013. p. 43–58.

LA ROVERE, Maria Teresa *et al.* Baroreflex sensitivity and heart-rate variability in prediction of total cardiac mortality after myocardial infarction. **Lancet**, [*s. l.*], v. 351, n. 9101, p. 478–484, 1998.

LAI, Ying-Cheng; YE, Nong. Recent Developments in Chaotic Time Series Analysis. **International Journal of Bifurcation and Chaos**, [*s. l.*], v. 13, n. 06, p. 1383–1422, 2003.

LILJEQUIST, David; ELFVING, Britt; ROALDSEN, Kirsti Skavberg. Intraclass correlation – A discussion and demonstration of basic features. **PLOS ONE**, [*s. l.*], v. 14, n. 7, p. e0219854, 2019.

LIN, Kun *et al.* Combination of Ewing test, heart rate variability, and heart rate turbulence analysis for early diagnosis of diabetic cardiac autonomic neuropathy. **Medicine (United States)**, [*s. l.*], v. 96, n. 45, p. 1–5, 2017.

LIU, Chengyu *et al.* Analysis of heart rate variability using fuzzy measure entropy. **Computers in Biology and Medicine**, [*s. l.*], v. 43, n. 2, p. 100–108, 2013.

MAHESHWARI, Sonam; KUMAR, Ankur. Empirical Mode Decomposition: Theory & Applications. **International Journal of Electronic and Electrical Engineering**, [*s. l.*], v. 7, n. 8, p. 873–878, 2014.

MATSUTANI, Daisuke *et al.* Visit-to-visit HbA1c variability is inversely related to baroreflex sensitivity independently of HbA1c value in type 2 diabetes. **Cardiovascular Diabetology**, [*s. l.*], v. 17, n. 1, p. 1–10, 2018.

MCCRATY, Rollin; SHAFFER, Fred. Heart rate variability: New perspectives on physiological mechanisms, assessment of self-regulatory capacity, and health risk. **Global Advances in Health and Medicine**, [*s. l.*], v. 4, n. 1, p. 46–61, 2015.

MISHRA, Vipin K. *et al.* An efficient method for analysis of EMG signals using improved empirical mode decomposition. **AEU - International Journal of Electronics and Communications**, [*s. l.*], v. 72, 2017.

MISHRA, Vipin K. *et al.* Analysis of ALS and normal EMG signals based on empirical mode decomposition. **IET Science, Measurement and Technology**, [*s. l.*], v. 10, n. 8, p. 963–971, 2016.

MOHANTY, Monalisa *et al.* Classification of ventricular arrhythmias using empirical mode decomposition and machine learning algorithms. **Progress in Artificial Intelligence**, [*s. l.*], 2021.

MOTATAIANU, Anca *et al.* Cardiac autonomic neuropathy in type 1 and type 2 diabetes patients. **BMC Neurology**, [*s. l.*], v. 18, n. 1, p. 1–9, 2018.

MUKKAMALA, Ramakrishna *et al.* Towards Ubiquitous Blood Pressure Monitoring via Pulse Transit Time: Theory and Practice. **IEEE Transactions on Biomedical Engineering**, [*s. l.*], v. 62, n. 8, p. 1879–1901, 2015.

MÜLLER, Andreas; GUIDO, Sarah. **Introduction to Machine Learning with Python**. [*S. l.: s. n.*], 2016.

MURPHY, Kevin P. **Machine Learning, a Probabilistic Perspective**. [*S. l.: s. n.*], 2012.

NAIK, Ganesh R.; SELVAN, S. Easter; NGUYEN, Hung T. Single-Channel EMG Classification with Ensemble-Empirical-Mode-Decomposition-Based ICA for

Diagnosing Neuromuscular Disorders. **IEEE Transactions on Neural Systems and Rehabilitation Engineering**, [*s. l.*], v. 24, n. 7, 2016.

NASTESKI, Vladimir. An overview of the supervised machine learning methods. [*s. l.*], 2017.

NEDERGAARD, Rasmus Bach *et al.* Features characterising cardiac autonomic neuropathy in diabetes using ensembled classification. **Clinical Neurophysiology**, [*s. l.*], v. 154, p. 200–208, 2023.

O'BRIEN, I. A.; O'HARE, P.; CORRALL, R. J.M. Heart rate variability in healthy subjects: effect of age and the derivation of normal ranges for tests of autonomic function. **Heart**, [*s. l.*], v. 55, n. 4, p. 348–354, 1986.

ORINI, Michele *et al.* Introduction to Complex Cardiovascular Physiology. *In*: BARBIERI, Riccardo; SCILINGO, Enzo Pasquale; VALENZA, Gaetano (org.). **Complexity and nonlinearity in cardiovascular signals**. [*S. l.*]: Springer, 2017. p. 3–44.

PACHORI, Ram Bilas *et al.* An improved online paradigm for screening of diabetic patients using RR-interval signals. **Journal of Mechanics in Medicine and Biology**, [*s. l.*], v. 16, n. 1, p. 1–23, 2016.

PACHORI, Ram Bilas *et al.* Application of empirical mode decomposition for analysis of normal and diabetic RR-interval signals. **Expert Systems with Applications**, [*s. l.*], v. 42, n. 9, p. 4567–4581, 2015.

PACHORI, Ram Bilas; PATIDAR, Shivnarayan. Epileptic seizure classification in EEG signals using second-order difference plot of intrinsic mode functions. **Computer Methods and Programs in Biomedicine**, [*s. l.*], v. 113, n. 2, p. 494–502, 2014.

PAN, Weifeng *et al.* Multi-Frequency Components Entropy as Novel Heart Rate Variability Indices in Congestive Heart Failure Assessment. **IEEE Access**, [*s. l.*], v. 7, p. 37708–37717, 2019.

PAN, Jiapu; TOMPKINS, Willis J. A Real-Time QRS Detection Algorithm. **IEEE Transactions on Biomedical Engineering**, [*s. l.*], v. BME-32, n. 3, 1985.

PEDREGOSA, Fabian *et al.* Scikit-learn: Machine Learning in Python Gaël Varoquaux Bertrand Thirion Vincent Dubourg Alexandre Passos PEDREGOSA, VAROQUAUX, GRAMFORT ET AL. Matthieu Perrot. **Journal of Machine Learning Research**, [*s. l.*], v. 12, p. 2825–2830, 2011.

PETRY, Daiana; MARQUES, Claudia Mirian de Godoy; MARQUES, Jefferson Luiz Brum. Baroreflex Sensitivity with Different Lags for the Evaluation of Cardiovascular Autonomic Neuropathy in Subjects with Diabetes. [*s. l.*], p. 1–22, 2020.

PISKORSKI, J.; GUZIK, P. Geometry of the Poincaré plot of RR intervals and its asymmetry in healthy adults. **Physiological Measurement**, [*s. l.*], v. 28, n. 3, p. 287–300, 2007.

POP-BUSUI, Rodica. Cardiac Autonomic Neuropathy in Diabetes: A clinical perspective. **Diabetes Care**, [*s. l.*], v. 33, n. 2, p. 434, 2010.

POP-BUSUI, Rodica *et al.* Diabetic neuropathy: A position statement by the American diabetes association. **Diabetes Care**, [*s. l.*], v. 40, n. 1, p. 136–154, 2017.

POP-BUSUI, Rodica *et al.* Utility of using electrocardiogram measures of heart rate variability as a measure of cardiovascular autonomic neuropathy in type 1 diabetes patients. **Journal of Diabetes Investigation**, [*s. l.*], v. 13, n. 1, p. 125–133, 2022.

POP-BUSUI, Rodica. What Do We Know and We Do Not Know About Cardiovascular Autonomic Neuropathy in Diabetes. **Journal of Cardiovascular Translational Research 2012 5:4**, [*s. l.*], v. 5, n. 4, p. 463–478, 2012.

PUDJIHARTONO, Nicholas *et al.* A Review of Feature Selection Methods for Machine Learning-Based Disease Risk Prediction. **Frontiers in Bioinformatics**, [*s. l.*], v. 2, p. 927312, 2022.

RAJALA, Satu; LINDHOLM, Harri; TAIPALUS, Tapio. Comparison of photoplethysmogram measured from wrist and finger and the effect of measurement location on pulse arrival time. **Physiological Measurement**, [*s. l.*], v. 39, n. 7, 2018.

RAJENDRA ACHARYA, U. *et al.* Automated identification of normal and diabetes heart rate signals using nonlinear measures. **Computers in Biology and Medicine**, [*s. l.*], v. 43, n. 10, p. 1523–1529, 2013.

RAKSHIT, Manas; DAS, Susmita. An efficient ECG denoising methodology using empirical mode decomposition and adaptive switching mean filter. **Biomedical Signal Processing and Control**, [*s. l.*], v. 40, 2018.

RASCHKA, Sebastian. Model Evaluation, Model Selection, and Algorithm Selection in Machine Learning. [*s. l.*], 2018.

RASCHKA, Sebastian; MIRJALILI, Vahid. **Python Machine Learning: Machine Learning and Deep Learning with Python, scikit-learn, and TensorFlow 2**. [*S. l.: s. n.*], 2019.

REMESEIRO, Beatriz; BOLON-CANEDO, Veronica. A review of feature selection methods in medical applications. **Computers in Biology and Medicine**, [*s. l.*], v. 112, n. February, p. 103375, 2019.

RICHMAN, J S; MOORMAN, J R. Physiological time-series analysis using approximate entropy and sample entropy. **American journal of physiology. Heart and circulatory physiology**, [*s. l.*], v. 278, n. 6, p. H2039-49, 2000.

ROLIM, Luiz Clemente; DE SOUZA, José Sérgio Tomaz; DIB, Sérgio Atala. Tests for early diagnosis of cardiovascular autonomic neuropathy: Critical analysis and relevance. **Frontiers in Endocrinology**, [*s. l.*], v. 4, n. NOV, p. 2–5, 2013.

ROY, Bhaskar; GHATAK, Sobhendu. Nonlinear Methods to Assess Changes in Heart Rate Variability in Type 2 Diabetic Patients - PubMed. **Arquivos Brasileiros de Cardiologia**, [*s. l.*], v. 101, n. 4, p. 317–327, 2013.

S. B. KOTSIANTIS; D. KANELLOPOULOS; P. E. PINTELAS. Data Preprocessing for Supervised Learning. **INTERNATIONAL JOURNAL OF COMPUTER SCIENCE**, [*s. l.*], v. 1, n. 1, 2006.

SALANKAR, Nilima; MISHRA, Pratikshya; GARG, Lalit. Emotion recognition from EEG signals using empirical mode decomposition and second-order difference plot. **Biomedical Signal Processing and Control**, [*s. l.*], v. 65, 2021.

SASSI, Roberto *et al.* Advances in heart rate variability signal analysis: joint position statement by the e-Cardiology ESC Working Group and the European Heart Rhythm Association co-endorsed by the Asia Pacific Heart Rhythm Society. **Europace**, [*s. l.*], v. 17, n. 9, p. 1341–1353, 2015.

SEDGWICK, Philip. Limits of agreement (Bland-Altman method). **BMJ**, [*s. l.*], v. 346, n. 7900, 2013.

SELVAN, Sharanya Senthamil *et al.* Complexity Analysis in the PR, QT, RR and ST Segments of ECG for Early Assessment of Severity in Cardiac Autonomic Neuropathy. **Applied Sciences 2022, Vol. 12, Page 5746**, [*s. l.*], v. 12, n. 11, p. 5746, 2022.

SHAFFER, Fred; GINSBERG, J. P. An Overview of Heart Rate Variability Metrics and Norms. **Frontiers in Public Health**, [*s. l.*], v. 5, n. September, p. 1–17, 2017.

SHAFFER, Fred; MCCRATY, Rollin; ZERR, Christopher L. A healthy heart is not a metronome: an integrative review of the heart's anatomy and heart rate variability. **Frontiers in Psychology**, [*s. l.*], v. 5, n. September, p. 1–19, 2014.

SHI, Manhong *et al.* Early Detection of Sudden Cardiac Death by Using Ensemble Empirical Mode Decomposition-Based Entropy and Classical Linear Features from Heart Rate Variability Signals. **Frontiers in Physiology**, [*s. l.*], v. 11, n. February, p. 1–16, 2020.

SILVA, Anne Kastelianne França da *et al.* Sensibilidade, Especificidade e Valor Preditivo dos Índices da Variabilidade da Frequência Cardíaca no Diabetes Mellitus Tipo 1. **Arquivos Brasileiros de Cardiologia**, [*s. l.*], v. 108, n. 3, p. 255–262, 2017.

SILVA-E-OLIVEIRA, Julia *et al.* Heart rate variability based on risk stratification for type 2 diabetes mellitus. **Einstein (Sao Paulo, Brazil)**, [*s. l.*], v. 15, n. 2, p. 141–147, 2017.

SILVERTHORN, Dee Unglaub. **Human Physiology: An Integrated Approach**. 8th. ed. United Kingdom: Pearson Educations, 2019.

SOH, Desmond Chuang Kiat *et al.* A computational intelligence tool for the detection of hypertension using empirical mode decomposition. **Computers in Biology and Medicine**, [*s. l.*], v. 118, 2020.

SOLÀ, Josep; DELGADO-GONZALO, Ricard. **The Handbook of Cuffless Blood Pressure Monitoring, A Practical Guide for Clinicians, Researchers, and Engineers.** [*S. l.: s. n.*], 2019.

SOOD, Surabhi *et al.* Application of empirical mode decomposition-based features for analysis of normal and CAD heart rate signals. **Journal of Mechanics in Medicine and Biology**, [*s. l.*], v. 16, n. 1, p. 1–20, 2016.

SOUZA NETO, E P *et al.* Assessment of cardiovascular autonomic control by the empirical mode decomposition. **Methods of information in medicine**, [*s. l.*], v. 43, n. 1, 2004.

SPALLONE, Vincenza. Update on the Impact, Diagnosis and Management of Cardiovascular Autonomic Neuropathy in Diabetes: What Is Defined, What Is New, and What Is Unmet. **Diabetes & Metabolism Journal**, [*s. l.*], v. 43, n. 1, p. 3, 2019.

SUBASI, Adbdulhamit. **Practical Guide for Biomedical Signals Analysis Using Machine Learning Techniques: A MATLAB Based Approach**. [*S. l.*]: Academic Press, 2019.

SUDA, Eneida Y. *et al.* Later stages of diabetic neuropathy affect the complexity of the neuromuscular system at the knee during low-level isometric contractions. **Muscle and Nerve**, [*s. l.*], v. 57, n. 1, p. 112–121, 2018.

SVAČINOVÁ, J. *et al.* Diagnostic Significance of a Mild Decrease of Baroreflex Sensitivity with Respect to Heart Rate in Type 1 Diabetes Mellitus. **Physiological Research**, [*s. l.*], v. 62, n. 6, p. 605–613, 2013.

TANK, Jens *et al.* **Reference Values of Indices of Spontaneous Baroreceptor Reflex Sensitivity**. [*S. l.: s. n.*], 2000.

TARVAINEN, Mika P. *et al.* Cardiac autonomic dysfunction in type 2 diabetes - effect of hyperglycemia and disease duration. **Frontiers in Endocrinology**, [*s. l.*], v. 5, n. AUG, p. 1–9, 2014a.

TARVAINEN, Mika P. *et al.* Complexity of heart rate variability in type 2 diabetes - Effect of hyperglycemia. **Proceedings of the Annual International Conference of the IEEE Engineering in Medicine and Biology Society, EMBS**, [*s. l.*], p. 5558–5561, 2013.

TARVAINEN, Mika P. *et al.* Kubios HRV - Heart rate variability analysis software. **Computer Methods and Programs in Biomedicine**, [*s. l.*], v. 113, n. 1, p. 210–220, 2014b.

TAYEL, Mazhar; ALSABA, Eslam. Poincaré Plot for Heart Rate Variability. **International Journal of Medical, Health, Biomedical, Bioengineering and Pharmaceutical Engineering**, [*s. l.*], v. 9, n. 9, p. 708–711, 2015.

TESFAYE, Solomon *et al.* Diabetic neuropathies: Update on definitions, diagnostic criteria, estimation of severity, and treatments. **Diabetes Care**, [*s. l.*], v. 33, n. 10, p. 2285–2293, 2010.

TESFAYE, S; SELVARAJAH, D. Advances in the epidemiology, pathogenesis and management of diabetic peripheral neuropathy. **Diabetes/Metabolism Research and Reviews**, [*s. l.*], n. 28, p. 8–14, 2012.

TOICHI, Motomi *et al.* A new method of assessing cardiac autonomic function and its comparison with spectral analysis and coefficient of variation of R-R interval. **Journal of the Autonomic Nervous System**, [*s. l.*], v. 62, n. 1–2, p. 79–84, 1997.

VALENZA, Gaetano *et al.* Measures of sympathetic and parasympathetic autonomic outflow from heartbeat dynamics. **Journal of Applied Physiology**, [*s. l.*], v. 125, n. 1, p. 19–39, 2018.

VEST, Adriana N. *et al.* An open-source benchmarked toolbox for cardiovascular waveform and interval analysis. **Physiological Measurement**, [*s. l.*], v. 39, n. 10, p. aae021, 2018.

VINIK, Aaron I. *et al.* Cardiac Autonomic Neuropathy in Diabetes: A Predictor of Cardiometabolic Events. **Frontiers in Neuroscience**, [*s. l.*], v. 12, n. AUG, p. 1–11, 2018.

VINIK, Aaron I. The conductor of the autonomic orchestra. **Frontiers in Endocrinology**, [*s. l.*], v. 3, n. JUN, p. 1–13, 2012.

VINIK, A. I.; CASELLINI, C.; NÉVORET, M. L. Alternative Quantitative Tools in the Assessment of Diabetic Peripheral and Autonomic Neuropathy. **International Review of Neurobiology**, [*s. l.*], v. 127, p. 235–285, 2016.

VINIK, Aaron I; ERBAS, Tomris; CASELLINI, Carolina M. Diabetic cardiac autonomic neuropathy, inflammation and cardiovascular disease. **Journal of Diabetes Investigation**, [*s. l.*], v. 4, n. 1, p. 4–18, 2013.

VINIK, Aaron I.; ZIEGLER, Dan. Diabetic cardiovascular autonomic neuropathy. **Circulation**, [*s. l.*], v. 115, n. 3, p. 387–397, 2007.

WEHLER, D. *et al.* Reliability of heart-rate-variability features derived from ultra-short ECG recordings and their validity in the assessment of cardiac autonomic neuropathy. **Biomedical Signal Processing and Control**, [*s. l.*], v. 68, p. 102651, 2021.

WILLIAMS, Scott *et al.* Cardiac Autonomic Neuropathy in Type 1 and 2 Diabetes: Epidemiology, Pathophysiology, and Management. **Clinical Therapeutics**, [*s. l.*], v. 44, n. 10, p. 1394–1416, 2022.

WON, Jong Chul; PARK, Tae Sun. Recent Advances in Diagnostic Strategies for Diabetic Peripheral Neuropathy. **Endocrinology and metabolism (Seoul, Korea)**, [*s. l.*], v. 31, n. 2, p. 230–8, 2016.

WONG, Mico Yee Man; POON, Carmen Chung Yan; ZHANG, Yuan Ting. An evaluation of the cuffless blood pressure estimation based on pulse transit time technique: A half year study on normotensive subjects. **Cardiovascular Engineering**, [*s. l.*], v. 9, n. 1, p. 32–38, 2009.

XIAO, Ming Xia *et al.* Combination of R-R interval and crest time in assessing complexity using multiscale cross-approximate entropy in normal and diabetic subjects. **Entropy**, [*s. l.*], v. 20, n. 7, p. 1–15, 2018.

ZAFRIR, Barak *et al.* Resting heart rate and measures of effort-related cardiac autonomic dysfunction predict cardiovascular events in asymptomatic type 2 diabetes. **European Journal of Preventive Cardiology**, [*s. l.*], v. 23, n. 12, p. 1298–306, 2016.

ZIEMSSEN, Tjalf; SIEPMANN, Timo. The Investigation of the Cardiovascular and Sudomotor Autonomic Nervous System—A Review. **Frontiers in Neurology**, [*s. l.*], v. 10, n. February, 2019.

ZYGMUNT, Agnieszka; STANCZYK, Jerzy. Methods of evaluation of autonomic nervous system function. **Archives of Medical Science**, [*s. l.*], v. 6, n. 1, p. 11–18, 2010.

ATTACHMENT A – ETHICS COMMITTEE

UNIVERSIDADE FEDERAL DE SANTA CATARINA - UFSC

PARECER CONSUBSTANCIADO DO CEP

DADOS DA EMENDA

Título da Pesquisa: Verificação de Alterações Precoces no Sistema Neuromotor em Indivíduos com Neuropatia Diabética Periférica

Pesquisador: Jefferson Luiz Brum Marques

Área Temática:

Versão: 5

CAAE: 58989616.1.0000.0121

Instituição Proponente: Universidade Federal de Santa Catarina

Patrocinador Principal: Financiamento Próprio

DADOS DO PARECER

Número do Parecer: 3.326.385

Apresentação do Projeto:

Trata-se de uma nova emenda de um projeto aprovado em 2016 cujas emendas foram aprovadas em momentos posteriores. Trata-se de uma pesquisa aplicada, quanto à natureza; quantitativa, quanto à abordagem; transversal, quanto ao tempo; exploratória, quanto
aos objetivos; experimental, quanto aos procedimentos coordenada pelo prof. dr. Jefferson Luiz Brum Marques a fim de verificar as alterações precoces no sistema neuromotor em indivíduos com neuropatia Diabética periférica. A justificativas emenda pelos pesquisadores é a seguinte: "o objetivo inicial se refere a uma investigação muscular e sensorial utilizando técnicas de eletromiografia de superfície, estudos de condução nervosa e pressão plantar para avaliação de alterações ocasionadas pela neuropatia diabética periférica. O segundo objetivo referente a emenda, é realizar uma investigação do sistema autônomo utilizando eletrocardiograma por meio da análise da variabilidade cardíaca e testes de pupilometria. Dessa forma, a combinação de técnicas para avaliação das funções nervosas periféricas e autonômicas pode ser interessante para avaliar e identificar manifestações precoces de neuropatia diabética. Portanto, as funções periféricas sensoriais, motoras e autonômicas serão avaliadas de forma conjunta por meio dos seguintes métodos: eletromiografia multicanal de superfície, pressão plantar, testes eletrofisiológicos (condução nervosa), ECG e pupilometria e, ao final, os resultados serão comparados de forma conjunta." Portanto, trata-se da inclusão de novos procedimentos como coleta de dados. Os pesquisadores anexaram todos os instrumentos e demais documentos

Endereço: Universidade Federal de Santa Catarina, Prédio Reitoria II, R: Desembargador Vitor Lima, nº 222, sala 401
Bairro: Trindade **CEP:** 88.040-400
UF: SC **Município:** FLORIANOPOLIS
Telefone: (48)3721-6094 **E-mail:** cep.propesq@contato.ufsc.br

pertinentes às modificações de interesse para o desenvolvimento da pesquisa.

Objetivo da Pesquisa:

Objetivo Primário:

O objetivo primário deste trabalho é utilizar a eletromiografia multicanal de superfície e avaliação da pressão plantar com o intuito de investigar se existem indícios de perda da UM unida a reinervação em pacientes com diabetes, antes mesmo de apresentarem sintomas clínicos de neuropatia periférica. Também o obejetivo deste trabalho é realizar um estudo eletrofisiológico para análise da condução nervosa e identificação de anormalidades das funções nervosas periféricas de nervos motores e nervos sensoriais em pacientes diabéticos com neuropatia periférica estabelecida e em pacientes que ainda não apresentam sintomas suficientes para o diagnóstico da doença.

Objetivo Secundário:

O objetivo secundário deste trabalho é avaliar as funções nervosas autonômicas em pacientes diabéticos sem sintomas ou sinais de neuropatia em pacientes diabéticos em diferentes estágios de neuropatia periférica, utilizando técnicas de avaliação da resposta pupilar (pupilômetro) e avaliação das funções cardiovasculares com a aquisição de sinais de eletrocardiograma e pressão arterial.

Avaliação dos Riscos e Benefícios:

Os pesquisadores mencionam com detalhes todos os riscos relativos aos novos procedimentos para a coleta de dados no formulário da Plataforma Brasil e no TCLE reapresentado de acordo com a inclusão dos procedimentos.

Comentários e Considerações sobre a Pesquisa:

Documentos anexados frente a nova emenda. Cronograma reorganizado para atender às novas demandas propostas.

Considerações sobre os Termos de apresentação obrigatória:

Adequado de acordo com a Resolução 466/2012.

Recomendações:

não se aplica.

Conclusões ou Pendências e Lista de Inadequações:

Conclusão: aprovado.

Considerações Finais a critério do CEP:

UNIVERSIDADE FEDERAL DE SANTA CATARINA - UFSC

O presente projeto, seguiu nesta data para análise da CONEP e só tem o seu início autorizado após a aprovação pela mesma.

Este parecer foi elaborado baseado nos documentos abaixo relacionados:

Tipo Documento	Arquivo	Postagem	Autor	Situação
Informações Básicas do Projeto	PB_INFORMAÇÕES_BÁSICAS_1257577_E2.pdf	20/03/2019 15:12:20		Aceito
Recurso Anexado pelo Pesquisador	Observacoes_emenda_2.pdf	20/03/2019 15:10:18	Mateus Andre Favretto	Aceito
Outros	Questionario_1_emenda_2.pdf	20/03/2019 15:09:08	Mateus Andre Favretto	Aceito
Projeto Detalhado / Brochura Investigador	Pj_detalhado_Comite_etica_emenda_2.pdf	20/03/2019 15:08:23	Mateus Andre Favretto	Aceito
TCLE / Termos de Assentimento / Justificativa de Ausência	TCLE_emenda_2.pdf	20/03/2019 15:07:31	Mateus Andre Favretto	Aceito
Declaração de Instituição e Infraestrutura	Termo_de_consordancia_HU.pdf	20/03/2019 15:06:59	Mateus Andre Favretto	Aceito
Folha de Rosto	Folha_de_Rosto_Assinada.pdf	17/07/2016 20:37:21	Mateus Andre Favretto	Aceito

Situação do Parecer:
Aprovado

Necessita Apreciação da CONEP:
Sim

FLORIANOPOLIS, 15 de Maio de 2019

Assinado por:
Nelson Canzian da Silva
(Coordenador(a))

Endereço: Universidade Federal de Santa Catarina, Prédio Reitoria II, R: Desembargador Vitor Lima, nº 222, sala 401
Bairro: Trindade **CEP:** 88.040-400
UF: SC **Município:** FLORIANOPOLIS
Telefone: (48)3721-6094 **E-mail:** cep.propesq@contato.ufsc.br